Modeling of Bioenergy Production

Nuttapol Lerkkasemsan

Dissertation submitted to the faculty of the Virginia Polytechnic Institute and State University in partial fulfillment of the requirements for the degree of

Doctor of Philosophy

In

Chemical Engineering

Luke E. Achenie, Chair

Erdogan Kiran

Stephen Michael Martin

Preston L. Durrill

April 30, 2014, Blacksburg, VA

Keywords: Biodiesel, Pyrolysis, Life Cycle Analysis, Life Cycle Cost, ANFIS

Modeling of Bioenergy Production

Nuttapol Lerkkasemsan

Abstract

In this dissertation we address three different sustainability concepts: [1] modeling of biodiesel production via heterogeneous catalysis, [2] life cycle analysis for pyrolysis of switchgrass for using in power plant, and [3] modeling of pyrolysis of biomass. Thus we deal with Specific Aim 1, 2 and 3.

In Specific Aim 1, the models for esterification in biodiesel production via heterogeneous catalysis were developed. The models of the reaction over the catalysts were developed in two parts. First, a kinetic study was performed using a deterministic model to develop a suitable kinetic expression; the related parameters were subsequently estimated by numerical techniques. Second, a stochastic model was developed to further confirm the nature of the reaction at the molecular level. The deterministic and stochastic models were in good agreement.

In Specific Aim 2, life cycle analysis and life cycle cost for pyrolysis of switchgrass for using in power plant model were developed. The greenhouse gas (GHG) emission for power

generation was investigated through life cycle assessment. The process consists of cultivation, harvesting, transportation, storage, pyrolysis, transportation and power generation. Here pyrolysis oil is converted to electric power through co-combustion in conventional fossil fuel power plants. The conventional power plants which are considered in this work are diesel engine power plant, natural gas turbine power plant, coal-fired steam-cycle power plant and oil-fired steam-cycle power plant. Several scenarios are conducted to determine the effect of selected design variables on the production of pyrolysis oil and type of conventional power plants.

In Specific Aim 3, pyrolysis of biomass models were developed. Since modeling of pyrolysis of biomass is complex and challenging because of short reaction times, temperatures as high as a thousand degrees Celsius, and biomass of varying or unknown chemical compositions. As such a deterministic model is not capable of representing the pyrolysis reaction system. We propose a new kinetic reaction model, which would account for significant uncertainty. Specifically we have employed fuzzy modeling using the adaptive neuro-fuzzy inference system (ANFIS) in order to describe the pyrolysis of biomass. The resulting model is in better agreement with experimental data than known deterministic models.

Acknowledgements

The author wishes to express his gratitude to Dr. Luke E. Achenie for his guidance and support that resulted in the completion of this work. Additionally, the author would like to thank his committee members Dr. Erdogan Kiran, Dr. Stephen Michael Martin, and Dr. Preston L. Durrill for their comments and suggestions during the evolution of this work.

The author would also like to acknowledge the following people:

- Nourredine Abdoulmoumine (Dr. Agblevor's lab in the Biological Systems Engineering), who provided the experimental data
- The staff of the chemical engineering department of Virginia Tech: Mrs. Diane Cannaday, Mrs. Tina Russell, Mrs. Nora Bentley, Mrs. Jane Price, Mr. Riley Chan
- The members of the Applied Physics and Modeling Lab at Virginia Tech (in no particular order): Zhenxing Wang, Chris Christie, and Naresh Pavurala

The author is also grateful for the following financial support:

- The 4-year student fellowship from the Ministry of Science and Technology, Thailand

- The augmented funding from the Institute for Critical Technology and Applied Science at Virginia Tech
- The Hord graduate fellowship from the Department of Chemical Engineering at Virginia Tech

Table of Contents

General Introduction..... 1

Chapter 1 - Specific Aim 1..... 3

1. Chapter 1 - Mechanistic Modeling of Biodiesel Production via Heterogeneous Catalysis 4

1.1. Introduction and literature review 5

1.2. Model development 22

1.3. Result, discussion, and conclusion 48

Reference 73

Chapter 2 Specific Aim 2..... 77

2. Chapter 2 - LCA and LCC Model for Switchgrass Pyrolysis for Use in Power Plant 78

2.1. Introduction and literature review 79

2.2. Model development 125

2.3. Result, discussion, and conclusion 146

Reference 169

Chapter 3 Specific Aim 3..... 177

3. Chapter 3 - Fuzzy Modeling of Biomass Pyrolysis 178

3.1. Introduction and literature review 179

3.2. Deterministic and fuzzy model development 199

3.3. Result, discussion and conclusion 203

Reference 230

Chapter 4 Summary and Conclusions..... 233

4. Summary and Conclusions 234

4.1. Overall Summary 234

4.2. Research contribution 237

4.3. Research papers and presentations 239

4.4. Recommendation and continued research 241

Appendices 243

Appendix A: Nomenclature 243

Appendix B: Esterification of palmitic acid on SO_4/ZrO_2-550°C 245

Appendix C: Esterification of palmitic acid on $AcAl_2O_3$ 247

Appendix D: Experimental data for esterification of FFA on SO_4/ZrO_2-550°C for verifying model 249

Appendix E: Result of esterification from experiment for $AcAl_2O_3$ for verifying model 250

Appendix F: Notation for ANFIS membership function 251

List of Figures

Figure 1.1 The mechanism of thermal decomposition of triglycerides [17]..... 13
Figure 1.2 Transesterification of triacylglycerol to produce three fatty acid alkyl esters by base catalysis..... 14
Figure 1.3 Esterification of a free fatty acid to an alkyl fatty acid ester by acid catalysis..... 14
Figure 1.4 Traditional biodiesel processes with an acidic pre treatment step followed by alkaline catalysis. (A) Reactor; (B) Separation (centrifuge or decanter); (D) Product purification and alcohol recovery[22]..... 17
Figure 1.5 Fitting of Eley-Rideal model to experimental data for palmitic acid esterification over SO_4/ZrO_2-550°C at 40, 60 and 80°C..... 51
Figure 1.6 Illustration of palmitic acid esterification over SO_4/ZrO_2-550°C..... 53
Figure 1.7 Fitting of Eley-Rideal model to experimental data for palmitic acid esterification over $AcAl_2O_3$ at 40, 60 and 80°C... 55
Figure 1.8 Illustration of palmitic acid esterification over $AcAl_2O_3$ 57
Figure 1.9 Prediction of Esterification of Palmitic Acid over Zirconia Sulfate..... 59
Figure 1.10 Prediction of Esterification of Palmitic Acid on Alumina..... 59
Figure 1.11 Stochastic simulation on SO_4/ZrO_2-550°C at 40°C 62
Figure 1.12 Comparison of Stochastic simulation vs. Deterministic model on SO_4/ZrO_2-550°C at 40°C 62
Figure 1.13 Stochastic simulation on SO_4/ZrO_2-550°C at 60°C 63
Figure 1.14 Comparison of Stochastic simulation vs. Deterministic model on SO_4/ZrO_2-550°C at 60°C 63
Figure 1.15 Stochastic simulation on SO_4/ZrO_2-550°C at 80°C 64
Figure 1.16 Comparison of Stochastic simulation vs. Deterministic model on SO_4/ZrO_2-550°C at 80°C 64
Figure 1.17 Stochastic simulation on $AcAl_2O_3$ at 40°C..... 66
Figure 1.18 Comparison of Stochastic simulation vs. Deterministic model on $AcAl_2O_3$ at 40°C..... 66
Figure 1.19 Stochastic simulation on $AcAl_2O_3$ at 60°C..... 67
Figure 1.20 Comparison of Stochastic simulation vs. Deterministic model on $AcAl_2O_3$ at 60°C..... 67
Figure 1.21 Stochastic simulation on $AcAl_2O_3$ at 80°C..... 68

Figure 1.22 Comparison of Stochastic simulation vs. Deterministic model on $AcAl_2O_3$ at 80°C..... 68
Figure 2.1 Outline of generic life cycle assessment (LCA) process (after ISO 14040)[25]..... 93
Figure 2.2 The general methodological framework for LCA (ISO 14040)[29]..... 96
Figure 2.3 Life cycle inventories which account energy, raw materials, wastes, emission and products from all product's life cycle [24]..... 99
Figure 2.4 Pollution prevention assessment boundaries in the context of LCA [20]..... 102
Figure 2.5 Life Cycle Assessment of switchgrass to energy.... 125
Figure 2.6 Calculating harvesting distance from farm to central pyrolysis plant..... 136
Figure 2.7 dependence of emission from switchgrass transportation on pyrolysis plant capacity..... 147
Figure 2.8 Switchgrass price versus Pyrolysis plant capacity. 148
Figure 2.9 Pyrolysis oil price versus Pyrolysis plant capacity 150
Figure 2.10 Price of electricity in different power plants versus pyrolysis plant capacity..... 153
Figure 2.11 Dependency shape of switchgrass price on land fraction and field..... 160
Figure 2.12 Dependency of pyrolysis oil price on land fraction and field shape..... 161
Figure 2.13 Electricity price for substituting pyrolysis oil in diesel engine power plant vary with land fraction and land shape 162
Figure 2.14 Electricity price for substituting pyrolysis oil in natural gas turbine power plant vary with land fraction and land shape..... 162
Figure 2.15 Electricity price for substituting pyrolysis oil in oil-fired steam-cycle power plant vary with land fraction and land shape..... 163
Figure 2.16 Electricity price for substituting pyrolysis oil in coal-fired steam-cycle power plant vary with land fraction and land shape..... 163
Figure 3.1 kinetic mechanism for Thurner et al[14] work..... 188
Figure 3.2 Six independent reaction from Alves et al [15].... 189
Figure 3.3 Reaction scheme from Bradbury et at [17]..... 190

Figure 3.4 Pyrolysis reaction scheme for Koufopanos et al [19] 191
Figure 3.5 the reaction scheme by Varhegyi et al [20]..... 192
Figure 3.6 A two-input first-order Sugeno fuzzy model with two rules..... 194
Figure 3.7 ANFIS architecture..... 194
Figure 3.8 FIS mapping..... 202
Figure 3.9 Pyrolysis of Canarygrass at different temperature using first order kinetic reproduced from Boateng et al [73]. 203
Figure 3.10 FIS represent membership function for time of the reaction..... 205
Figure 3.11 FIS represent membership function for temperature 205
Figure 3.12 FIS represent membership function for output, which is production from pyrolysis reaction..... 206
Figure 3.13 wt% of gas vs number of train data pairs..... 208
Figure 3.14 %wt of gas depend on temperature (C) and time of reaction (s)..... 209
Figure 3.15 ANFIS result against experimental data at 600°c to 1050°c..... 210
Figure 3.16 wt% of gas vs number of test data pairs..... 211
Figure 3.17 testing ANFIS model with the testing data..... 212
Figure 3.18 Comparison result from two different models left side is first order kinetic reaction and right side is ANFIS model..... 214
Figure 3.19 Power law model against experimental data at different temperature..... 216
Figure 3.20 Power law model against experimental data at different temperature with optimum order of reaction..... 217
Figure 3.21represent membership function for time of the reaction..... 218
Figure 3.22 FIS represent membership function for temperature 219
Figure 3.23 FIS represent membership function for output which is production from pyrolysis reaction..... 219
Figure 3.24 FIS mapping..... 221
Figure 3.25 % conversion vs number of train data pairs..... 221
Figure 3.26 %conversion depend on temperature (C) and time of reaction (s)..... 222
Figure 3.27 ANFIS model against experimental data at 600 to 1000°C..... 223
Figure 3.28 %conversion vs number of test data pairs..... 224
Figure 3.29 testing ANFIS model with the testing data..... 225

Figure 3.30 Power law model vs ANFIS model for pyrolysis of wood 227

List of Tables

Table 1.1 Published results on heterogeneous catalyst, experimental conditions and respective results obtained, found in literature research, for biodiesel production..... 19
Table 1.2 Stoichiometric table for a Batch system..... 26
Table 1.3 Kinetic parameters of palmitic acid esterification on SO_4/ZrO_2-550°C..... 51
Table 1.4 Kinetic parameters of palmitic acid esterification on $AcAl_2O_3$ 56
Table 1.5 Reaction parameters determined by stochastic model on SO_4/ZrO_2-550°C..... 61
Table 1.6 Reaction parameters determined by stochastic model on $AcAl_2O_3$ 65
Table 2.1 ISO documents on life cycle assessment (LCA)[30].... 93
Table 2.2 more likely and less likely items to be included in current practice..... 113
Table 2.3 Activity Categories for Cost Allocation [46]..... 115
Table 2.4 Switchgrass cultivars and characteristics for upland varieties [49]..... 122
Table 2.5 Switchgrass cultivars and characteristics for lowland varieties [95]..... 123
Table 2.6 Biomass yield of several switchgrass varieties cultivars grown in southern Iowa from 1998 to 2001[54]..... 124
Table 2.7 The estimated costs of pre-harvest machinery in establishing per hectare [57][58][59][60]..... 128
Table 2.8 The operating expense in establishing per hectare [57][58][59][60]..... 128
Table 2.9 Total cost and prorated yearly in establishing per hectare..... 129
Table 2.10 The estimated GHG emission for establishing switchgrass per hectare [57][58][59][61][60]..... 129
Table 2.11 The estimated pre-harvest machinery operations cost in reseeding per hectare [57][58][59][60]..... 130
Table 2.12 The estimated operating expense in reseeding year per hectare [57][58][59][60]..... 130
Table 2.13 Total cost and prorated yearly in reseeding per hectare..... 131
Table 2.14 The estimated GHG emission for reseeding switchgrass per hectare [57][58] [59][61][60]..... 131

Table 2.15 The estimated costs per hectare of pre-harvesting machinery operations for production year per hectare [57][58][59][60]..... 132
Table 2.16 The estimated operating expense in production year per hectare [57][58][59][60]..... 132
Table 2.17 The estimated cost of harvest machinery operation in production year per hectare [57][58][59][60]..... 133
Table 2.18 The total cost and prorated yearly in production year per hectare..... 133
Table 2.19 estimated GHG emission for pre-harvest machinery operations, fertilizer, and herbicide per hectare [57][58][59][60][61]..... 134
Table 2.20 estimated GHG emission for harvest machinery operations per hectare [57][58][59][61][60]..... 134
Table 2.21 Initial construction costs of the selected storage systems (storage losses are not included)[68]..... 137
Table 2.22 Storage systems and expected dry matter loss[68].. 138
Table 2.23 Biorefinery capital cost components based on the reference plant size[69]..... 140
Table 2.24 Biomass fast pyrolysis annual operating cost components based on the reference plant size[69]..... 140
Table 2.25 Production from switchgrass pyrolysis[15]..... 140
Table 2.26 Properties of pyrolysis oil [15]..... 141
Table 2.27 Power plant efficiency..... 142
Table 2.28 Specification on wt% of pyrolysis liquid component (to be able to use as fuel in boilers, engines and turbines)[73] 142
Table 2.29 Power Generation capital, operation and maintenance cost per kWyr for different power plants[81]..... 145
Table 2.30 Slope of electricity produced by different power plants vary with pyrolysis plant capacity..... 152
Table 2.31 variation of total emission (of different power plants) with pyrolysis plant capacity..... 155
Table 2.32 Slope and intercept in linear relation for dependence of electric cost on distance between pyrolysis plant and power plant..... 157
Table 2.33 Slope and intercept for dependence of total GHG emission on distance between pyrolysis plant and power plant. 158
Table 2.34 Life-cycle assessment of green house gas emissions (kt eq. CO_2 per Twh)[86] 159

Table 2.35 parameters for Land fraction and field shape effect to the total GHG emission equation..... 165

General Introduction

This dissertation analyzes the mechanism of bio-oil production and the use of bio-oil in replacing fossil fuels in power plants. We studied two popular bio-oil production processes: biodiesel production and pyrolysis oil production.

Biodiesel is a liquid bio-fuel obtained by chemical processes from vegetable oils or animal fats and an alcohol. The biodiesel can be used in diesel engines alone or blended with diesel. We studied the mechanisms of biodiesel production via heterogeneous catalysts, including SO_4ZrO_2-550°C and $AcAl_2O_3$.

Pyrolysis oil is a liquid product of anaerobic distillation of biomass, such as wood or other biomass sources. With sufficient temperature in an air-tight chamber, biomass is transformed into volatile components and char. When the volatile components cool down, some of them formed liquid, the so-called pyrolysis oil. The pyrolysis oil can substitute for fossil fuels in power plants. We studied the viability of switchgrass pyrolysis use in power plants through life cycle analysis and life cycle cost. In this dissertation, we also examined biomass pyrolysis behavior. Since biomass pyrolysis behavior is

difficult to model due to its complexity and uncertainty, we employed a new uncertainty approach for our model.

Chapter 1 - Specific Aim 1

Mechanistic Modeling of Biodiesel Production via Heterogeneous Catalysis

Lerkkasemsan N, Abdoulmoumine N, Achenie L, Agblevor F. Mechanistic Modeling of Palmitic Acid Esterification via Heterogeneous Catalysis. Industrial & Engineering Chemistry Research 2011;50:1177 – 1186.

1. Chapter 1 - Mechanistic Modeling of Biodiesel Production via Heterogeneous Catalysis

In this aim, we develop models that explain the reaction over two heterogeneous catalysts, namely SO_4/ZrO_2-550°C (Sulfated Zirconia activated at 550°C) and $AcAl_2O_3$ (Acid Aluminium Oxide). First, we consider deterministic models for both catalysts. Next, we develop stochastic models for the catalytic reactions in biodiesel production. The stochastic models will act as additional validation for the deterministic models.

1.1. Introduction and literature review

1.1.1. Introduction

In recent years, biodiesel has been shown to be a promising alternative renewable energy source for petrol-diesel. As a result biodiesel production has been increasingly investigated by many scientists. This interest was prompted by environmental concerns of global warming and the mounting evidence of the depletion of natural crude oil reserves. At the current usage rate, petroleum reserves will be depleted by the end of the next century [1][2]. Biodiesel is gentler on the environment. For example, biodiesel is biodegradable and is also carbon neutral [3] because it is produced from renewable sources such as vegetable oil and animal fat. The traditional method of biodiesel production is through the esterification of vegetable oil and animal fat with alcohol using homogeneous catalysts such as NaOH or KOH. However, homogeneous basic catalysts are susceptible to free fatty acid (FFA) and water that are found in cheaper feedstock such as waste cooking oil.

The homogeneous basic catalysts can react with the free fatty acid to form soap through a saponification reaction. The water in the feedstock reverses some of the reaction steps. Therefore, water limits the yield of Fatty Acid Methyl Ester

(FAME); additionally it limits the choice of feedstock. One solution to this problem is to use homogeneous *acid* catalysts to convert FFA before using homogeneous *basic* catalysts. However, the homogeneous acid catalysts have a problem of corrosion. To address these problems, heterogeneous acid catalysts that can simultaneously react with both FFA and triacylglycerols have been developed. Moreover, it can be easily separated from the product and reused several times. These advantages can reduce biodiesel production costs thus making biodiesel price competitive with petrol diesel. The heterogeneous acid catalysts, which are considered in this specific aim are SO_4/ZrO_2 and $AcAl_2O_3$.

1.1.2. Literature review

There are several methods in biodiesel production; the following section will outline a few of those methods.

(1) Biodiesel making process

Some of the ways to make biodiesel are as follows:

(I) Direct use of pure vegetable oil or blending with petrol-diesel in various ratios.

(II) Microemulsions with solvent by blending diesel fuel with solvent such as alcohol.

(III) Thermal cracking to alkane, alkenes, alkadines, etc.

(IV) Transesterification with catalyst

(I) Direct use and blending

The direct use of vegetable oil in diesel engine was tested by Rudolph Diesel who was the inventor of diesel engine[4]. Because of low cost petrol-diesel at that time, using vegetable oil in diesel engine was not pursued. At the beginning of the 1980s, Bartholomew et al [5] addressed the concept of using food for fuel, indicating that food products such as vegetable oil, alcohol and some other forms of renewable resources should be the alternative fuel rather than petroleum. The most advanced

work with sunflower seed oil occurred in South Africa because of the oil embargo.

Caterpillar[6] Brazil, in 1980, used pre-combustion chamber engines with a mixture of 10% vegetable oil with petrol-diesel in order to maintain total power without any modifications or adjustments of the engine. At that point, it was not practical to substitute 100% vegetable oil for diesel fuel, but a blend of 20% vegetable oil and 80% diesel fuel was successful.

A blend of 95% used cooking oil and 5% diesel fuel was used power the engines of a fleet of buses in the early 1980s which was address by Anon [7]. Blending or preheating was needed in order to compensate for cooler ambient temperatures. Incidentally, there were no coking and carbon build-up problems in this operation. The key to success was suggested to be filtering and the only problem reported was lubricating oil contamination. The viscosity of lubricating oil increased due to polymerization of polyunsaturated vegetable oils. The lubricating oil had to be changed between 4,000 and 4,500 miles.

Mixtures of degummed soybean oil and petrol-diesel fuel in the ratios of 1:2 and 1:1 were tested[8]. The thickening and potential gelling of the lubricant existed for the 1:1 blend, but it did not occur with the 1:2 blend. The results indicated

that the 1:2 blends should be suitable as fuel for agricultural equipment during periods of diesel fuel shortages.

Two severe problems associated with the use of vegetable oils (directly or blended with petrol-diesel fuels) were oil deterioration and incomplete combustion[9]. Polyunsaturated fatty acids were very susceptible to polymerization, gum formation caused by oxidation during storage or by complex oxidative, thermal polymerization at the higher temperature and pressure of combustion. The gum did not combust completely, resulting in carbon deposits and lubricating oil thickening.

From Pryde et al[1], the advantages of direct use and blending vegetable oils in diesel fuel are:

(A) Portability (Liquid fuel)

(B) Heat content (88% of diesel no.2 fuel)

(C) Ready availability

(D) Renewability

(E) Lower sulfur and aromatic content

The disadvantages are:

(A) Higher viscosity

(B) Lower volatility

(C) The reactivity of unsaturated hydrocarbon chains

There are several problems that appear after long periods of time, especially with direct-injection engines[10]. Some are as follows:

(A) Carbon deposit

(B) Thickening and gelling of the lubricating oil as a result of contamination by vegetable oils

(C) Coking and trumpet formation on the injectors to such an extent that fuel atomization does not occur properly or is even prevented as a result of plugged orifices

(D) Lubricating problems

(E) Oil ring sticking

In addition, the vegetable oil and animal fats also have high viscosity, which is 11 to 17 times higher than petroleum diesel. They also have lower volatilities that cause incomplete combustion. In addition, vegetable oil can form large agglomerations, which are caused by the polymerization of unsaturated fatty acids at high temperature as well as gumming. This problem occurs because vegetable oil contains many unsaturated fatty acids. Because of these problems, the direct use and blending methods are not popular.

(II) Microemulsions

The main idea of creating microemulsions is to try to reduce the viscosity of vegetable oil with solvents such as methanol, ethanol, and 1-butanol. This method can eliminate the problem of high viscosity that plagues vegetable oil[11]. A microemulsion is a system of water, oil, and amphiphilic compounds (surfactant and co-surfactant); it is a transparent, single optically isotropic, and thermodynamically stable liquid.

Ziejewski et al.[12]prepared an emulsion of 53.3% (v/v) alkali-reined and winterized sunflower oil, 13.3% (v/v) 1-butanol. This non-ionic emulsion had a viscosity of $6.31 \times 10^{-6} \frac{m^2}{s}$ at 40°C, a cetane number of 25, sulfur content of 0.01%, free fatty acids of 0.01%, and ash content of less than 0.01%. Lower viscosities and better spray patterns were obtained by increasing the amount of 1-butanol. Short-term performances of both ionic and non-ionic microemulsions of aqueous ethanol in soybean oil were nearly as good as that of No.2 diesel, despite the lower cetane number and energy content. However, there are still problems after using this fuel for a long term. Problems such as injector needle sticking, carbon deposits, incomplete combustion, and increasing viscosity of lubricating oils were reported[10].

(III) Thermal Cracking (Pyrolysis)

Thermal cracking or pyrolysis involves heating in the absence of air or oxygen and cleavage of chemical bonds to yield small molecule [13]. This is often done with the aid of a catalyst[10]. The first pyrolysis of vegetable oil was conducted in China in an attempt to synthesize petroleum from vegetable oil during World War II.

Pyrolysis chemistry is difficult to characterize because of the variety of reaction paths and the variety of reaction products that may be obtained from the reactions that take place. Many investigators have studied the pyrolysis of triglycerides with the aim of obtaining products suitable for diesel engines [14][15][16][17]. The pyrolyzed material can be vegetable oils, animal fats, natural fatty acids, and methyl esters of fatty acids. The products include alkanes, alkenes, alkadienes, aromatics, and carboxylic acids. The mechanisms for the thermal decomposition of a triglyceride are given in Figure 1.1.

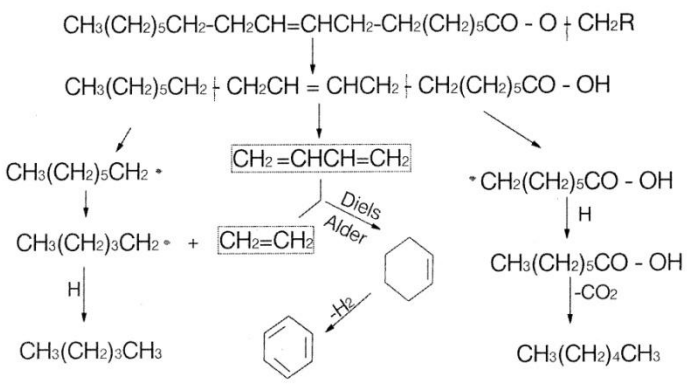

Figure 1.1 The mechanism of thermal decomposition of triglycerides [17]

Different types of vegetable oils reveal large differences in composition when they are thermally decomposed. For example, pyrolyzed soybean oil contains 79% carbon and 12% hydrogen[17]. The biodiesel produced in this process has low viscosity and a high Cetane number compared to pure vegetable oils. Moreover, pyrolyzed vegetable oil has acceptable amounts of sulfur, water and sediment. However, they are unacceptable in terms of ash, carbon residues, and pour points. The equipment of thermal cracking or pyrolysis is expensive for modest throughputs. In addition, while the products are chemically similar to petroleum-derived gasoline and diesel fuel, the removal of oxygen during the thermal processing also removes any environmental benefits of using an oxygenated fuel [10]. It also produced some low value material.

(IV) Transesterification

Biodiesel can be produced by the transesterification of triacylglycerols through base catalysis (Figure 1.2) or esterification of free fatty acids and triacylglycerols by acid catalysis (Figure 1.3).

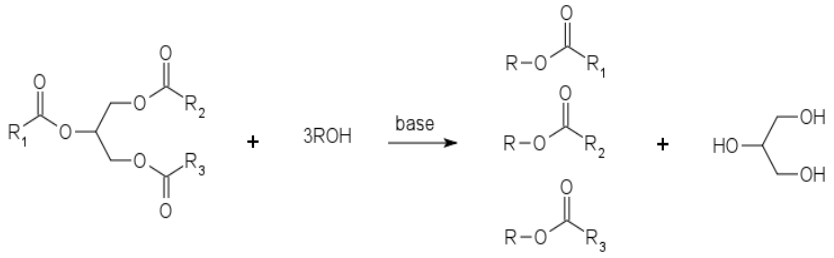

Figure 1.2 Transesterification of triacylglycerol to produce three fatty acid alkyl esters by base catalysis

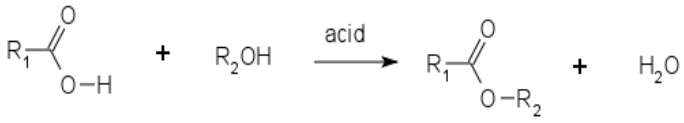

Figure 1.3 Esterification of a free fatty acid to an alkyl fatty acid ester by acid catalysis

The most common catalyst for both esterification and transesterification reaction are homogeneous catalyst, especially homogeneous basic catalysts. Vicente et al [18] reported the transesterification of sunflower seed oil and

methanol at 65°C using four different homogeneous basic catalysts, namely sodium hydroxide, potassium hydroxide, sodium methoxide, and potassium methoxide. The ratio of methanol per sunflower oil was 6:1 with 1wt% of catalyst. The report showed that the biodiesel yield after the separation process and purification process were higher than 98 wt% for the methoxide catalysts, because the yield losses due to triglyceride saponification and methyl ester dissolution in glycerol were negligible. The biodiesel yield for the sodium and potassium hydroxide were lower, 85.9 and 91.67 wt% respectively. However, the cost of methoxide catalysts is higher than hydroxide catalysts and more difficult to manipulate since they are very hygroscopic. Therefore, applications that employ homogeneous catalysts prefer sodium or potassium hydroxide because they are inexpensive compared to methoxide. Moreover, sodium hydroxide is the fastest catalyst, in the sense that it achieves 100 wt% of methyl ester concentration in the biodiesel phase in just 30 minutes. Unfortunately, when a basic homogeneous catalyst is used for the transesterification of feeds with FFAs, soaps are produced as by-products through the unwanted saponification reaction of carboxylic acids with the base catalyst[19].

$$ROOH + NaOH \text{ (or } MeONa) \rightarrow ROO^{-}Na^{+} + H_2O \text{ (or } MeOH) \quad (1.1)$$

$$ROOMe + H_2O \Leftrightarrow ROOH + MeOH \quad (1.2)$$

The water that is produced by hydrolysis (1.1) reacts with the esters to form more FFA that consumes the base catalyst to produce soap, according to reaction (1.2). Because of these problems, homogeneous basic catalysts are susceptible to water and FFA, which are found in cheap feedstock such as waste cooking oil. Therefore, homogeneous basic catalysts are more suitable for refined vegetable oil, which can raise the production cost of biodiesel. This means that the cost of biodiesel cannot be lower to be competitive with petrol-diesel because of high price feedstock. Moreover, the homogeneous basic catalysts are also nonrenewable catalysts.

Several methods have been proposed to solve these problems, but the most useful method seems to be pre-esterification with acid catalysis.

(2) Methods to solve homogeneous problem

(I) Pre-esterification method

The homogeneous acid catalyzed pre-esterification of FFA is a common practice in reducing FFA levels in feedstock with high FFA, before performing the base catalysts transesterification

[20][21]. The disadvantage of the pre-esterification method consists of the necessity to remove the homogeneous acid catalyst from the oil after pre-esterification. To improve the process, the solution is the use of a heterogeneous esterification catalyst[21]. The biodiesel production process by pre-esterification method is shown in (Figure 1.4).

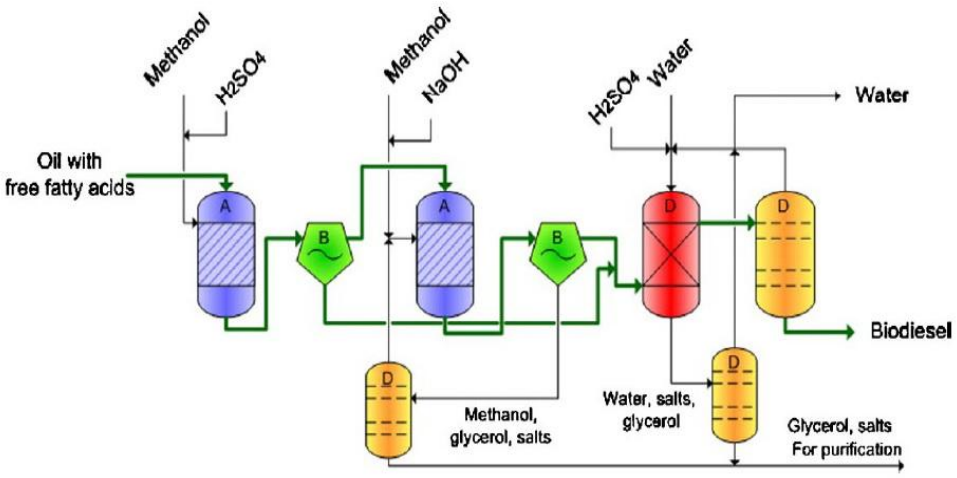

Figure 1.4 Traditional biodiesel processes with an acidic pre treatment step followed by alkaline catalysis. (A) Reactor; (B) Separation (centrifuge or decanter); (D) Product purification and alcohol recovery[22]

(II) Use of acid catalysts

Homogeneous acid catalysis is less complex than the two-step process namely, pre-esterification with homogeneous acid catalyst followed by alkali-catalysis [23]. However, this process is associated with problems linked with the corrosive nature of the liquid acid catalyst and to the high quantity of byproduct obtained[24]. There is a way to perform triglyceride

transesterification and FFA esterification in a single step, using low concentrations of a homogeneous Lewis acid catalyst. However, this process also has its shortcomings linked to the need to remove catalysts from products by downstream purification [24]. A solid acid catalyst could solve these problems[21].

(III) Heterogeneous Catalysts

The use of heterogeneous catalysts can easily solve the problem of separation of products and catalysts after the esterification reaction. There are two types of heterogeneous catalysts, namely (a) heterogeneous basic catalysts such as MgO and hydrotalcites (CHT) and (b) heterogeneous acid catalysis such as titanium oxide supported on silica, TiO_2/SiO_2 (TS); Vanadyl phosphate $VOPO_4 \cdot 2H_2O$ (VOP) and metal-substituted Vanadyl Phosphate $Me(H_2O)xVO(1-x)PO_4 \cdot 2H_2O$ (MeVOP). Di Serio et al [25]studied MgO, CHT, TS, VOP and MeVOP. The study showed that MgO and CHT had high activities. However, in the presence of FFAs both catalysts form soap via saponification reaction. Therefore, the heterogeneous basic catalyst is also as vulnerable as the homogeneous basic catalyst. On the other hand, The presence of FFAs has minute negative effect to the solid acid catalysts. Therefore, the solid acid catalysts can be

useful for producing biodiesel from low quality feedstock, which contain substantial amount of FFAs such as waste cooking oil. Using cheaper feedstock without having to refine it can lead to the reduction in the cost of biodiesel production. Furthermore, heterogeneous catalysis is readily to apply to continuous fix bed reactor. The utilization of heterogeneous catalyst thus means more flexibility and less downstream separation. It also means less catalyst replacements in the fixed bed catalytic reactor, which leads to a higher quality of the final biodiesel product [26]. Furthermore, heterogeneous catalysis results in cleaner glycerol, which further improves the profitability of the process. The absence of the alkaline catalyst neutralization step and the necessity to replace the consumed catalyst can simplify the production line and reduce the cost of production.

The performances of several heterogeneous catalysts are shown in Table 1.1.

Table 1.1 Published results on heterogeneous catalyst, experimental conditions and respective results obtained, found in literature research, for biodiesel production

Catalysts	**Results**
SO_4/ZrO_2	Good results in the reaction conversion and yield for SO_4/ZrO_2, in a large range of temperatures[27][28]

Catalysts	Results
Dibutyltin oxide ($(C_4H_9)_2SnO$)	Soya oil transesterification. Molar ratio oil/methanol/catalyst: 100/400/1, 10 hours of residence reaction time. Higher conversion (35%) for dibutyltin oxide. [29]
Supported catalysts Fe-Zn in cyanid complexes, with and without t-buthanol (complex agent) and with a co-polymer ($EO_{20}PO_{70}EO_{20}$)	Higher activity and selectivity using complex agent in the catalytic matrix [30]
SiO_2/H_2SO_4, SiO_2/KOH and Al_2O_3/KOH, SiO_2/HCl, $SiO_2/ZnCl_2$, SiO_2/ Al_2O_3 and Al_2O_3/ H_2SO_4	Mamona and soy oil transesterification, with methanol, temperatures of 25C and 65C, ratio support/catalyst of 50%(w/w), ratio oil/methanol of 1:6, mass ratio of 5g oil/0.25g of catalyst. Best results for supported alumina catalysts for alkaline catalysis. While the silica catalysts showed best results for acid catalysis. [31]

Catalysts	Results
K_2CO_3, Na_2CO_3 and $CaCO_3$	Mamona oil transesterification with methanol, ratio oil/methanol/catalyst of 100/600/1. Reaction time of 10 hours. K_2CO_3 showed best catalystic activity and higher yields in biodiesel production. $CaCO_3$ did not show any catalytic activity. [32]
Zeolite Y	Employment of used fried oils. Good biodiesel yield. [33]
Hydrotalcites of Mg and Al (ratio Mg/Al of 3). Modified with Zn, Sn, Ba, Mn, Ce and Ca, with 5% catalyst (wt.%)	Soy oil transesterification with methanol, 70°C, reaction time of 3 hours, ratio methanol/oil of 9:1. Good results regarding biodiesel yield and product quality. [34]

In the current specific aim, we will show that the Eley-Rideal model is suitable for studying the kinetics of palmitic acid esterification on sulfated zirconium oxide and activated acidic alumina catalysts. Furthermore, the Gillespie model is used to investigate the consistency of the model.

1.2. Model development

1.2.1. Deterministic kinetic models for transesterification reaction for palmitic acid

SO_4/ZrO_2-550^{o}C and $AcAl_2O_3$ were used to perform the kinetic experiments at 40, 60 and 80^{o}C at 10 wt% and 100 wt%. Eleven models (including Langmuir-Hinshelwood and Eley-Rideal models) were tested. The total active site on SO_4/ZrO_2-550^{o}C was determined to be 2.05 wt%. For Alumina, due to the lack of actual experimental data, we used total active site, which was measured via chemisorption of ethylene on alumina, from literature; this was reported to be 35 %mole [35]. We assumed that an Eley-Rideal mechanism occurred with palmitic acid on the catalyst surface and reaction of bulk fluid methanol as the rate-determining step. For $AcAl_2O_3$ however, we assumed that methanol was adsorbed on the catalyst surface and the palmitic acid was in the bulk fluid. We assumed that the methanol adsorption was the rate- determining step.

(1) Rate law Model

In chemical reaction kinetics, the power law model is popular model. However, rate laws in heterogeneous catalysis rarely follow power law models and hence are inherently more difficult to formulate from the data [36]. In order to develop

an in-depth understanding and insight as to how the rate laws are formed from heterogeneous catalytic data, we will postulate catalytic mechanisms and derive rate laws for the various mechanisms. The mechanisms will typically have an adsorption step, a surface reaction step, and a desorption step, one of which is usually a rate-determining step.

By knowing the different forms that catalytic rate equations can take, it will be easier to view the trends in the data and deduce the appropriate rate law. After knowing the form of the rate law, one can then numerically evaluate the rate law parameters and postulate a reaction mechanism and rate-determining step that is consistent with the rate data. Finally, one can use the rate law to design catalytic reactors.

To find a rate law for the esterification reaction, which occurs over the surface of the catalysts, we employ both the Langmuir-Hinshelwood model and the Eley-Rideal model. The models are derived in the following sections.

(I) Langmuir-Hinshelwood model

In this model, palmitic acid and methanol, which are the reactants, are adsorbed on the surface of the catalyst and react with each other. After the reaction, the products, which are water and biodiesel, are desorbed back to the bulk fluid.

Therefore, we can formulate the model using the following elementary steps:

$A + S \overset{k_{AB}, k_{-AB}}{\Longleftrightarrow} A \cdot S$ -Adsorption of palmitic acid (1.3)

$M + S \overset{k_{AM}, k_{-AM}}{\Longleftrightarrow} M \cdot S$ -Adsorption of methanol (1.4)

$A \cdot S + M \cdot S \overset{k_S, k_{-S}}{\Longleftrightarrow} E \cdot S + W \cdot S$ -Reaction of adsorbed species (1.5)

$E \cdot S \overset{k_{DB}\, k_{-DB}}{\Longleftrightarrow} E + S$ -Desorption of ester (1.6)

$W \cdot S \overset{k_{DW}, k_{-DW}}{\Longleftrightarrow} W + S$ -Desorption of water (1.7)

Here the rate equations from reactions (1.3) to (1.7) can be written as below:

$-r_{AB} = k_{AB}\left(C_A C_v - \frac{C_{A\cdot S}}{K_{AB}}\right); K_{AB} = \frac{k_{AB}}{k_{-AB}}$ -Adsorption of palmitic acid (1.8)

$-r_{AM} = k_{AM}\left(C_M C_v - \frac{C_{M\cdot S}}{K_{AM}}\right); K_{AM} = \frac{k_{AM}}{k_{-AM}}$ -Adsorption of methanol (1.9)

$-r_S = k_S\left(C_{A\cdot S} C_{M\cdot S} - \frac{C_{E\cdot S} C_{W\cdot S}}{K_S}\right); K_S = \frac{k_S}{k_{-S}}$ -Reaction of Adsorbed species (1.10)

$-r_{DB} = k_{DB}\left(C_{E\cdot S} - \frac{C_E C_v}{K_{DB}}\right); K_{DB} = \frac{k_{DB}}{k_{-DB}}$ -Desorption of ester (1.11)

$-r_{DW} = k_{DW}\left(C_{W\cdot S} - \frac{C_W C_v}{K_{DW}}\right); K_{DW} = \frac{k_{DW}}{k_{-DW}}$ -Desorption of water (1.12)

The rate-determining step in the Langmuir-Hinshelwood model can be chosen assuming five different pseudo steady state hypotheses as follows.

(A) The reaction over the reactant is the rate-determining step. The $k_{AB}, k_{AM}, k_{DB}, k_{DW}$ are large and we can set.

$$-\frac{r_{AB}}{k_{AB}} \cong 0 \qquad C_{A\cdot S} = K_{AB} C_A C_v \qquad (1.13)$$

$$-\frac{r_{AM}}{k_{AM}} \cong 0 \qquad C_{M\cdot S} = K_{AM} C_M C_v \qquad (1.14)$$

$$-\frac{r_{DB}}{k_{DB}} \cong 0 \qquad C_{E\cdot S} = \frac{C_E C_v}{K_{DB}} \qquad (1.15)$$

$$-\frac{r_{DW}}{k_{DW}} \cong 0 \qquad C_{W\cdot S} = \frac{C_W C_v}{K_{DW}} \qquad (1.16)$$

$$C_T = C_v + C_{A\cdot S} + C_{M\cdot S} + C_{E\cdot S} + C_{W\cdot S}$$

-Total site equation (1.17)

From (1.10)

$$-r_S = k_S \left(C_{A\cdot S} C_{M\cdot S} - \frac{C_{E\cdot S} C_{W\cdot S}}{K_S} \right) \qquad ; \quad K_S = \frac{k_S}{k_{-S}}$$

Substitute (1.11) to (1.16) into (1.17)

$$-r_S = k_S K_{AB} K_{AM} \left(C_A C_M - \frac{C_E C_W}{K_{DB} K_{DW} K_S K_{AB} K_{AM}} \right) C_v^2 \qquad (1.18)$$

From (1.17) the vacant site equation can be expressed as seen below:

$$C_v = \frac{C_T}{1+K_{AB}C_A+K_{AM}C_M+\frac{C_E}{K_{DB}}+\frac{C_W}{K_{DW}}} \tag{1.19}$$

Substitute (1.18) into (1.19)

$$-r_S = \frac{K_1 K_{AB} K_{AM}\left(C_A C_M - \frac{C_E C_W}{K_S K_{AB} K_{AM} K_{DB} K_{DW}}\right)}{\left(1+K_{AB}C_A+K_{AM}C_M+\frac{C_E}{K_{DB}}+\frac{C_W}{K_{DW}}\right)^2} \tag{1.20}$$

Table 1.2 Stoichiometric table for a Batch system

Species	**Symbol**	**Initially**	**Change**	**Remaining**	**Concentration**
$C_{15}H_{31}COOH$	A	N_{A_0}	$-N_{A_0}X$	$N_{A_0}(1-X)$	$C_{A_0}(1-X)$
CH_3OH	M	N_{M_0}	$-N_{A_0}X$	$N_{A_0}(\theta_M-X)$	$C_{A_0}(\theta_M-X)$
$C_{15}H_{31}OOCH_3$	E	N_{E_0}	$N_{A_0}X$	$N_{A_0}(\theta_E+X)$	$C_{A_0}(\theta_E+X)$
H_2O	W	N_{W_0}	$N_{A_0}X$	$N_{A_0}(\theta_W+X)$	$C_{A_0}(\theta_W+X)$

Since these are liquid-phase reactions the density ρ is considered to be constant; therefore, $V = V_0$. Thus

$$C_A = C_{A_0}(1-X) \tag{1.21}$$

$$C_M = C_{A_0}(100-X) \tag{1.22}$$

$$C_E = C_{A_0}X \tag{1.23}$$

$$C_W = C_{A_0}X \tag{1.24}$$

where $C_{A_0} = 0.246863\ \frac{mol}{dm^3}$

Substitute (1.21) to (1.24) into (1.20)

Therefore, the rate equation for the reaction limited is expressed as:

$$rate = \frac{K_1\left(K_{AB}K_{AM}C_{A_0}(1-X)(100-X)-\frac{C_{A_0}X*X}{K_S K_{DB}K_{DW}}\right)}{\left(1+K_{AB}C_{A_0}(1-X)+K_{AM}C_{A_0}(100-X)+\frac{C_{A_0}X}{K_{DB}}+\frac{C_{A_0}X}{K_{DW}}\right)^2} \quad (1.25)$$

(B) Adsorption of palmitic acid is the rate-determining step. The $k_{AM}, k_S, k_{DB}, k_{DW}$ are large by comparison, and we can set.

$$-\frac{r_{AM}}{k_{AM}} \cong 0 \qquad C_{M\cdot S} = K_{AM}C_M C_v \quad (1.14)$$

$$-\frac{r_S}{k_S} \cong 0 \qquad C_{A\cdot S} = \frac{C_{E\cdot S}C_{W\cdot S}}{K_S C_{M\cdot S}} \quad (1.26)$$

$$-\frac{r_{DB}}{k_{DB}} \cong 0 \qquad C_{E\cdot S} = \frac{C_E C_v}{K_{DB}} \quad (1.15)$$

$$-\frac{r_{DW}}{k_{DW}} \cong 0 \qquad C_{W\cdot S} = \frac{C_W C_v}{K_{DW}} \quad (1.16)$$

From (1.8)

$$-r_{AB} = -r_C = k_{AB}\left(C_A C_v - \frac{C_{A\cdot S}}{K_{AB}}\right)$$

Substitute (1.3) to (1.15) and (1.26) into (1.8) to obtain

$$-r_{AB} = k_{AB}\left(C_A - \frac{C_E C_W}{K_{DB}K_{AB}K_{DW}K_S K_{AM}C_M}\right)C_v \quad (1.27)$$

From (1.17) we can derive the vacant site equation as seen below:

$$C_v = \frac{C_T}{1+\frac{C_E C_W}{K_S K_{AM} K_{DB} K_{DW} C_M}+K_{AM} C_M+\frac{C_E}{K_{DB}}+\frac{C_W}{K_{DW}}} \quad (1.28)$$

Substitute (1.28) into (1.27)

$$-r_{AB} = \frac{K_1\left(C_A-\frac{C_E C_W}{K_{DB} K_{AB} K_{DW} K_S K_{AM} C_M}\right)}{1+\frac{C_E C_W}{K_S K_{AM} K_{DB} K_{DW} C_M}+K_{AM} C_M+\frac{C_E}{K_{DB}}+\frac{C_W}{K_{DW}}} \quad (1.29)$$

Substitute (1.21) to (1.24) into (1.29)

$$rate = \frac{K_1\left(C_{A_0}(1-X)-\frac{C_{A_0}X^2}{K_{DB} K_{AB} K_{DW} K_S K_{AM} (100-X)}\right)}{1+\frac{C_{A_0}X^2}{(100-X)K_{DB} K_{DW} K_S K_{AM}}+K_{AM} C_{A_0}(100-X)+\frac{C_{A_0}X}{K_{DB}}+\frac{C_{A_0}X}{K_{DW}}} \quad (1.30)$$

(C) Adsorption of methanol is the rate-determining step. The k_{AB} , k_S , k_{DB} , k_{DW} are large by comparison, and we can set.

$$-\frac{r_{AB}}{k_{AB}} \cong 0 \qquad C_{A\cdot S} = K_{AB} C_A C_v \quad (1.13)$$

$$-\frac{r_S}{k_S} \cong 0 \qquad \frac{C_{W\cdot S} C_{E\cdot S}}{K_S C_{A\cdot S}} = C_{M\cdot S} \quad (1.26)$$

$$-\frac{r_{DB}}{k_{DB}} \cong 0 \qquad C_{E\cdot S} = \frac{C_E C_v}{K_{DB}} \quad (1.15)$$

$$-\frac{r_{DW}}{k_{DW}} \cong 0 \qquad C_{W\cdot S} = \frac{C_W C_v}{K_{DW}} \quad (1.16)$$

From (1.9)

$$-r_{AM} = k_{AM}\left(C_M C_v - \frac{C_{M\cdot S}}{K_{AM}}\right)$$

Substitute (1.13), (1.26), (1.15) and (1.16) into (1.9) to obtain

$$-r_{AM} = k_{AM}\left(C_M - \frac{C_W C_E}{K_S K_{AM} K_{AB} K_{DW} K_{DB} C_A}\right) C_v \qquad (1.31)$$

From (1.17)

$$C_v = \frac{C_T}{1+K_{AB} C_A + \frac{C_W C_E}{K_S K_{AB} K_{DW} K_{DB} C_A} + \frac{C_E}{K_{DB}} + \frac{C_W}{K_{DW}}} \qquad (1.32)$$

Substitute (1.32) into (1.31)

$$-r_{AM} = \frac{K_1\left(C_M - \frac{C_W C_E}{K_S K_{AM} K_{AB} K_{DW} K_{DB} C_A}\right)}{1+K_{AB} C_A + \frac{C_W C_E}{K_S K_{AB} K_{DW} K_{DB} C_A} + \frac{C_E}{K_{DB}} + \frac{C_W}{K_{DW}}} \qquad (1.33)$$

Substitute (1.21) to (1.24) into (1.33)

$$rate = \frac{K_1\left(C_{A_0}(100-X) - \frac{{C_{A_0}}^2 X^2}{K_S K_{AM} K_{AB} K_{DW} K_{DB}(1-X)}\right)}{1+K_{AB} C_{A_0}(1-X) + \frac{{C_{A_0}}^2 X^2}{K_{DW} K_{DB} K_S K_{AB}(1-X)} + \frac{C_{A_0} X}{K_{DB}} + \frac{C_{A_0} X}{K_{DW}}} \qquad (1.34)$$

(D) Desorption of palmetate is a rate-determining step. The k_{AB}, k_{AM}, k_S, k_{DW} are large by comparison, and we can set.

$$-\frac{r_{AB}}{k_{AB}} \cong 0 \qquad C_{A\cdot S} = K_{AB} C_A C_v \qquad (1.13)$$

$$-\frac{r_{AM}}{k_{AM}} \cong 0 \qquad C_{M\cdot S} = K_{AM} C_M C_v \qquad (1.14)$$

$$-\frac{r_S}{k_S} \cong 0 \qquad C_{E\cdot S} = \frac{K_S C_{A\cdot S} C_{M\cdot S}}{C_{W\cdot S}} \qquad (1.26)$$

$$-\frac{r_{DW}}{k_{DW}} \cong 0 \qquad C_{W\cdot S} = \frac{C_W C_v}{K_{DW}} \qquad (1.16)$$

From (1.11)

$$-r_{DB} = k_{DB}\left(C_{E\cdot S} - \frac{C_E C_v}{K_{DB}}\right)$$

Substitute (1.13), (1.14), (1.16) and (1.26) into (1.11) to obtain

$$-r_{DB} = k_{DB}\left(\frac{K_S K_{AB} K_{AM} K_{DW} C_M C_A}{C_W} - \frac{C_E}{K_{DB}}\right) C_v \qquad (1.35)$$

From (1.17)

$$C_v = 1 + K_{AB} C_A + K_{AM} C_M + \frac{K_S K_{AB} K_{AM} K_{DW} C_A C_M}{C_W} + \frac{C_W}{K_{DW}} \qquad (1.36)$$

Substitute (1.35) into (1.36)

$$-r_{DB} = \frac{K_1\left(\frac{K_S K_{AB} K_{AM} K_{DW} C_M C_A}{C_W} - \frac{C_E}{K_{DB}}\right)}{1 + K_{AB} C_A + K_{AM} C_M + \frac{K_S K_{AB} K_{AM} K_{DW} C_A C_M}{C_W} + \frac{C_W}{K_{DW}}} \qquad (1.37)$$

Substitute (1.21) to (1.24) into (1.37) and simplify to obtain

$$rate = \frac{K_1\left(K_S K_{AB} K_{AM} K_{DW} C_{A_0}(100-X)(1-X) - \frac{C_{A_0} X^2}{K_{DB}}\right)}{X + K_{AB} C_{A_0} X(1-X) + K_{AM} C_{A_0} X(100-X) + K_S K_{AB} K_{AM} K_{DW} C_{A_0}(1-X)(100-X) + \frac{C_{A_0} X^2}{K_{DW}}} \qquad (1.38)$$

(E) Desorption of water is the rate-determining step. The $k_{AB}, k_{AM}, k_S, k_{DB}$ are large by comparison, and we can set.

$$-\frac{r_{AB}}{k_{AB}} \cong 0 \qquad C_{A\cdot S} = K_{AB} C_A C_v \qquad (1.13)$$

$$-\frac{r_{AM}}{k_{AM}} \cong 0 \qquad C_{M\cdot S} = K_{AM} C_M C_v \qquad (1.14)$$

$$-\frac{r_S}{k_S} \cong 0 \qquad C_{W\cdot S} = \frac{K_S C_{A\cdot S} C_{M\cdot S}}{C_{E\cdot S}} \qquad (1.15)$$

$$-\frac{r_{DB}}{k_{DB}} \cong 0 \qquad C_{E\cdot S} = \frac{C_E C_v}{K_{DB}} \qquad (1.16)$$

From (1.12)

$$-r_{DW} = k_{DW}\left(\frac{K_S K_{AB} K_{DB} K_{AM} C_A C_M}{C_E} - \frac{C_W}{K_{DW}}\right) C_v \qquad (1.39)$$

From (1.17)

$$C_v = \frac{C_T}{1 + K_{AB} C_A + K_{AM} C_M + \frac{C_E}{K_{DB}} + \frac{K_S K_{AB} K_{AM} K_{DB} C_M C_A}{C_E}} \qquad (1.40)$$

Substitute (1.40) to (1.39)

$$-r_{DW} = \frac{K_1\left(\frac{K_S K_{AB} K_{DB} K_{AM} C_A C_M}{C_E} - \frac{C_W}{K_{DW}}\right)}{1 + K_{AB} C_A + K_{AM} C_M + \frac{C_E}{K_{DB}} + \frac{K_S K_{AB} K_{AM} K_{DB} C_M C_A}{C_E}} \qquad (1.41)$$

Substitute (1.21) to (1.24) into (1.41) and simplify to obtain

$$rate = \frac{K_1\left(K_S K_{AB} K_{DB} K_{AM} C_{A_0}(1-X)(100-X) - \frac{C_{A_0} X^2}{K_{DW}}\right)}{X + K_{AB} C_{A_0} X(1-X) + K_{AM} C_{A_0} X^2 + \frac{C_{A_0} X^2}{K_{DB}} + K_S K_{AB} K_{AM} K_{DB} C_{A_0}(100-X)(1-X)} \qquad (1.42)$$

(II) Eley-Rideal model

In this model, the mechanism is for the reaction between an adsorbed molecule and a molecule in the fluid phase. There are two major models in this work. The first model assumes that palmitic acid is an adsorbed molecule. The second model assumes that methanol is an adsorbed molecule.

(A) Palmitic acid is an adsorbed molecule

$A + S \overset{k_{AB}, k_{-AB}}{\Longleftrightarrow} A \cdot S$ -Adsorption of palmitic acid (1.43)

$A \cdot S + M \overset{k_S, k_{-S}}{\Longleftrightarrow} E \cdot S + W$ -Adsorbed palmitic acid with methanol (1.44)

$E \cdot S \overset{k_{DB}\, k_{-DB}}{\Longleftrightarrow} E + S$ -Desorption of ester (1.45)

$-r_{AB} = k_{AB}\left(C_A C_v - \left(\frac{C_{A\cdot S}}{K_{AB}}\right)\right); K_{AB} = \frac{k_{AB}}{k_{-AB}}$ -Adsorption of palmitic acid (1.46)

$-r_S = k_S\left(C_{A\cdot S} C_M - \left(\frac{C_{E\cdot S} C_W}{K_S}\right)\right); K_S = \frac{k_S}{k_{-S}}$ -Adsorbed palmitic acid with methanol (1.47)

$-r_{DB} = k_{DB}\left(C_{E\cdot S} - \left(\frac{C_E C_v}{K_{DB}}\right)\right); K_{DB} = \frac{k_{DB}}{k_{-DB}}$ -Desorption of ester (1.48)

$C_T = C_v + C_{A\cdot S} + C_{E\cdot S}$ -Total site equation (1.49)

◊ Adsorption of palmitic acid is a rate-determining step. The k_S and k_{DB} are large by comparison, and we can set.

$$-\frac{r_S}{k_S} \cong 0 \qquad C_{A\cdot S} = \frac{C_{E\cdot S} C_W}{K_S C_M} \qquad (1.50)$$

$$-\frac{r_{DB}}{k_{DB}} \cong 0 \qquad C_{E\cdot S} = \frac{C_E C_v}{K_{DB}} \qquad (1.51)$$

From (1.46)

$$-r_{AB} = k_{AB}\left(C_A C_v - \left(\frac{C_{A\cdot S}}{K_{AB}}\right)\right)$$

Substitute (1.50) and (1.51) into (1.46)

$$-r_{AB} = k_{AB}\left(C_A - \left(\frac{C_E C_W}{K_{DB} K_S C_M K_{AB}}\right)\right) C_v \qquad (1.52)$$

From (1.49)

$$C_v = \frac{C_T}{1+\frac{C_W C_E}{K_{DB} K_S C_M}+\frac{C_E}{K_{DB}}} \qquad (1.53)$$

Substitute (1.53) into (1.52)

$$-r_{AB} = \frac{K_1\left(C_A-\left(\frac{C_E C_W}{K_{DB} K_S C_M K_{AB}}\right)\right)}{1+\frac{C_W C_E}{K_{DB} K_S C_M}+\frac{C_E}{K_{DB}}} \qquad (1.54)$$

Substitute (1.51) to (1.24) into (1.54)

$$rate = \frac{K_1\left(C_{A_0}(1-X)-\left(\frac{C_{A_0}X^2}{K_{DB}K_S K_{AB}(100-X)}\right)\right)}{1+\frac{C_{A_0}X^2}{K_{DB}K_S(100-X)}+\frac{C_{A_0}X}{K_{DB}}} \quad (1.55)$$

◊ Reaction of methanol with palmitic acid is a rate-determining step. The k_{AB} and k_{DB} are large, and we can set.

$$-\frac{r_{AB}}{k_{AB}} \cong 0 \qquad C_{A\cdot S} = K_{AB}C_A C_v \quad (1.56)$$

$$-\frac{r_{DB}}{k_{DB}} \cong 0 \qquad C_{E\cdot S} = \frac{C_E C_v}{K_{DB}} \quad (1.51)$$

From (1.47)

$$-r_S = k_S\left(C_{A\cdot S}C_M - \left(\frac{C_{E\cdot S}C_W}{K_S}\right)\right)$$

Substitute (1.51) and (1.56) into (1.47)

$$-r_S = k_S\left(K_{AB}C_A C_M - \left(\frac{C_W C_E}{K_{DB}K_S}\right)\right)C_v \quad (1.57)$$

From (1.49)

$$C_v = \frac{C_T}{1+K_{AB}C_A+\frac{C_E}{K_{DB}}} \quad (1.58)$$

Substitute (1.58) into (1.57)

$$-r_S = \frac{K_1\left(K_{AB}\,C_A C_M - \left(\frac{C_W C_E}{K_{DB}\,K_S}\right)\right)}{1+K_{AB}\,C_A + \frac{C_E}{K_{DB}}} \qquad (1.59)$$

Substitute (1.21) to (1.24) into (1.59)

$$-r_S = \frac{K_1\left(K_{AB}\,{C_{A_0}}^2(1-X)(100-X) - \left(\frac{{C_{A_0}}^2 X^2}{K_{DB}\,K_S}\right)\right)}{1+K_{AB}\,C_{A_0}(1-X) + \frac{C_{A_0}X}{K_{DB}}} \qquad (1.60)$$

◊ Desorption of ester is a rate-determining step. The k_{AB} and $k_S$are large by comparison, and we can set.

$$-\frac{r_{AB}}{k_{AB}} \cong 0 \qquad C_{A\cdot S} = K_{AB} C_A C_v \qquad (1.56)$$

$$-\frac{r_S}{k_S} \cong 0 \qquad C_{A\cdot S} = \frac{C_{E\cdot S} C_W}{K_S C_M};\ C_{E\cdot S} = \frac{K_S C_M C_{A\cdot S}}{C_W} \qquad (1.50)$$

From (1.48)

$$-r_{DB} = k_{DB}\left(C_{E\cdot S} - \left(\frac{C_E C_v}{K_{DB}}\right)\right)$$

$$-r_{DB} = k_{DB}\left(\frac{K_S C_M K_{AB} C_A}{C_W} - \left(\frac{C_E}{K_{DB}}\right)\right) C_v \qquad (1.61)$$

From (1.49)

$$C_v = \frac{C_T}{1+K_{AB}\,C_A + \frac{K_S K_{AB} C_M C_A}{C_W}} \qquad (1.62)$$

Substitute (1.61) into (1.62)

$$-r_{DB} = \frac{K_1\left(\frac{K_S K_{AB} C_M C_A}{C_W} - \left(\frac{C_E}{K_{DB}}\right)\right)}{1 + K_{AB} C_A + \frac{K_S K_{AB} C_M C_A}{C_W}} \quad (1.63)$$

Substitute (1.21) to (1.24) into (1.63)

$$-r_{DB} = \frac{K_1\left(\frac{K_{AB} K_S C_{A_0}(1-X)(100-X)}{X} - \left(\frac{C_{A_0} X}{K_{DB}}\right)\right)}{1 + K_{AB} C_{A_0}(1-X) + \frac{K_S K_{AB} C_{A_0}(1-X)(100-X)}{X}} \quad (1.64)$$

Simplify to obtain

$$rate = \frac{K_1\left(K_{AB} K_S C_{A_0}(1-X)(100-X) - \left(\frac{C_{A_0} X^2}{K_{DB}}\right)\right)}{X + K_{AB} C_{A_0} X(1-X) + K_S K_{AB} C_{A_0}(1-X)(100-X)} \quad (1.65)$$

(B) Methanol is an adsorbed molecule

$M + S \overset{k_{AM}, k_{-AM}}{\Longleftrightarrow} M \cdot S$ -Adsorption of methanol (1.66)

$M \cdot S + A \overset{k_S, k_{-S}}{\Longleftrightarrow} W \cdot S + E$ -Adsorbed methanol with palmitic acid (1.67)

$W \cdot S \overset{k_{DW}\, k_{-DW}}{\Longleftrightarrow} W + S$ -Desorption of water (1.68)

$-r_{AM} = k_{AM}\left(C_M C_v - \frac{C_{M \cdot S}}{K_{AM}}\right); K_{AM} = \frac{k_{AM}}{k_{-AM}}$ -Adsorption of methanol (1.69)

$-r_S = k_S\left(C_{M \cdot S} C_A - \frac{C_{W \cdot S} C_E}{K_S}\right); K_S = \frac{k_S}{k_{-S}}$ -Reaction of adsorbed methanol with palmitic acid (1.70)

$$-r_{DW} = k_{DW}\left(C_{W\cdot S} - \frac{C_W C_v}{K_{DW}}\right); K_{DW} = \frac{k_{DW}}{k_{-DW}}$$ -Desorption of water (1.71)

$$C_T = C_v + C_{M\cdot S} + C_{W\cdot S}$$ -Total site equation (1.72)

◊ Adsorption of methanol is a rate-determining step. The k_S and k_{DW} are large by comparison, and we can set.

$$-\frac{r_S}{k_S} \cong 0 \qquad C_{M\cdot S} = \frac{C_{W\cdot S} C_E}{K_S C_A}$$ (1.73)

$$-\frac{r_{DW}}{k_{DW}} \cong 0 \qquad C_{W\cdot S} = \frac{C_W C_v}{K_{DW}}$$ (1.74)

From (1.69)

$$-r_{AM} = k_{AM}\left(C_M C_v - \frac{C_{M\cdot S}}{K_{AM}}\right)$$

Substitute (1.73) and (1.74) into (1.69)

$$-r_{AM} = k_{AM}\left(C_M - \frac{C_W C_E}{K_{DW} K_S K_{AM} C_A}\right) C_v$$ (1.74)

From (1.72)

$$C_v = \frac{C_T}{1 + \frac{C_W C_E}{K_{DW} K_S C_A} + \frac{C_E}{K_{DW}}}$$ (1.75)

Substitute (1.75) into (1.74)

$$-r_{AM} = \frac{K_1\left(C_M - \frac{C_W C_E}{K_{DW} K_S K_{AM} C_A}\right)}{1 + \frac{C_W C_E}{K_{DW} K_S C_A} + \frac{C_E}{K_{DW}}}$$ (1.76)

Substitute (1.61) to (1.64) into (1.76)

$$rate = \frac{K_1\left(C_{A_0}(100-X)-\frac{C_{A_0}X^2}{K_{DW}K_S K_{AM}}\right)}{1+\frac{C_{A_0}X^2}{K_{DW}K_S(1-X)}+\frac{C_{A_0}X}{K_{DW}}} \qquad (1.77)$$

◊ Reaction is a rate-determining step. The k_{AM} and k_{DW} are large by comparison, and we can set.

$$-\frac{r_{AM}}{k_{AM}} \cong 0 \qquad C_{M\cdot S} = K_{AM}C_M C_v \qquad (1.78)$$

$$-\frac{r_{DW}}{k_{DW}} \cong 0 \qquad C_{W\cdot S} = \frac{C_W C_v}{K_{DW}} \qquad (1.74)$$

From (1.70)

$$-r_S = k_S\left(C_{M\cdot S}C_A - \frac{C_{W\cdot S}C_E}{K_S}\right)$$

$$-r_S = k_S\left(K_{AM}C_M C_A - \frac{C_E C_W}{K_{DW}K_S}\right)C_v \qquad (1.79)$$

From (1.72)

$$C_v = \frac{C_T}{1+K_{AM}C_M+\frac{C_W}{K_{DW}}} \qquad (1.80)$$

Substitute (1.80) into (1.79)

$$-r_S = \frac{K_1\left(K_{AM}C_M C_A-\frac{C_E C_W}{K_{DW}K_S}\right)}{1+K_{AM}C_M+\frac{C_W}{K_{DW}}} \qquad (1.81)$$

Substitute (1.21) to (1.24) into (1.81)

$$rate = \frac{K_1\left(K_{AM}\,{C_{A_0}}^2(100-X)(1-X)-\frac{{C_{A_0}}^2X^2}{K_{DW}\,K_S}\right)}{1+K_{AM}\,C_{A_0}(100-X)+\frac{C_{A_0}X}{K_{DW}}} \qquad (1.82)$$

◊ Desorption of water is a rate-determining step. The k_{AM} and k_S are large by comparison, and we can set

$$-\frac{r_{AM}}{k_{AM}} \cong 0 \qquad C_{M\cdot S} = K_{AM} C_M C_v \qquad (1.78)$$

$$-\frac{r_S}{k_S} \cong 0 \qquad C_{M\cdot S} = \frac{C_{W\cdot S} C_E}{K_S C_A}\,; C_{W\cdot S} = \frac{K_S C_A C_{M\cdot S}}{C_E} \qquad (1.73)$$

From (1.71)

$$-r_{DW} = k_{DW}\left(C_{W\cdot S} - \frac{C_W C_v}{K_{DW}}\right)$$

$$-r_{DW} = k_{DW}\left(\frac{K_{AM} K_S C_M C_A}{C_E} - \frac{C_W}{K_{DW}}\right) C_v \qquad (1.83)$$

From (1.80)

$$C_v = \frac{C_T}{1+K_{AM} C_M + \frac{K_{AM} K_S C_M C_A}{C_E}} \qquad (1.84)$$

Substitute (1.84) into (1.83)

$$-r_{DW} = \frac{K_1\left(\frac{K_{AM} K_S C_M C_A}{C_E} - \frac{C_W}{K_{DW}}\right)}{1+K_{AM} C_M + \frac{K_{AM} K_S C_M C_A}{C_E}} \qquad (1.85)$$

Substitute (1.21) to (1.24) into (1.85)

$$-r_{DW} = \frac{K_1\left(\frac{K_S K_{AM} C_{A_0}(100-X)(1-X)}{X} - \frac{C_{A_0}X}{K_{DW}}\right)}{1+K_{AM} C_{A_0}(100-X)+\frac{K_S K_{AM} C_{A_0}(100-X)(1-X)}{X}} \qquad (1.86)$$

Multiply $\frac{X}{X}$ to (1.86)

$$-r_{DW} = \frac{K_1\left(K_S K_{AM} C_{A_0}(100-X)(1-X) - \frac{C_{A_0} X^2}{K_{DW}}\right)}{X + K_{AM} C_{A_0} X(100-X) + K_S K_{AM} C_{A_0}(100-X)(1-X)} \quad (1.87)$$

(2) Model for reactor

In the experiment, the batch reactor was used. The equation of the batch reactor was derived as (Fogler,2006).

$$\frac{dN_A}{dt} = \int^{V} r_A dV \quad (1.88)$$

Assume that the reaction mixture is perfectly mixed so that there is no variation in the rate of reaction throughout the reactor volume. Therefore, we can take r_A out of the integral. The reaction is also in the liquid phase, and the volume is constant. Therefore, the eq. (1.3.1.II-1) can be transformed into the following equation:

$$\frac{dN_A}{dt} = r_A V \quad (1.89)$$

Divided by V

$$\frac{dC_A}{dt} = r_A \quad (1.90)$$

From (1.21)

$$C_A = C_{A_0}(1 - X)$$

The (1.90) can be transformed into

$$C_A \frac{dX}{dt} = -r_A \qquad (1.91)$$

We substituted the entire rate law model into (1.91). Then, we tested the models with the reaction rates from the experiment.

1.2.2. Stochastic Simulation Models

Computer simulations can be vital in investigating a chemical reaction. The simulation can aid in the exploration of complex dynamics of reaction. There are two main approaches in computer simulation, namely deterministic and stochastic(Mira, et al.,2003). The deterministic approach uses a set of differential and/or algebraic equations to explain the time dependence of the concentrations in the chemical system.

In the stochastic approach, we assume that each reaction proceeds independently and randomly and can occur with a certain probability associated with the thermodynamic properties of the reacting molecules. The stochastic chemical kinetics describes interactions involving a discrete number of molecules. The stochastic algorithm is appropriate when the number of molecules in a system is small. In a given initial number of molecules, there are many possible time evolutions, each of which has their

own probability. The summation of all the probabilities has to add up to one.

There is a link between deterministic and stochastic simulation. The reaction rate constants of the deterministic simulation can be interpreted in terms of probabilities in the stochastic simulation. The differential equations in the deterministic simulation are similar to the stochastic approach.

(1) Stochastic approach

The nature of chemical reactions is stochastic (de Levie,2000). Each reaction is a discrete event that takes place with a given probability. An aspect of this simulation is that it can determine whether a proposed reaction mechanism is consistent with the observed result. The stochastic algorithm is as follows (Gillespie,2007):

Notation

- $P_0(\tau|x,t)$ is the probability that no reaction will occur in the time interval $[t,t+\tau)$.
- $p(\tau,j|x,t)d\tau$ is the probability that the next reaction will be j^{th} reaction and occur during the time interval $[t+\tau,t+\tau+d\tau)$.

- X(t)=x is a number of molecules of any species.
- $a_j(X(t))$is a propensity function of j^{th}reaction.
- $\nu_j$is a state-change vector of j^{th}reaction.
- $c_j$is a reaction rate constant of j^{th}reaction.

If the time of the reaction is very small, the assumption is that what happens over $[t, t+\tau)$ is independent of what happens over $[t+\tau, t+\tau+d\tau)$.

$$P_0(\tau + d\tau|x,t) = P_0(\tau|x,t) \cup P_0(\tau|x,t+\tau)d\tau$$

$$= P_0(\tau|x,t) \times P_0(\tau|x,t+\tau)d\tau$$

$$= P_0(\tau|x,t) \times (1 - \sum p(\tau,j|x,t)\, d\tau) \qquad (1.92)$$

From the definition of the propensity function

$$P_0(\tau + d\tau|x,t) = P_0(\tau|x,t)(1 - \sum_{k=1}^{M} a_k(x)d\tau) \qquad (1.93)$$

From the proof in (Higham,2008)

$$p(\tau,j|x,t) = \frac{a_j(x)}{a_{sum}\,(x)}\left(a_{sum}\,(x)e^{-a_{sum}\,(x)\tau}\right) \qquad (1.94)$$

$\frac{a_j(x)}{a_{sum}\,(x)}$ is the next reaction index which corresponds to a discrete random variable that controls the chance of picking the j^{th} reaction while $a_{sum}\,(x)e^{-a_{sum}\,(x)\tau}$ is the time until the next

reaction and is the density function for a continuous random variable with an exponential distribution.

Assuming good mixing and negligible surface diffusion, the resulting algorithm can be summarized in the following pseudo code:

Step 1: Evaluate $\{a_k(X(t))\}_{k=1}^{M}$ and $a_{sum}(X(t)) \coloneqq \sum_{k=1}^{M} a_k(X(t))$.

Step 2: Draw two independent uniform (0,1) random numbers, ξ_1 and ξ_2

Step 3: Set j to be the smallest integer satisfying

$$\sum_{k=1}^{j} a_k\big(X(t)\big) > \xi_1 a_{sum}(X(t)).$$

Step 4: Set $\tau = \frac{ln(\frac{1}{\xi_2})}{a_{sum}(X(t))}$

Step 5: Set $X(t+\tau) = X(t) + \nu_j$

Return to step 1

(2) SO_4/ZrO_2-550°C stochastic simulation

There are six sub-chemical reactions that occur during the esterification of palmitic acid over SO_4/ZrO_2-550°C. The solution contains seven species and X_n represents the n^{th} species. The six sub-reactions are illustrated below:

$$X_1 + X_2 \xrightarrow{C_1} X_3 \quad (1) \quad a_1 = C_1 X_1 X_2 \quad (1.95)$$

$$X_3 \xrightarrow{C_2} X_1 + X_2 \quad (2) \quad a_2 = C_2 X_2 \quad (1.96)$$

$$X_3 + X_4 \xrightarrow{C_3} X_5 + X_6 \quad (3) \quad a_3 = C_3 X_3 X_4 \quad (1.97)$$

$$X_5 + X_6 \xrightarrow{C_4} X_3 + X_4 \quad (4) \quad a_4 = C_4 X_5 X_6 \quad (1.98)$$

$$X_5 \xrightarrow{C_5} X_7 + X_2 \quad (5) \quad a_5 = C_5 X_5 \quad (1.99)$$

$$X_2 + X_7 \xrightarrow{C_6} X_5 \quad (6) \quad a_6 = C_6 X_2 X_7 \quad (1.100)$$

Here,

- X_1 is palmitic acid
- X_2 is a vacant site on the catalyst
- X_3 is palmitic acid attached to the catalyst
- X_4 is the methanol
- X_5 is palmitic acid methyl ester attached to the catalyst
- X_6 is water
- X_7 is palmitic acid methyl ester

In step 5, the state vectors (ν_j) of reactions 1 to 6 are:

$$\nu_1 = \begin{bmatrix} -1 \\ -1 \\ 1 \\ 0 \\ 0 \\ 0 \\ 0 \end{bmatrix} \nu_2 = \begin{bmatrix} 1 \\ 1 \\ -1 \\ 0 \\ 0 \\ 0 \\ 0 \end{bmatrix} \nu_3 = \begin{bmatrix} 0 \\ 0 \\ -1 \\ -1 \\ 1 \\ 1 \\ 0 \end{bmatrix} \nu_4 = \begin{bmatrix} 0 \\ 0 \\ 1 \\ 1 \\ -1 \\ -1 \\ 0 \end{bmatrix} \nu_5 = \begin{bmatrix} 0 \\ 1 \\ 0 \\ 0 \\ -1 \\ 0 \\ 1 \end{bmatrix} \nu_6 = \begin{bmatrix} 0 \\ -1 \\ 0 \\ 0 \\ 1 \\ 0 \\ -1 \end{bmatrix}$$

There is a link between deterministic and stochastic simulation. The rate constant (C_j) for stochastic simulation can be calculated from kinetic parameters (k_j) in the deterministic simulation as illustrated below:

$$C_1 = \frac{k_1}{n_A vol},\ C_2 = k_2,\ C_3 = \frac{k_3}{n_A vol},\ C_4 = \frac{k_4}{n_A vol},\ C_5 = k_5,\ C_6 = \frac{k_6}{n_A vol}$$

In addition $K_{AM} = \frac{k_1}{k_2},\ K_S = \frac{k_3}{k_4}$ and $K_{DB} = \frac{k_5}{k_6}$

(3) $AcAl_2O_3$ stochastic simulation

There are six sub-chemical reactions that occur during the esterification of palmitic acid over $AcAl_2O_3$. The solution contains seven species and X_n represents the n^{th} species. The six sub reactions are illustrated below:

$$X_1 + X_2 \xrightarrow{C_1} X_3 \qquad (1) \quad a_1 = C_1 X_1 X_2 \qquad (1.101)$$

$$X_3 \xrightarrow{C_2} X_1 + X_2 \qquad (2) \quad a_2 = C_2 X_2 \qquad (1.102)$$

$$X_3 + X_4 \xrightarrow{C_3} X_5 + X_6 \qquad (3) \quad a_3 = C_3 X_3 X_4 \qquad (1.103)$$

$$X_5 + X_6 \xrightarrow{C_4} X_3 + X_4 \qquad (4) \quad a_4 = C_4 X_5 X_6 \qquad (1.104)$$

$$X_5 \xrightarrow{C_5} X_7 + X_2 \qquad (5) \quad a_5 = C_5 X_5 \qquad (1.105)$$

$$X_2 + X_7 \xrightarrow{C_6} X_5 \qquad (6) \quad a_6 = C_6 X_2 X_7 \qquad (1.106)$$

Here,

- X_1 is methanol
- X_2 is vacant site of the catalyst
- X_3 is methanol attached on catalyst
- X_4 is pal mitic acid
- X_5 is palmitic acid methyl ester and methanol intermediate adsorbed on the catalyst
- X_6 is palmitic acid methyl ester
- X_7 is water

The rate constant (C_j) for stochastic simulation can be calculated from kinetic parameters (k_j) in the deterministic simulation as illustrated below:

$$C_1 = \frac{k_1}{n_A vol}, \quad C_2 = k_2, C_3 = \frac{k_3}{n_A vol}, C_4 = \frac{k_4}{n_A vol}, \quad C_5 = k_5, \quad C_6 = \frac{k_6}{n_A vol}$$

In addition $K_{AM} = \frac{k_1}{k_2}$, $K_S = \frac{k_3}{k_4}$ and $K_{DB} = \frac{k_5}{k_6}$

1.3. Result, discussion, and conclusion

1.3.1. SO_4/ZrO_2-550°C kinetic mechanisms

After testing all the models, the Eley-Rideal mechanism, which assumed that the surface reaction between adsorbed palmitic acid and methanol in the bulk fluid was the rate-determining step, was fitted to the experimental data. The mechanism consisted of three elementary reactions as described below:

$$A + S \overset{K_A}{\Leftrightarrow} A \cdot S \tag{1.43}$$

$$A \cdot S + M \overset{K_S}{\Leftrightarrow} E \cdot S + W \tag{1.44}$$

$$E \cdot S \overset{K_{DB}}{\Longleftrightarrow} E + S \tag{1.45}$$

Here, A is palmitic acid, S is an active site on the surface, M is methanol, W is water, E is palmitic methyl ester, and $A \cdot S$ and $E \cdot S$ are adsorbed intermediates. The kinetic model was built based on following assumptions:

(1) The surface reaction was the rate-determining step.

(2) The adsorption and desorption of reactants and products are fast and at equilibrium.

(3) The rate of the non-catalyzed reactions compared to the catalyzed reactions can be neglected.

(4) The diffusion rate of the product and reactant from the catalyst surface is fast and can be neglected.

(5) There are no differences in the activity and accessibility of sites on the catalyst surface.

(6) There are no palmitic methyl ester and water before the reaction.

Based on the assumptions above, the following kinetic rate law is derived:

$$rate = \frac{K_1\left(K_{AB}\,C_A C_M - \left(\frac{C_W C_E}{K_{DB}\,K_S}\right)\right)}{1+K_{AB}\,C_A + \frac{C_E}{K_{DB}}} \tag{1.59}$$

Here, K_S, K_{AB}, and K_D represent the equilibrium constants of the surface reaction, adsorption of palmitic acid, and desorption of palmitic methyl ester respectively. In the equation $K_1 = C_T k_s$, k_s is the forward reaction rate constant.

The concentration of the reactants and products can be expressed as

$$C_A = C_{A_0}(1 - X) \tag{1.21}$$

$$C_M = C_{A_0}(100 - X) \tag{1.22}$$

$$C_E = C_{A_0}X \tag{1.23}$$

$$C_W = C_{A_0}X \tag{1.24}$$

Therefore, the equation can be expressed as:

$$rate = \frac{K_1\left(K_{AB}\,{C_{A_0}}^2(1-X)(100-X) - \left(\frac{{C_{A_0}}^2X^2}{K_{DB}\,K_S}\right)\right)}{1+K_{AB}\,C_{A_0}(1-X)+\frac{C_{A_0}X}{K_{DB}}} \tag{1.60}$$

The result of this model against experimental data is shown in Figure 1.5.

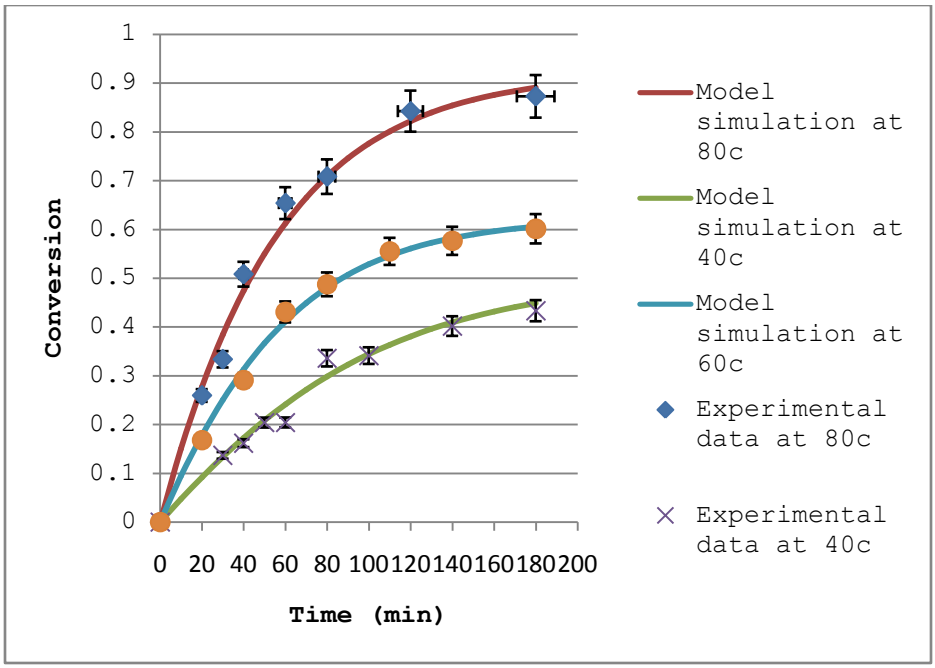

Figure 1.5 Fitting of Eley-Rideal model to experimental data for palmitic acid esterification over SO_4/ZrO_2-550°C at 40, 60 and 80°C

The coefficients of determination of the deterministic model were 0.98, 0.99, and 0.99 for SO_4/ZrO_2-550°C at 40, 60, and 80°C. Therefore, the esterification of palmitic acid over SO_4/ZrO_2-550°C obeys the Eley-Rideal mechanism. The reaction of adsorbed palmitic acid with methanol in the bulk fluid is the rate-determining step for SO_4/ZrO_2-550°C.

Table 1.3 Kinetic parameters of palmitic acid esterification on SO_4/ZrO_2-550°C

Temp (°C)	$K_1 \times 10^{-4}$	$K_{AB} \times 10^{-2}$	K_{DB}	$K_S \times 10^{-3}$
40	3.78	59.75	2.01	4.21
60	16.12	26.74	2.01	19.38
80	51.10	13.38	9.08	92.41

Table 1.3 shows the kinetic parameter of palmitic acid esterification on SO_4/ZrO_2-550℃ from stochastic model.

The plausible esterification mechanism for palmitic acid (with SO_4/ZrO_2-550°C), is shown in Figure 1.6. Firstly, palmitic acid is adsorbed on an active site of SO_4/ZrO_2-550°C. Next, palmitic acid on an active site reacts with methanol through esterification reaction. The reaction results in forming ester (palmetate) and water. Finally, the palmetate is desorbed from the catalyst.

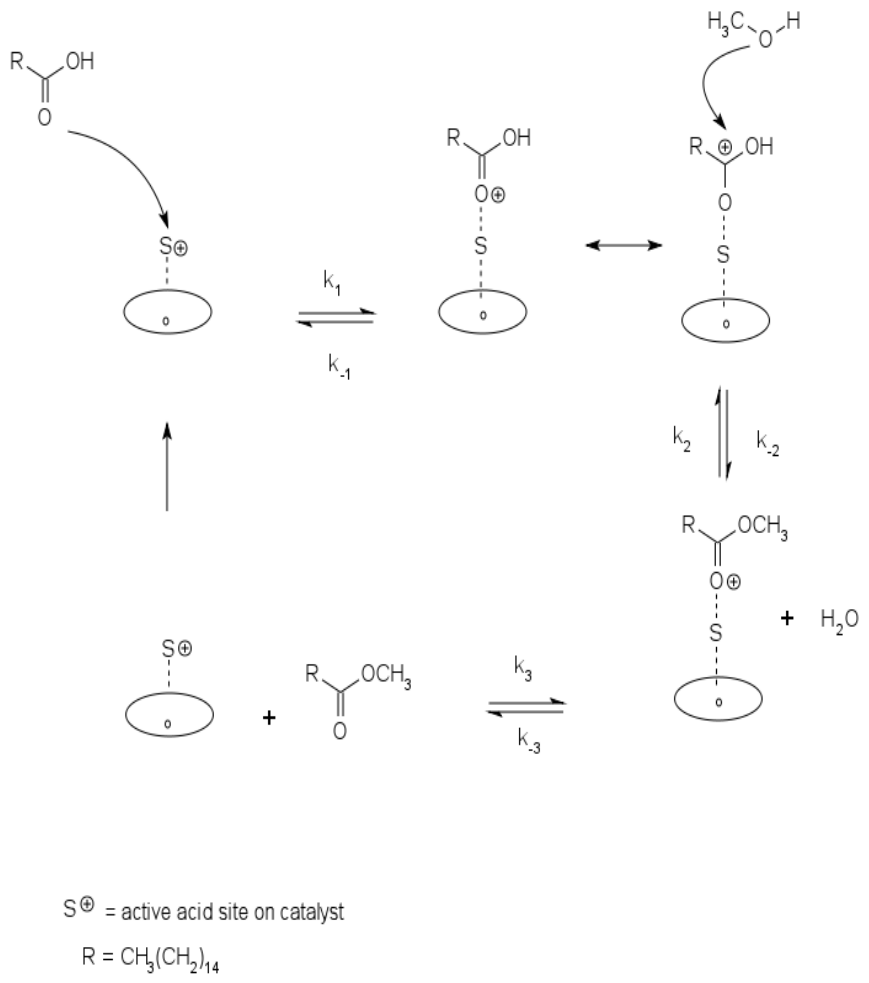

Figure 1.6 Illustration of palmitic acid esterification over SO_4/ZrO_2-550°C

1.3.2. $AcAl_2O_3$ kinetic model

After testing our earlier derived models, the Eley-Rideal mechanism, which assumed that methanol adsorption on the surface was the rate-determining step for $AcAl_2O_3$, was fitted to the

experimental data. The mechanisms consisted of three elementary reactions as described below:

$$M + S \overset{K_{AM}}{\Longleftrightarrow} M \cdot S \tag{1.66}$$

$$M \cdot S + A \overset{K_S}{\Leftrightarrow} W \cdot S + E \tag{1.67}$$

$$W \cdot S \overset{K_{DW}}{\Longleftrightarrow} W + S \tag{1.68}$$

Where M is methanol, S is an active site, A is palmitic acid, W is water, E is palmitic acid methyl ester, and $M \cdot S$ and $W \cdot S$ are surface intermediates. The kinetic model was built based on similar assumptions as in SO_4/ZrO_2-550°C The following kinetic rate law was derived:

$$rate = \frac{K_1\left(C_M - \frac{C_W C_E}{K_{DW} K_S K_{AM} C_A}\right)}{1 + \frac{C_W C_E}{K_{DW} K_S C_A} + \frac{C_E}{K_{DW}}} \tag{1.76}$$

Here, K_S, K_{AM}, and K_D represent the equilibrium constants of the surface reaction, adsorption of palmitic acid, desorption of palmitic acid methyl ester respectively. In the equation $K_1 = C_T k_{AM}$, k_{AM} is the forward rate constant of adsorption of methanol.

The concentration of the reactants and products can be expressed as:

$$C_A = C_{A_0}(1 - X) \tag{1.21}$$

$$C_M = C_{A_0}(100 - X) \tag{1.22}$$

$$C_E = C_{A_0}X \tag{1.23}$$

$$C_W = C_{A_0}X \tag{1.24}$$

Therefore, the equation can be expressed as:

$$rate = \frac{K_1\left(C_{A_0}(100-X) - \frac{{C_{A_0}X}^2}{K_{DW}K_S K_{AM}}\right)}{1 + \frac{{C_{A_0}X}^2}{K_{DW}K_S(1-X)} + \frac{C_{A_0}X}{K_{DW}}} \tag{1.77}$$

The result of this model against experimental data is shown in Figure 1.7.

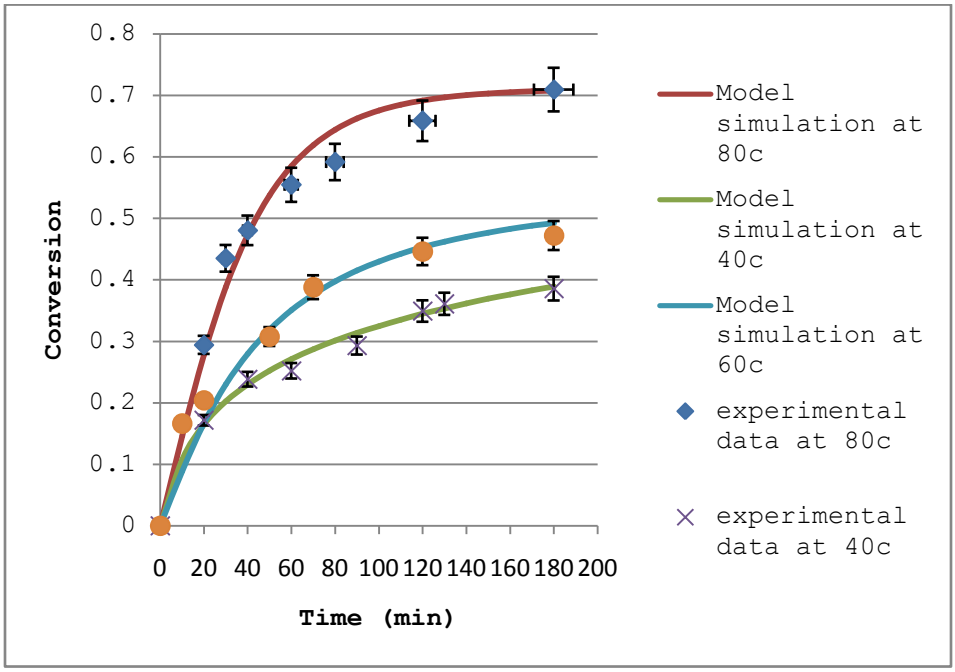

Figure 1.7 Fitting of Eley-Rideal model to experimental data for palmitic acid esterification over $AcAl_2O_3$ at 40, 60 and 80°C

The coefficients of determination of the deterministic model were 0.99, 0.98, and 0.96 for $AcAl_2O_3$ at 40, 60, and 80°C. Therefore, the esterification of palmitic acid with methanol on $AcAl_2O_3$ follows the Eley-Rideal mechanism. The adsorption of methanol on an active site on the catalyst was the rate-determining step in $AcAl_2O_3$. The kinetic parameters are shown in Table 1.4.

Table 1.4 Kinetic parameters of palmitic acid esterification on $AcAl_2O_3$

Temp (°C)	$K_1 \times 10^{-4}$	K_{AM}	K_{DB}	$K_S \times 10^{-1}$
40	1.36	2.01	2.17	0.02
60	0.91	0.14	2.01	0.21
80	1.50	0.08	2.01	1.14

The esterification mechanisms of palmitic acid, catalyzed by $AcAl_2O_3$ are shown in Figure 1.8. Firstly, methanol is adsorbed on an active site of $AcAl_2O_3$. Next, the methanol on active site reacts with palmitic acid through esterification reaction. The reaction result in forming of palmetate and water. Finally, water is desorbed from the active site.

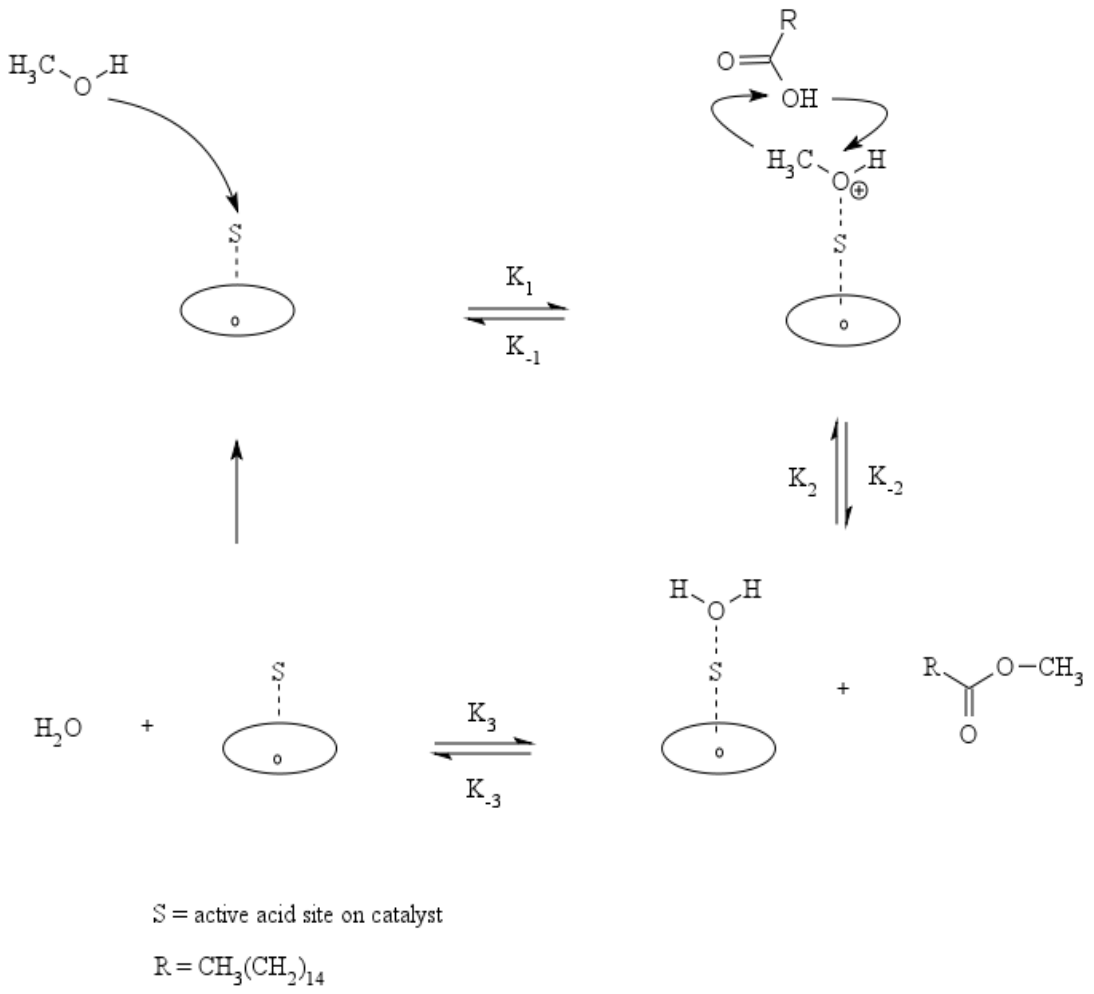

Figure 1.8 Illustration of palmitic acid esterification over $AcAl_2O_3$

1.3.3. Determined the heat of the reaction on both catalysts

To evaluate the efficiency of the catalysts, the activation energies were determined. The reaction rate constant is related to the reaction temperature through the Arrhenius equation. Therefore, the overall reaction heat of the reaction can be

calculated from equation below using the reaction rate constant K_S:

$$K_S = Aexp\left(-\frac{\Delta E}{RT}\right) \quad (1.107)$$

Both the frequency factor A and the heat of the reactionEa were obtain by plotting $ln(K_S)$ against $^1/_T$. The heat of the reaction of palmitic acid esterification was 70.81 kJ/mol and 93.71 KJ/mol for SO_4/ZrO_2-550°C and $AcAl_2O_3$ respectively.

1.3.4. Predicted conversion using the deterministic model

In order to validate the models, we used them to predict the percent conversion at 210 minutes and 240 minutes at all temperatures for all catalysts. We then compared the predicted values with actual experimental data.

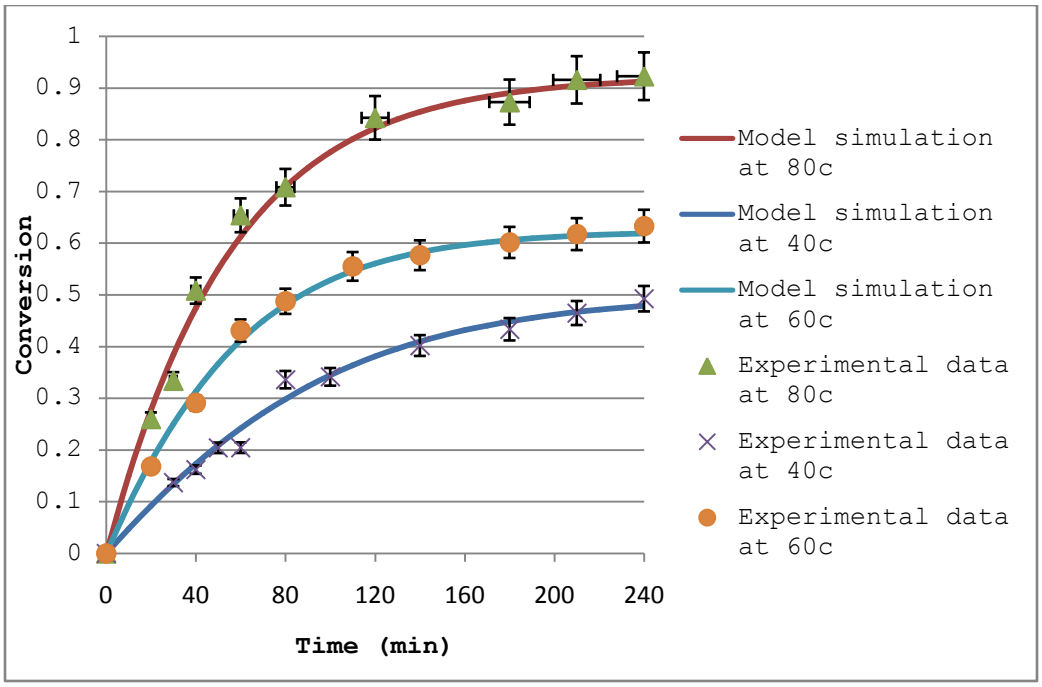

Figure 1.9 Prediction of Esterification of Palmitic Acid over Zirconia Sulfate

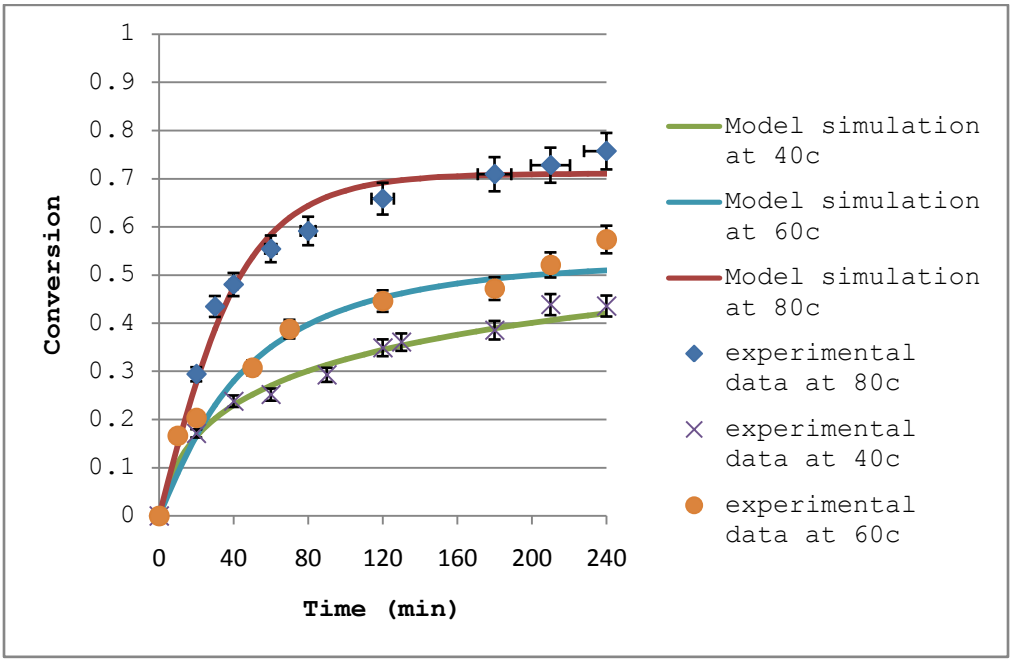

Figure 1.10 Prediction of Esterification of Palmitic Acid on Alumina

As can be seen in Figure 1.9 and Figure 1.10, the deterministic models used to predict the conversion at times

greater than 180 minutes showed good agreement. The values of the deterministic models are very close to the experimental data. Therefore, these rate law models can be used to predict the experimental data at different temperatures between 40^{o}C to 80^{o}C and at longer reaction times.

1.3.5. Discussion on deterministic model

This disparity between the adsorbed species is attributed to the nature of the acidic sites on the catalysts. Sulfated zirconium oxide has been reported to have Brönsted and Lewis acid sites. When the reaction was carried over pure zirconium oxide, the esterification yield was low; therefore, it was assumed that the catalyst activity was mostly due to the Brönsted acid sites generated by the sulfation. Activated acidic alumina, however, only has Lewis acid sites. The adsorption of palmitic acid is believed to be a nucleophilic interaction between the Brönsted acid site and the carboxylic moiety similar to homogeneous acid catalyzed esterification. On the activated acidic alumina, however, Lewis acid sites are predominant leading to the chemisoption of methanol. Therefore, Brönsted acid behaves differently from Lewis acid in the esterification of free fatty acid.

From the heat of the reaction of both catalysts, SO_4/ZrO_2-550°C seems to be a better catalyst in the esterification of palmitic acid. However, this catalyst requires sulfation and temperature activation before use. On the other hand, $AcAl_2O_3$ does not require sulfation, though three hours of activation at 550°C is required in order to remove moisture and atmospheric carbon from the surface. Therefore, it is more convenient for industrial use where easy-to-prepare catalysts are needed, although the operation cost of $AcAl_2O_3$ may be higher due to the higher heat of the reaction requiring higher temperature.

1.3.6. Result for SO_4/ZrO_2-550°C stochastic simulation

The reaction parameters of palmitic acid esterification over SO_4/ZrO_2-550°C were then determined in Table 1.5.

Table 1.5 Reaction parameters determined by stochastic model on SO_4/ZrO_2-550°C

Temp (°C)	k_1	k_2	k_3	k_4	k_5	k_6
40	0.30	0.5	1.28	304.04	4.02	2
60	0.80	3	6.55	337.84	1	0.5
80	1.14	8.5	6.92	74.88	4.54	0.5

Results of the stochastic simulations for SO_4/ZrO_2-550°C at different temperature are shown in Figure 1.11 to Figure 1.16.

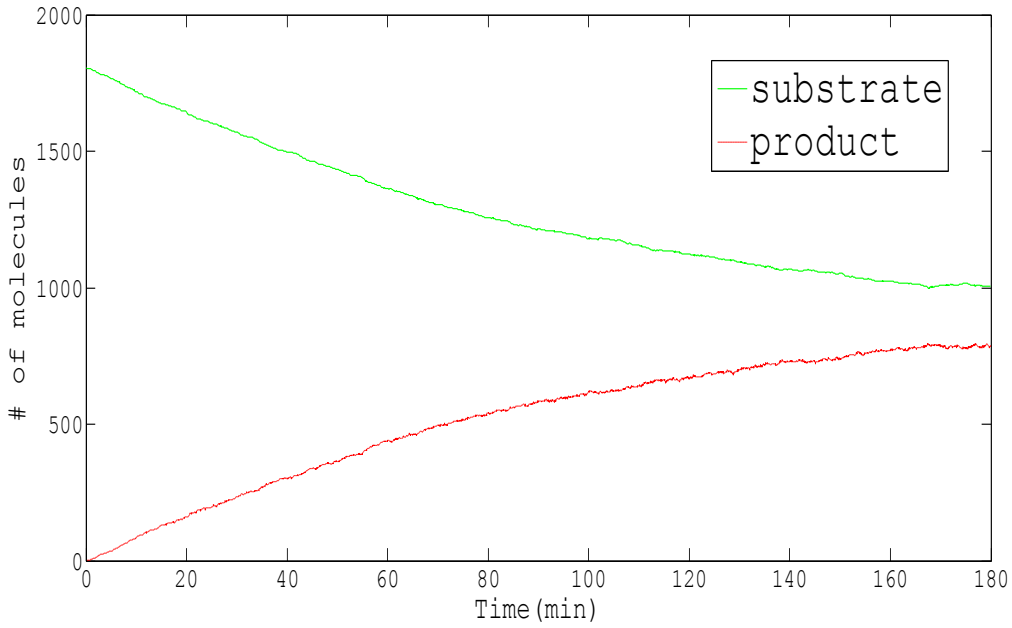

Figure 1.11 Stochastic simulation on SO_4/ZrO_2-550°C at 40°C

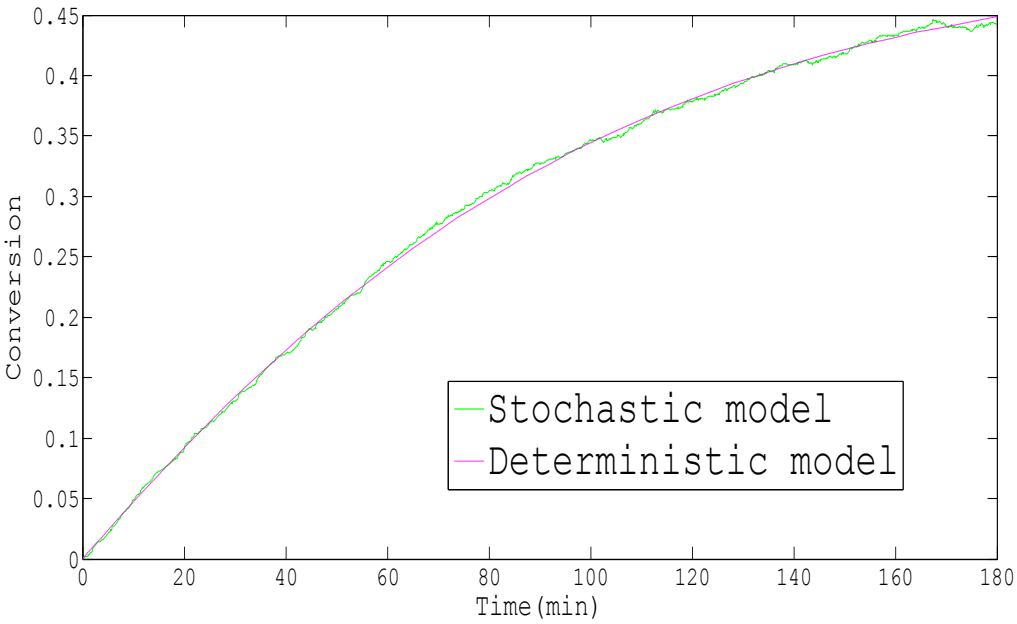

Figure 1.12 Comparison of Stochastic simulation vs. Deterministic model on SO_4/ZrO_2-550°C at 40°C

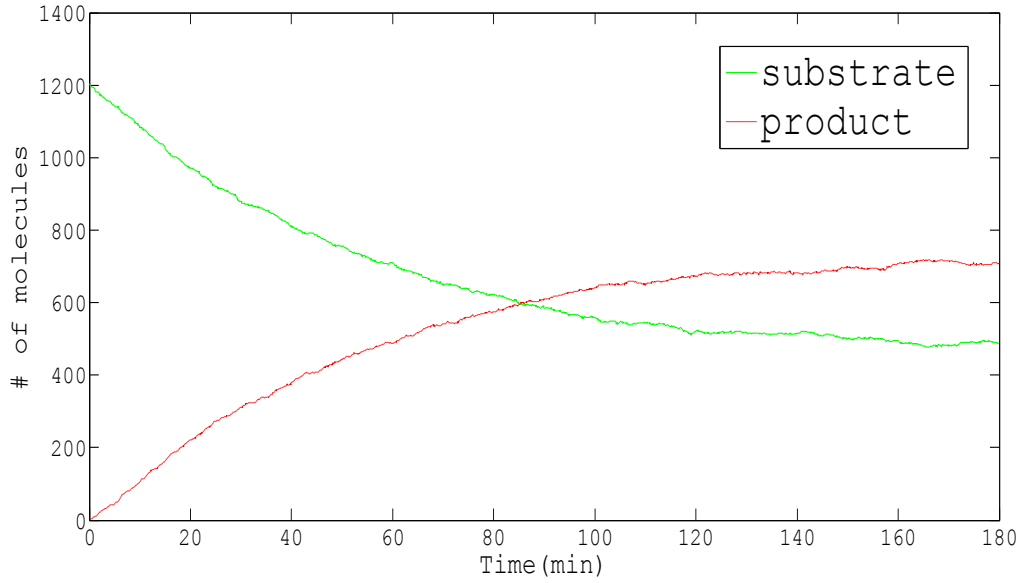

Figure 1.13 Stochastic simulation on SO_4/ZrO_2-550°C at 60°C

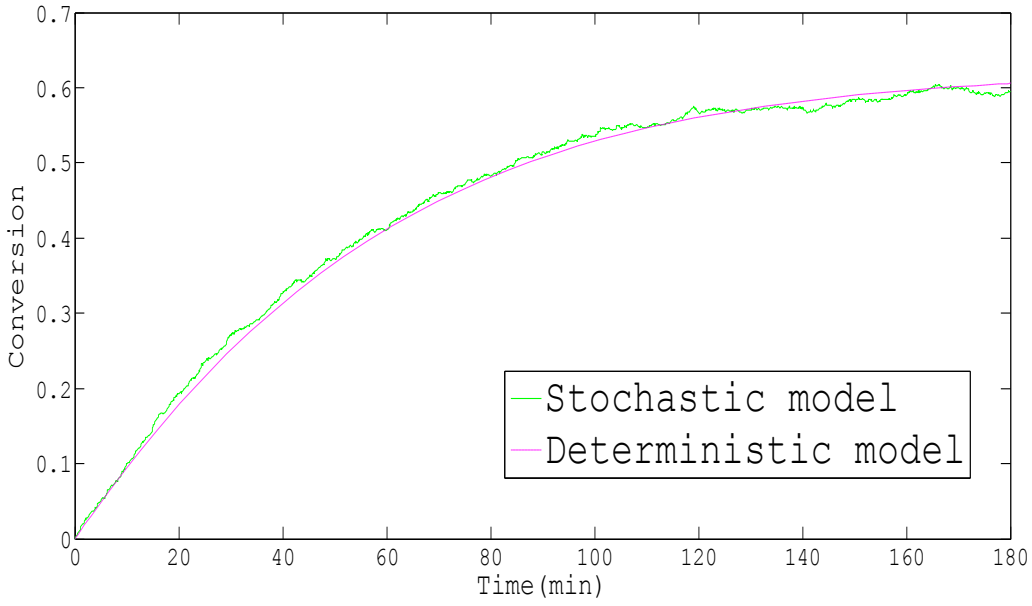

Figure 1.14 Comparison of Stochastic simulation vs. Deterministic model on SO_4/ZrO_2-550°C at 60°C

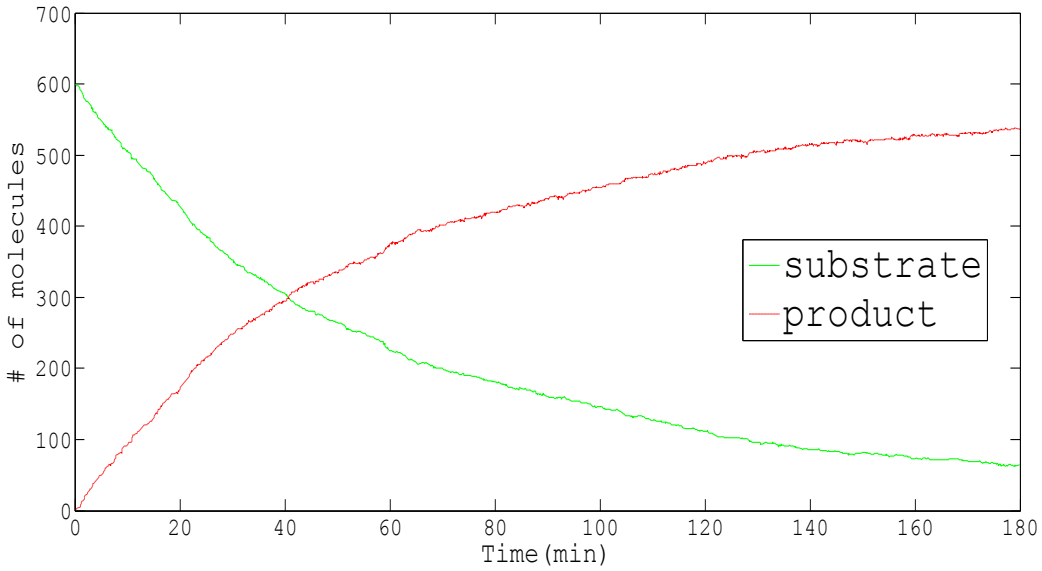

Figure 1.15 Stochastic simulation on SO_4/ZrO_2-550°C at 80°C

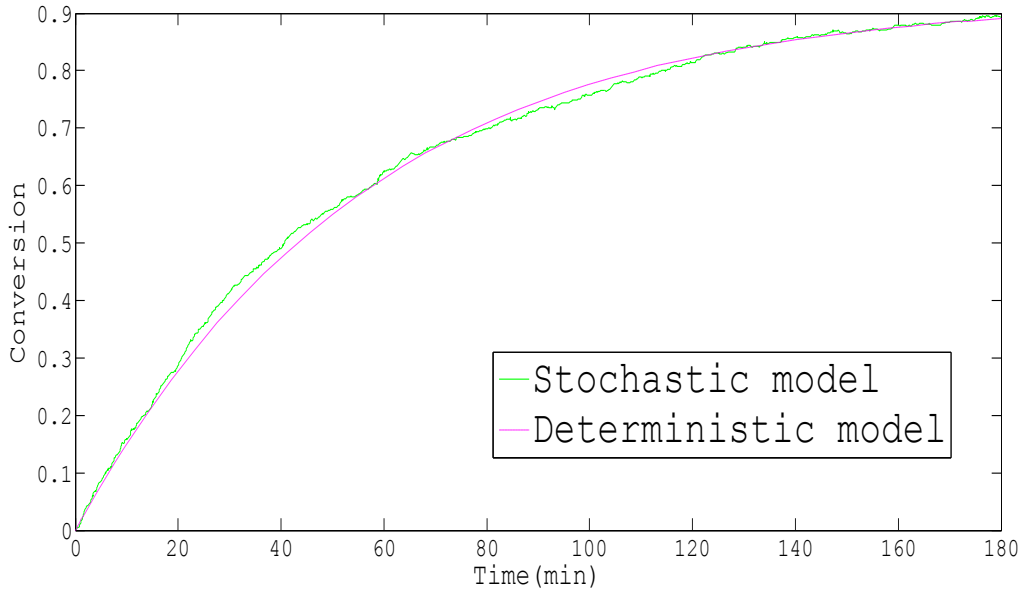

Figure 1.16 Comparison of Stochastic simulation vs. Deterministic model on SO_4/ZrO_2-550°C at 80°C

The stochastic simulation algorithms generated smooth graphs that are comparable to those produced in the deterministic model. However, the stochastic simulation generated smooth graphs as the number of molecules in the system increased. The number of molecules employed were 1800, 1200 and 600 for SO_4/ZrO_2 at temperatures of 40, 60 and 80°C, respectively. The stochastic simulation also further validated the Eley-Rideal mechanism over SO_4/ZrO_2 surface.

1.3.7. Result for $AcAl_2O_3$ stochastic simulation

The reaction parameters of palmitic acid esterification over SO_4/ZrO_2-550°C were then determined in Table 1.6.

Table 1.6 Reaction parameters determined by stochastic model on $AcAl_2O_3$

Temp (°C)	$k_1 \times 10^{-2}$	$k_2 \times 10^{-3}$	k_3	k_4	k_5	k_6
40	1.89	0.94	9.70	500.00	1.19	0.55
60	1.27	9.10	6.23	300.00	16.08	8.00
80	2.08	271.59	10.82	95.00	20.10	10.00

Results of stochastic simulations for Alumina at different temperature are shown below:

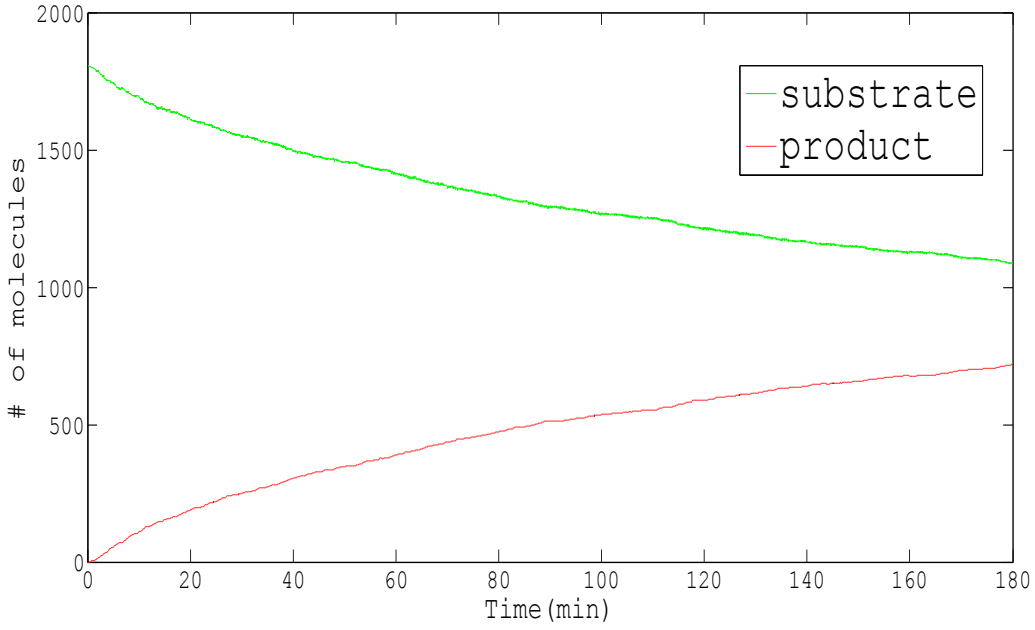

Figure 1.17 Stochastic simulation on $AcAl_2O_3$ at 40°C

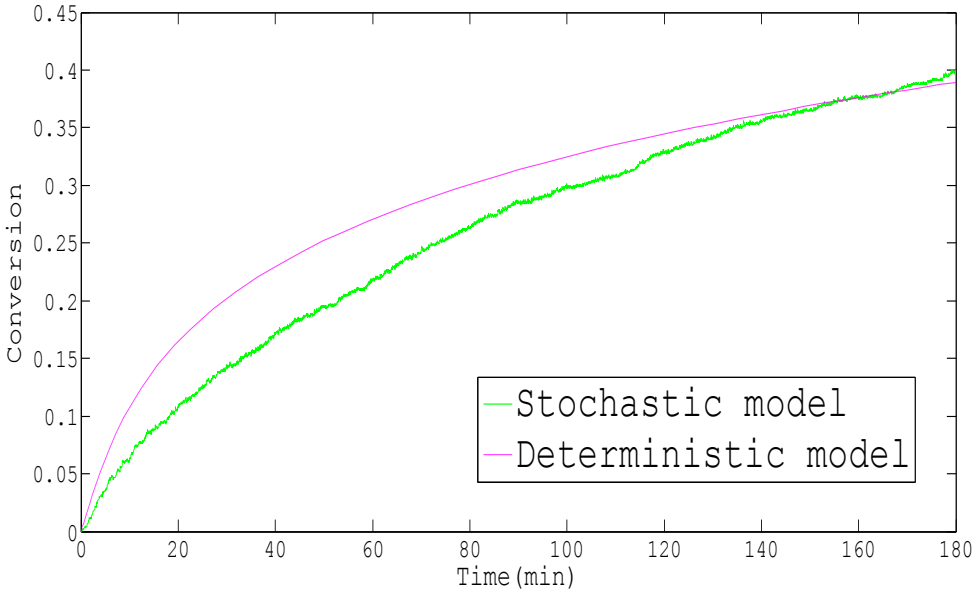

Figure 1.18 Comparison of Stochastic simulation vs. Deterministic model on $AcAl_2O_3$ at 40°C

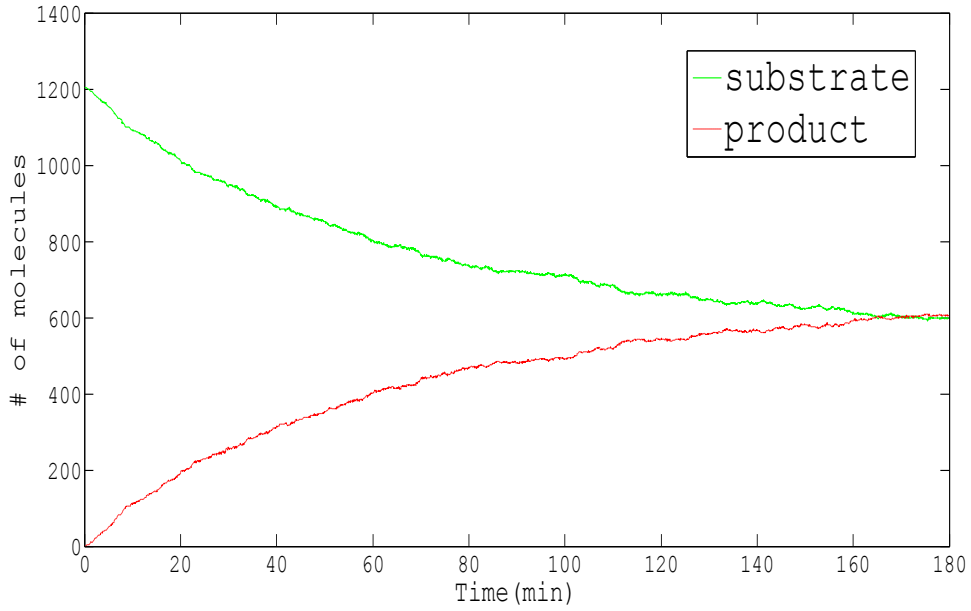

Figure 1.19 Stochastic simulation on $AcAl_2O_3$ at 60°C

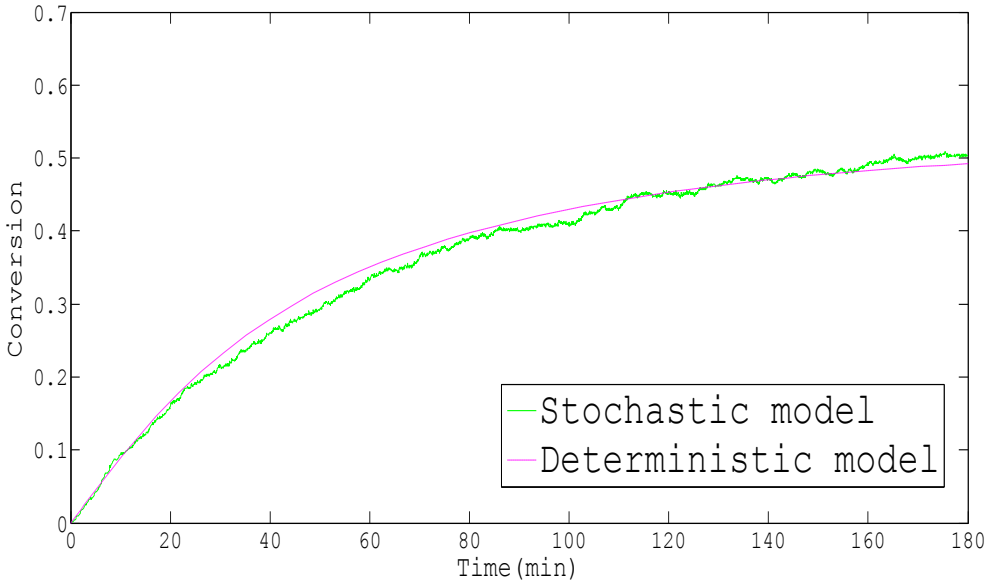

Figure 1.20 Comparison of Stochastic simulation vs. Deterministic model on $AcAl_2O_3$ at 60°C

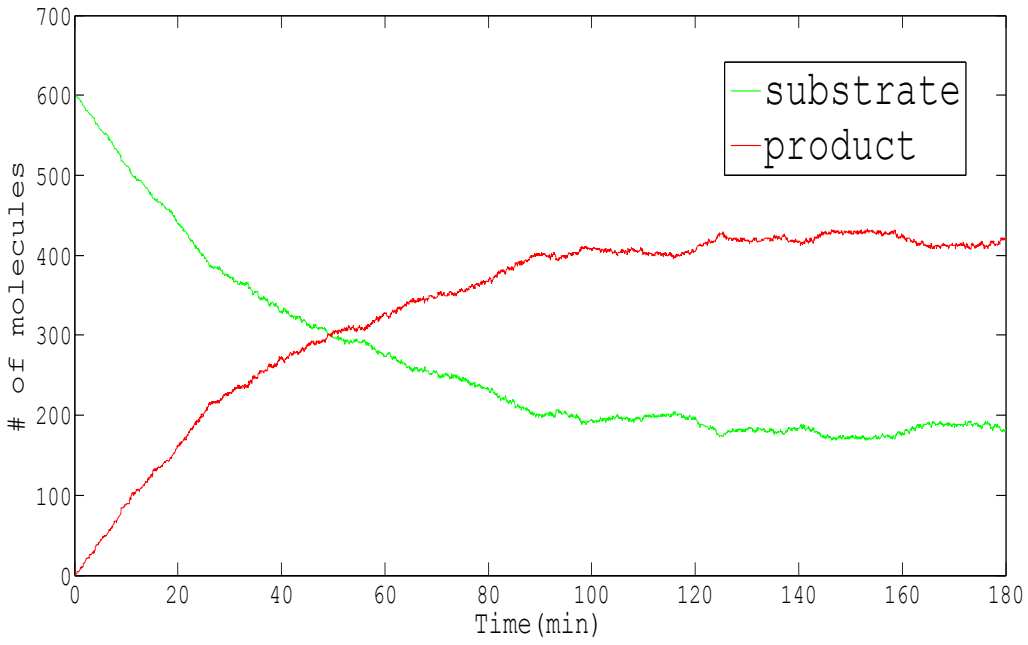

Figure 1.21 Stochastic simulation on $AcAl_2O_3$ at 80°C

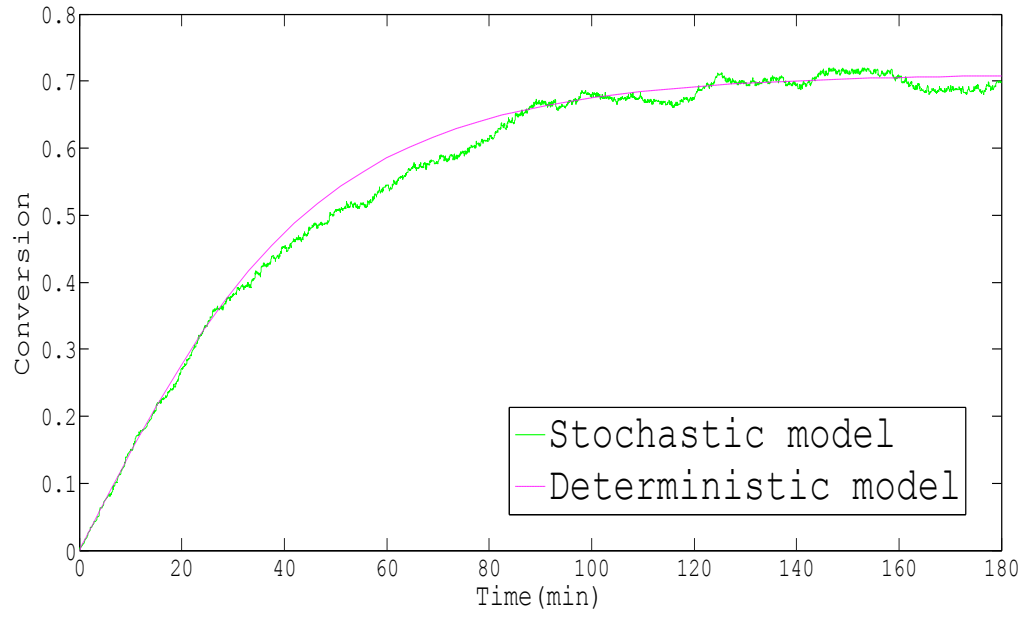

Figure 1.22 Comparison of Stochastic simulation vs. Deterministic model on $AcAl_2O_3$ at 80°C

The stochastic simulation generated smooth graphs as the number of molecules in the system increased. The number of molecules employed were 1800, 1200 and 600 for $AcAl_2O_3$ at temperatures of 40, 60 and 80^{o}C, respectively. The stochastic simulation also further validated the Eley-Rideal mechanism over $AcAl_2O_3$ surface.

1.3.8. Discussion on Stochastic modeling

We use stochastic simulation is used as a tool for observing the nature of the reaction, which occurs over the surface of the catalysts. The major difference at the molecular level between deterministic and stochastic is that the deterministic model mimics the experimental result whereas the stochastic model investigates the intrinsic nature of the reaction. The deterministic model does not take into account the stochastic nature of the chemical reaction. In a chemical reaction, each individual reaction is an event that occurs with a certain probability. Practically, the deterministic model is easier to set up and faster in terms of calculation compared to the stochastic model. The deterministic model however, is not adequate at describing the intrinsic nature of chemical reactions. In order to observe the reactions that occur over the surface of the catalyst, a small number of molecules in the system will be observed. When dealing with a small number of

molecules, the deterministic model cannot be used. In some systems such as biological processes, the reaction can be accurately simulated using a stochastic simulation.

In this specific aim, the stochastic simulation algorithms generated graphs that were comparable to those produced by the deterministic model. This is more the case as the number of molecules in the system increased. This was also observed as the temperature increased due to the increased frequency of collision and therefore there is a higher likelihood of reaction. The number of molecules employed were 1800, 1200 and 600 for both SO_4/ZrO_2 and $AcAl_2O_3$ at temperatures of 40, 60 and 80 ^0C, respectively. The stochastic simulation also further verifies the Eley-Rideal mechanism. The deterministic behavior represents the average of all these possible stochastic evolutions. Thus we note that the deterministic model and stochastic simulation are very close as illustrated in Figure 1.11 through 22 for both catalysts. Consequently, the deterministic result should be enough to describe the mechanism of the system. However, for other more complex catalyst, such as enzyme, the stochastic simulation could be essential in investigating the reaction mechanisms.

1.3.9. Conclusion

Our results show that Eley-Rideal mechanism is appropriate to explain the reaction mechanism, which occurs in the esterification of palmitic acid over both, SO_4/ZrO_2-550°C, and $AcAl_2O_3$. The reaction of adsorbed palmitic acid with methanol in bulk fluid is the rate-determining step for SO_4/ZrO_2-550°C. On the other hand, the adsorption of methanol on an active site on the catalyst was the rate-determining step in $AcAl_2O_3$. This difference in adsorbed species is attributed to the nature of the acid sites: SO_4/ZrO_2-550°C has mostly Brönsted acid sites whereas, $AcAl_2O_3$ has Lewis acid sites. Furthermore, the deterministic model and the stochastic simulation are in good agreement. It is therefore sufficient to use the deterministic model for the future kinetic investigation of free fatty esterification over heterogeneous catalysts. Furthermore, we showed that these models can be used to predict the conversion for different times. The heat of the reaction of SO_4/ZrO_2-550°C is 70.81 kJ/mol while that of $AcAl_2O_3$ is 93.70 kJ/mol indicating that SO_4/ZrO_2-550°C is better in the esterification for free fatty acids. Finally, this investigation of the esterification of free fatty acids serves as a model for further kinetic studies of transesterification of vegetable oil to biodiesel. Moreover, the combination of deterministic modeling and

stochastic simulation can be used as a model to study more complex catalyst such as enzyme catalyst.

Reference

[1] Pryde E. Vegetable Oils as Diesel Fuels: Overview. J Am Oil Chem Soc 1983;60:1557 – 1558.

[2] Shafiee S, Topal E. When Will Fossil Fuel Reserves Be Diminished? Energy Policy 2009;37:181 – 189.

[3] Kulkarni MG, Gopinath R, Meher LC, Dalai AK. Solid Acid Catalyzed Biodiesel Production by Simultaneous Esterification and Transesterification. Green Chem 2006;8:1056 – 1062.

[4] Shay EG. Diesel Fuel from Vegetable-Oils - Status and Opportunities. Biomass Bioenergy 1993;4:227 – 242.

[5] Bartholomew D. Viewpoint. J Am Oil Chem Soc 1981;58:286A – 288A.

[6] Arbon IM. Worldwide Use of Biomass in Power Generation and Combined Heat and Power Schemes. Proc Inst Mech Eng Part A J Power Energy 2002;216:41 – 57.

[7] Anon. Filtered Used Frying Fat Powers Diesel Fleet. J Am Oil Chem Soc 1982;59:A780–1.

[8] Adams C, Peters J, Rand M, Schroer B, Ziemke M. Investigation of Soybean Oil as a Diesel Fuel Extender: Endurance Tests. J Am Oil Chem Soc 1983;60:1574 – 1579.

[9] Peterson CL, Auld DL, Korus RA. Winter Rape Oil Fuel for Diesel-Engines - Recovery and Utilization. J Am Oil Chem Soc 1983;60:1579 – 1587.

[10] Ma FR, Hanna MA. Biodiesel Production: A Review. Bioresour Technol 1999;70:1 – 15.

[11] Schwab AW, Bagby MO, Freedman B. Preparation and Properties of Diesel Fuels from Vegetable-Oils. Fuel 1987;66:1372 – 1378.

[12] Ziejewski M, Kaufman KR, Schwab AW, Pryde EH. Diesel-Engine Evaluation of a Nonionic Sunflower Oil Aqueous- Ethanol Microemulsion. J Am Oil Chem Soc 1984;61:1620 – 1626.

[13] WEISZ PB, HAAG WO, RODEWALD PG. Catalytic Production of High-Grade Fuel (Gasoline) from Biomass Compounds by Shape-Selective Catalysis. Science (80-) 1979;206:57 – 58.

[14] Alencar JW, Alves PB, Craveiro AA. Pyrolysis of Tropical Vegetable-Oils. J Agric Food Chem 1983;31:1268 – 1270.

[15] Billaud F, Dominguez V, Broutin P, Busson C. Production of Hydrocarbons by Pyrolysis of Methyl-Esters from Rapeseed Oil. J Am Oil Chem Soc 1995;72:1149 – 1154.

[16] Crossley A, Heyes T, Hudson B. The Effect of Heat on Pure Triglycerides. J Am Oil Chem Soc 1962;39:9 – 14.

[17] Schwab A, Dykstra G, Selke E, Sorenson S, Pryde E. Diesel Fuel from Thermal Decomposition of Soybean Oil. J Am Oil Chem Soc 1988;65:1781 – 1786.

[18] Vicente G, Martínez M, Aracil J. Integrated Biodiesel Production: A Comparison of Different Homogeneous Catalysts Systems. Bioresour Technol 2004;92:297 – 305.

[19] Pasias S, Barakos N, Alexopoulos C, Papayannakos N. Heterogeneously Catalyzed Esterification of FFAs in Vegetable Oils. Chem Eng Technol 2006;29:1365 – 1371.

[20] Kulkarni MG, Dalai AK. Waste Cooking Oil - An Economical Source for Biodiesel: A Review. Ind Eng Chem Res 2006;45:2901 – 2913.

[21] Lotero E, Liu Y, Lopez DE, Suwannakarn K, Bruce DA, Goodwin JG. Synthesis of Biodiesel via Acid Catalysis. Ind Eng Chem Res 2005;44:5353 – 5363.

[22] Fjerbaek L, Christensen K V, Norddahl B. A Review of the Current State of Biodiesel Production Using Enzymatic Transesterification. Biotechnol Bioeng 2009;102:1298 – 1315.

[23] Zhang Y, Dube MA, McLean DD, Kates M. Biodiesel Production from Waste Cooking Oil: 1. Process Design and Technological Assessment. Bioresour Technol 2003;89:1–16.

[24] Di Serio M, Tesser R, Dimiccoli M, Cammarota F, Nastasi M, Santacesaria E. Synthesis of Biodiesel via Homogeneous Lewis Acid Catalyst. J Mol Catal A Chem 2005;239:111 – 115.

[25] Di Serio M, Cozzolino M, Giordano M, Tesser R, Patrono P, Santacesaria E. From Homogeneous to Heterogeneous Catalysts in Biodiesel Production. Ind Eng Chem Res 2007;46:6379 – 6384.

[26] Gomes JF, Puna JF, Bordado J, Correia MJN. Development of Heterogeneous Catalysts for Transesterification of Triglycerides. React Kinet Catal Lett 2008;95:273 – 279.

[27] Kiss AA, Omota F, Dimian AC, Rothenberg G. The Heterogeneous Advantage: Biodiesel by Catalytic Reactive Distillation. Top Catal 2006;40:141 – 150.

[28] West AH, Posarac D, Ellis N. Simulation, Case Studies and Optimization of A Biodiesel Process with A Solid Acid Catalyst. Int J Chem React Eng 2007;5:1 – 8.

[29] Rosa M, Oliveira A. Synthesization of Biodiesel by Tin (IV) Complexes. Proc. 3rd Brazilian Congr. Pet. Gas, Brazil: Brazilian Petroleum and Gas Institute; 2005.

[30] Srivastava R, Srinivas D, Ratnasamy P. Fe-Zn Double-Metal Cyanide Complexes as Novel, Solid Transesterification Catalysts. J Catal 2006;241:34 – 44.

[31] Perin D, Armareg W, Perrin P. Heterogeneous Catalysis in the Transesterification of Mamona and Soy Oils. Proc. 29th Annu. Reun. Chem. Brazilian Soc., Brazil: 2006.

[32] Rosa M, Oliveira A. Carbonates Utilization as Heterogeneous Catalysts of Transesterification. Proc. 29th Annu. Reun. Chem. Brazilian Soc., Brazil: 2006.

[33] Brito A, Borges ME, Arvelo R, Garcia F, Diaz MC, Otero N. Reuse of Fried Oil to Obtain Biodiesel: Zeolites Y as a Catalyst. Int J Chem React Eng 2007;5:1548 – 1559.

[34] Santos A. Heterogeneous Catalysts for Biodiesel Production – Metanolysis of Soy Oil over Hidrotalcytes of Magnesium and Aluminium Changed. Master Thesis on Environmental Engineering, IST/UTL, Lisbon, 2007.

[35] Amenomiya Y, Cvetanovic RJ. Active Sites of Alumina and Silica-Alumina as Observed by Temperature Programmed Desorption. J Catal 1970;18:329 – 337.

[36] Fogler HS. Elements of Chemical Reaction Engineering. 4th ed. Upper Saddle River, NJ: Prentice Hall PTR; 2006.

Chapter 2 Specific Aim 2

LCA and LCC Model for Switchgrass Pyrolysis for Use in Power Plant

Lerkkasemsan N, Achenie LEK. Life Cycle Costs and Life Cycle Assessment for the Harvesting, Conversion, and the Use of Switchgrass to Produce Electricity. International Journal of Chemical Engineering 2013;2013:1 – 16.

2. Chapter 2 - LCA and LCC Model for Switchgrass Pyrolysis for Use in Power Plant

The second aim is to study the life cycle cost and life cycle assessment for the entire switchgrass production system including the pyrolysis facility and the downstream power plant facility. The life cycle cost will determine the feasibility of the process. On the other hand, the life cycle assessment will determine the GHG emission from the process; the GHG has an impact on the environmental. The process is likely to be viable if both criteria are satisfied. This means the process has to be profitable and have less impact on environmental when compared with the conventional process, which uses fossil fuel.

2.1. Introduction and literature review

2.1.1. Introduction

Our dependence on fossil fuel has increased over the past century due to increasing energy consumption. The U.S. Department of Energy [1] stated that transportation energy demand is increasing at an annual rate of 0.2 percent from year 2010 to 2035. Total electricity consumption is also increasing at an annual rate of 0.8 percent from 3879 billion kilowatt-hours in 2010 to 4775 billion kilowatt-hours in 2035. On the other hand, the world oil reservoir is decreasing. From BP's estimates[2], world oil production has already reached its maximum and is expected to drop. At the present production rate, the world oil reservoir will last for forty-one years.

Renewable energy such as bio-oil will be an alternative source to make up the reduction of oil production rate. Faaij[3] reported that fossil fuel dominated the world's energy uses, supplying 80% of the total energy requirement. However, 10-15% of this demand could be covered by biomass resource. Biomass is an important energy resource for developing countries accounting for 50-90% of their total energy requirement.

Advantages of biomass energy include potential to reduce GHG emissions, substitution for depleting global crude oil

reservoir, potential impacts on waste management, and the conversion of waste resources into clean energy. Waste resources include natural forests wood, forestry residues, agricultural residues, industrial wastes, food processing wastes and municipal solid wastes.

With the increasing concern of Green House gas from petroleum sources, searching for clean and environmentally friendly energy resource has become more important[4]. Alley et al.[5]reported perturbation of Green House Gas such as Carbon dioxide (CO_2), Methane (CH_4), and Nitrous oxide (N_2O), which have been created by human activity such as utilization of fossil fuel and land-use change to the global climate. Measurement of carbon dioxide at Mauna Loa Observatory showed that the rate of release of carbon dioxide into the atmosphere has increased from less than 1 ppm per year in 1970 to more than 2 ppm per year in 2009. It is expected that the rate will increase exponentially[6].

Bio-oil is one of the promising clean energy substitutes since it can replace or be mixed with fossil fuel to use in a conventional technology engine. In this study, the bio-oil is produced and used in a conventional power plant. Hammons[7] reported a study of Green House Gas emissions from an electric

power plant in Europe. Carbon dioxide from fossil fuel combustion in a power plant is more than one third of the total carbon dioxide emission and the fraction is increasing. From AEO2012 [8], carbon dioxide produced from electricity generation is increasing at a rate of 0.2 percent per year until 4.9 percent from year 2010 to 2035. Brammer et al. [9] reported on the use of bio-oil in heat, power or combined heat and power (CHP)in 14 European countries. They reported that heat application is the most economically competitive followed by CHP application. Fan et al. [10] conducted life cycle assessment of electricity generation using fast pyrolysis bio-oil from short rotation forestry willow, poplar, collection of hard wood residue from existing forestry operations, and wasted wood from a sawmill available at the site of pyrolysis plant. They reported that using fast pyrolysis oil in power plants could save GHG emission about 77%-99% depending on the biomass feedstock and type of power plant. Solantauta et al. [11] reported the use of fast pyrolysis oil in diesel engine in power plant. The modification of the diesel engine by including an injection system helps the engine run smooth. Arbon[12] reported on the use of biomass in power generation. He discussed the use of pyrolysis and gasification product in a conventional combustion system such as steam turbine, boiler and

reciprocating engine. However, the development in technology is needed to reduce high capital cost of pyrolysis process. Chiaramonti et al.[13]reported on the use of pyrolysis in diesel engine, gas turbine, and natural gas/steam power plant.

Advantages of using fast pyrolysis oil as fuel are as follows: it is easy to store and transport; it has a higher energy density than gasification fuel gases; it can be distilled and used as a replacement for light fuel oil; and it can be used in a conventional fossil fuel power plant[13]. Arbogast et al. [14] reported the economic study of pyrolysis oil. The authors concluded that waste biomass such as logging residues is the lowest cost material for pyrolysis oil. However, the supply of waste biomass material is limited. On the other hand, growing energy crop is more expensive. Fortunately with more concentrated production of energy crop, the logistic cost can be reduced.

Growing energy crop provides a more stable energy source thus reducing the limitation of pyrolysis oil production. Boateng et al. [15] stated that pyrolysis oil from switchgrass as an energy crop has a yield greater than 60%. The energy conversion efficiencies of switchgrass range between 52% and 81%. This specific aim focuses on life cycle assessment and life

cycle cost of using switchgrass as an energy crop from field to power plant.

2.1.2. Literature review and background

(1) Literature review and background-LCA

(I) General Introduction

The International Scientific Society of Environmental Chemists (SETAC)[16] defines LCA as "a process to evaluate the environmental burdens associated with a product, process, or activity by identifying and quantifying energy and materials used as well as waste released to the environment." Clearly, LCA focuses only on the environmental impacts from the production system; economic and social aspects are not considered [17].

In recent years, clean and green technologies have attracted significant attention from not only governments but also many manufacturers, since pollution and environmental contamination problems have begun to be more serious problems. Therefore, the evaluation of environmental impact from any products has become more important. The purpose of evaluation of any environmental impact through Life Cycle assessment is to reduce or choose processes that have less impact on the environment. In other words, Life Cycle Assessment is a systematic path that enables achievement of cleaner and greener products and process concepts in industry[18]. Recently,

substantial research has been delivered in the field of clean and green production.

The LCA frame work was developed by the International Organization for Standardization in ISO 14000 series which consist of (a) ISO14000 on principle and frame work, (b) ISO14041 on goal and scope definition and inventory analysis, (c) ISO14042 on life cycle impact assessment, and (d) ISO14043 on life cycle interpretation[19].

(II) The history of LCA

The concept of exploring the life cycle of a product or function initially developed in the United States in the 1950s to 1960s. It was mainly focused on public purchasing. At that time, the "use cost" was often the dominant part of the total cost[20]. Novick [21] was the first person to introduce the life cycle concept in a report by the RAND Corporation. The report was focused on Life Cycle Analysis of cost. At that time, the main application of life cycle analysis was to estimate weapon systems costs. They included the cost of purchasing, the use cost, the development cost and the cost of end-of-life operations. Life Cycle Analysis became the tool for improved budget management, which linked all the cost together as total cost of ownership.

This life cycle concept was already fully developed when environmental policy became a major issue in all industrialized societies. The conceptual jump from life cycle cost analysis to the first life cycle-based waste and energy analysis, and later the broader environmental LCA, was developed through a series of small steps. The first attempt to consider all product systems was started in the early 1960s[20]. The work mainly studied energy requirements. Research such as fuel cycle research was conducted in the United States by the Department of Energy. Even though they mainly focused on energy requirements, these studies also included limited estimates of environmental releases. In 1969, the Coca Cola Company was the first to document the use of LCA to compare resource consumption and environmental releases related with beverage container[22]. However, at that time, the environmental aim was on resource use and waste management. The scope of LCA has since widened.

With the oil shortages in the early 1970s, the U.S. and British governments commissioned extensive industrial energy analysis. However, after the oil crisis, the interest in the LCA approach for evaluating energy use also faded. In the mid 1970s, Arthur D. Little and Midwest Research Institute (MRI) studied environmental issues in landmark studies. LCA studies on the environment in the United States continued at a slow but steady

pace of around two or three studies per year. The exact number of studies are not known because most studies were conducted for private clients[20]. In 1979, Boustead published the *Handbook of Industrial Energy Analysis*[23]. His early interest was to evaluate the total energy used in the production of various types of beverage containers including glass, plastic, and aluminum. Later on, he extended his method to many different materials.

In the 1980s, the Green movement in Europe drew public attention into LCA on issues related to recycling. As a result, the raw materials and solid waste considerations were added into LCA. In the 1990s, the Society of Environmental Toxicology and Chemistry (SETAC) held a workshop in which terms to describe LCA were defined. Those discussions laid the framework for how we view LCA today[24].

Many industry leaders initially expressed interest in LCA as they tried to demonstrate the environmental superiority of their product over a competitor's product. Consumers who were interested in environmentally friendly products could use LCA to compare products. This information could help guide consumers in making better purchasing decisions. Nowadays, product comparison is still the goal of many groups. LCA is now often used to

identify opportunities to alter a product, or process, to improve the company profile that makes it look greener. Both government and private industry have used LCA. For example, EPA hired Midwest Research Institute in 1976 to study resource and environmental profile analysis of five milk container systems with selected health and economic considerations. In January 1978, Goodyear Tire and Rubber Company hired Franklin Associates to study family-size soft drink containers[20].

In 2002, the United Nations Environment Programme (UNEP) and SETAC formed the UNEP/SETAC Life Cycle Initiative to assist development and uptake of LCA[25]. This LCA was built based on practices in many European countries, the USA and Japan. The purpose was to enable users to put life cycle thinking into practice. This generated focus on the new manufacturers, which were centered in Asia, Africa and South America. Since the production centers of modern manufacturing shifted through the effects of globalization, LCA practitioners followed. Further techniques for calculating the environmental impacts of production and consumption systems were also developed.

(III) LCA links to Environmental Policy

In the 1980s, the link to public policy was made based on concepts first developed in the Netherland at the Department of

Environmental Management headed by Pieter Winsemius. After the first stage of environmental policy, with command-and-control instruments directly used at main sources, there was a change to a systems aspect. LCA shifted to a more general formulation of environmental policy goals in the Dutch Environmental Policy Plans[26]. This shift from a source-oriented to an effect-oriented approach established a scope for environmental LCA from an environmental policy point of view, as contrasted to a business long-term cost view or a consumer interest point of view. His environmental approach is now dominant in LCA. It looks for integration over the environmental compartments' policies regarding water, air and soil. His overall policy strategy was based on: acidification; eutrophication; diffusion of toxic substances; disposal of waste; and disturbance, which includes noise, odor, and local-only air pollution. Later, climate change, dehydration and squandering were added.

The theme-oriented policy formed the basis for a broadened view on environmental policy. It also covered volume policy, product policy and substance policy. People and organizations were also the target groups of environmental policy. This approach inspired environmental policy of the EU[27]. In the 1990s, with additions and adaptations, the Life Cycle Impact Assessment method became dominant in LCA. The most widely

publicized use of LCA is ecolabeling. The development of the International Standards Organization (ISO) standard on Environmental Management Systems, which was known as the ISO 14000 series, made significant improvements and understanding possible in LCA. Considerable activity is made in the United States at the federal level in integrating a life-cycle approach with the formation of new policies such as solid waste management strategies, the regulatory development process (EPA rule making).

LCA is useful in decisions requiring comparisons of environmental outcomes and can be extended through tools such as Multi-Criteria Assessment, where quantitative and qualitative information is ranked and assessed across different environmental criteria. Systematic tools to assess, monitor, document, manage and maintain environmental performance are often modeled on ISO 14001 or similar environmental management systems, which in turn have their origins in quality management.

LCA is mainly used as background information for environmental reports or "environmental assessments" to demonstrate environmental benefits, burdens or burdens foregone. For example, 'eco-footprints' use LCA data in order to calculate results.

(IV) Why is LCA important

LCA is essential for justifying the selection of one product over another or for selecting the modifications made to any process in the life-cycle in order to decrease environmental impacts from all the stages.

It appears that any improvement made to operations or activities without careful consideration would result in possible secondary effects. Mostly, any change in any part of the product or process system can result in an unwanted shifting of burdens to another part of the system. This problem can be solved by employing life-cycle framework because identifying these unwanted shifts between any parts of system, as well as between media such as air, water, and solid waste, is the key concept behind LCA.

For example, the Environmental Protection Agency's (EPA's) Office of Water studied effluents from industrial laundries. The EPA tried to identify hazardous solvents that were being released when shop towels were washed. These towels were used to clean and degrease in many different shops, such as repair shops and print shops. The EPA set up regulations for disposal of the shop towels from this industry. At that time, the EPA realized that this would result in simply transferring the pollutant

loading to the landfill. When the regulation was written, a different approach should have been used so that a broader field of information was considered. Therefore, the Office of Water used the LCA to evaluate different shop towel systems as it wrote the new regulation for industrial laundries [20].

(V) LCA standards and process

International standards assist in the specification, definition, method, and protocols related to LCA studies. ISO 14040 describes the principles and framework for life cycle assessment. The original standard was produced in 1997 and updated in 2006 [28]. In this standard, reporting and critical review parameters and limitations of LCA are also indicated. However, there is no detailed description of the LCA technique. It does not specify how to undertake individual phases of the LCA. More detail is provided in ISO 14044 [29]. The ISO 14044 and ISO14040 have replaced other former LCA-related standards. The purpose of the standards is to provide more detail on LCA application in practice. The International Organization for Standardization (ISO) has issued a series of standards and technical reports for LCA, which can be referred to as the 14040 series. Table 2.1 shows the series within the documents.

Table 2.1 ISO documents on life cycle assessment (LCA)[30]

Number	Type	Title	Year
14040	International standard	Principles and framework	1996, 2006
14041	International standard	Goal and scope definition and inventory analysis	1998[1]
14042	International standard	Life cycle impact assessment	2000[1]
14043	International standard	Life cycle interpretations	2000[1]
14044	International standard	Requirements and guidelines	2006[2]
14047	Technical report	Examples of application of ISO 14042	2003
14048	Technical report	Data documentation format	2001
14049	Technical report	Examples of application of ISO 14041	2000

[1]Updated in 2006 and merged into 14044.

[2]Replaces 14041,14042, and 14043.

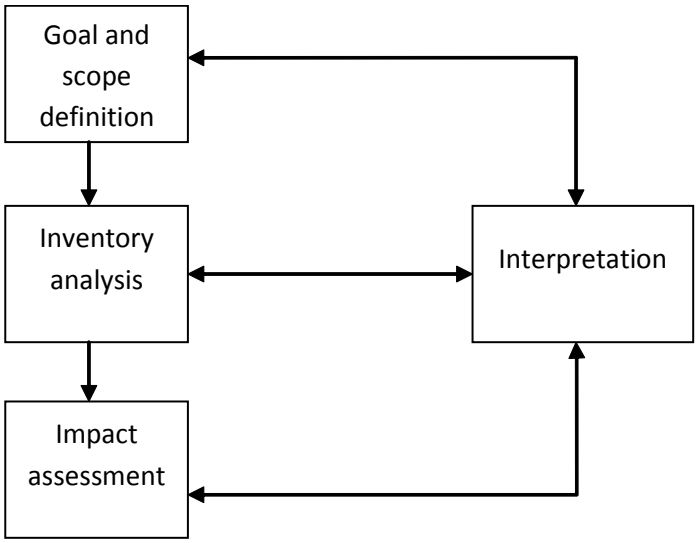

Figure 2.1 Outline of generic life cycle assessment (LCA) process (after ISO 14040)[25]

Figure 2.1 shows the outline of generic life cycle assessment as discussed in ISO 14040. This standard includes guidance on defining the goal and scope of an LCA study, development of the life cycle inventory, the life cycle impact assessment, and interpretation. A generic LCA method requires that all the main inputs to the processes that provide the service are taken into account.

For any LCA, appropriate framing of the question organizes part of the definition of the goal and scope. It includes setting the functional unit of the study. For example, if we compare LCA of two coffee machines based on the product level, the more durable and heavily built coffee machine has the higher environmental impact. However, if we compare the two coffee machines based on functional level, the more durable machine has a longer lifespan, which is capable of producing five times more cups of coffee than the other. This quality may reverse the outcome of the LCA comparison if we account for the functional unit impact per production of cups of coffee instead of impact per coffee machine.

From the previous example, the LCA is mostly used in comparing the total environmental impact of a product or service with alternative products or services. UNEP refers to LCA as a

tool to reveal “the world behind the product”[31]. Therefore, LCA is often considered to be a measurement that provides the answer to the question of which product is more environmentally friendly.

However, in some comparison, the process chain may be significantly different. For example, a wool carpet and a synthetic carpet would have very different process chains. Industrial inputs and processes dominate the synthetic carpet process chain. On the other hand, agricultural inputs and processes mostly influence the wool carpet process chain. This is an example of allocation of impacts. Sheep farming does not only produce wool but also produces other animal products, such as meat.

(VI) The LCA Methodology

The LCA methodology includes four components: goal definition and scoping, life-cycle inventory (LCI), impact assessment, and improvement assessment (interpretation) [32]. The relationships between these phases are illustrated in Figure 2.2.

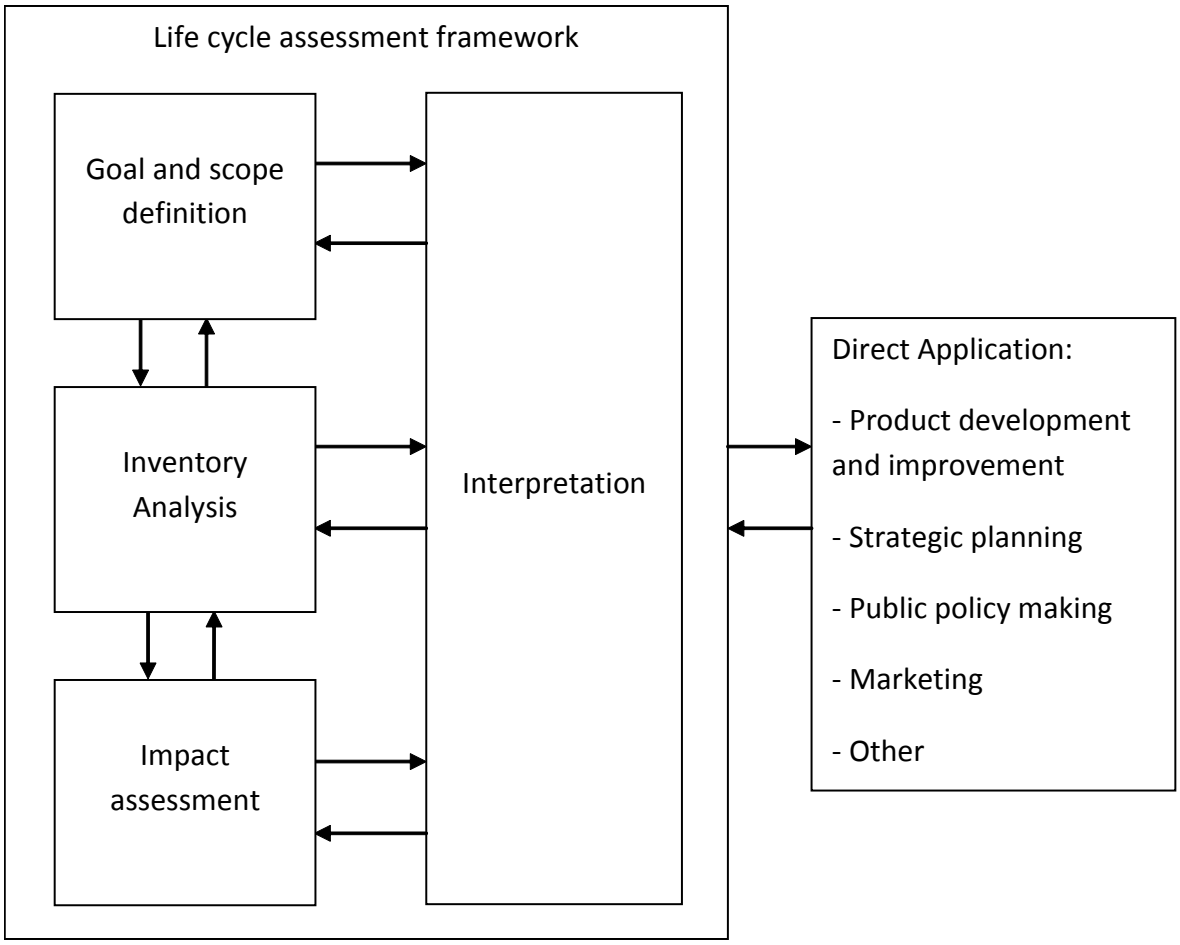

Figure 2.2 The general methodological framework for LCA (ISO 14040)[29]

(A) Goal and scope definition of LCA

The LCA begins here. The purpose for the activity must be defined. Typically LCI and LCA studies are performed in response to specific questions. In the goal and scope definition, no data is collected and no results are calculated. Here, it is a place where the plan of the LCA study is defined as clearly and unambiguously as possible.

The components involved in delivering the product or service should be included, as well as all inputs to those components and the inputs of those inputs, and so on. It also includes the outputs, emissions and wastes produced at all stages of the product or service delivery, which means that we calculate both pre-consumption and post-consumption. However, some distant process may be negligible only after thoroughly estimating the impact of that distant process to the center process.[25]

A given LCA should discuss the following topics[30]:

- ◊ The intended application;
- ◊ The reasons of carrying out the study;
- ◊ The intended audience;
- ◊ Whether the results are used in comparative assertions disclosed to the public.

(B) Inventory Analysis

"*Inventory*: An objective, data-based process of quantifying energy and raw material requirements, air emissions, waterborne effluents, solid waste, and other environmental releases throughout the life cycle of a product, process, or activity"[33].

The inventory is the result of compiling all environmental flows, including resource use inputs and waste or pollution outputs. Inventory data can only be converted into impact results through the use of appropriate algorithms or indicators of an environmental burden related to damage or importance. This is where primary fossil fuel energy used in delivering the product or service is converted into climate impacts, local air pollution, and so on. The inventory analysis technique will be used to deliver the work.

The LCI is built on the basis of the unit process, which is the central element of inventory analysis. A unit process is the "smallest element considered in the life cycle inventory analysis for which input and output data are quantified."[33] A unit process is treated as a black box that converts a bundle of inputs into a bundle of outputs. There are several types of inputs. For example, product (including components, materials, and services), waste for treatment, and natural resources (including fossils and land). There are also several types of outputs; for example product, waste for treatment, and residuals to the environment (including pollutants to air, water, and soil, waste heat, and noise). Figure 2.3 shows the inputs, namely raw materials and energy. Outputs include water effluent, air emissions, solid wastes, other environmental releases, and

products. All unit processes included have to be quantified. This means that the size of the inflows and outflows, per unit process must be specified.

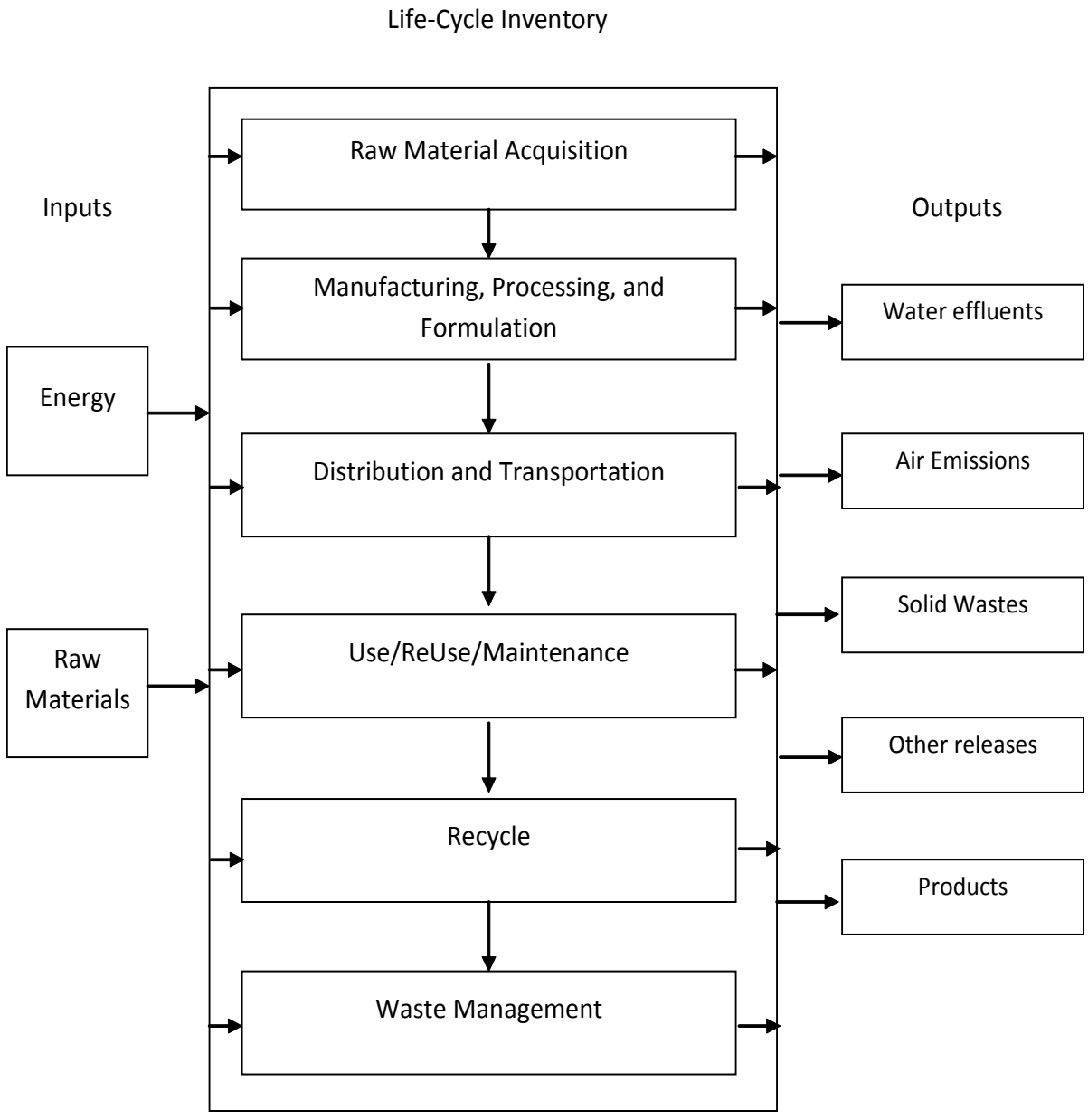

Figure 2.3 Life cycle inventories which account energy, raw materials, wastes, emission and products from all product's life cycle [24]

(C) Impact assessment

"*Impact assessment*: A technical, quantitative or semi quantitative process to characterize and assess the effects of the environmental loadings identified in the inventory component. The assessment should address both ecological and human health considerations as well as other effects such as habitat modification or noise pollution" [20].

Impact assessment is a "phase of life cycle assessment aimed at understanding and evaluating the magnitude and significance of the potential environmental impacts for a product system throughout the life cycle of the product." [30] The central element in impact assessment is the impact category and can be performed after the inputs and outputs of a system have been quantified by the life cycle inventory[34].

The impact assessment consists of three stages[20]:

- ◊ *Classification* of the process of aggregation of the life cycle inventory data into relatively homogeneous impact groups.
- ◊ *Characterization* of the model to convert or translate the LCI data into impact descriptors. For example, BOD data for wastewater discharges may be translated to fish mortality.

◊ *Valuation* is the assignment of relative values or weights to different impacts. When valuation is completed, the decision makers can directly compare the overall potential impacts of each product.

(D) Improvement assessment or interpretation

"*Improvement assessment*: A systematic evaluation of the needs and opportunities to reduce the environmental burden associated with energy and raw materials use and environmental releases throughout the whole life cycle of the product, process, or activity. This assessment may include both quantitative and qualitative measures of improvement, such as changes in product, process, and activity design; raw material use; industrial processing; consumer use; and waste management" [20].

From Figure 2.2, we can see that interpretation is performed by considering the other three phases of the LCA. The goal of the interpretation phase is to verify whether the results from the inventory analysis or the impact assessment fulfill the requirements defined in the goal and scoping phase. If the results do not satisfy the goal and scoping phase, the inventory analysis must be improved which will also improve

impact assessment. This improvement process will continue until the goal and scoping phase are fulfilled [35].

(VII) Application and example of LCA

(A) Pollution Prevention

Pollution prevention is another area, which should be viewed with life cycle impacts in mind. In order to do the pollution prevention assessment, the system boundaries are drawn very narrowly around the facility. In life cycle terms, these boundaries would then only include one stage, which is usually manufacturing.

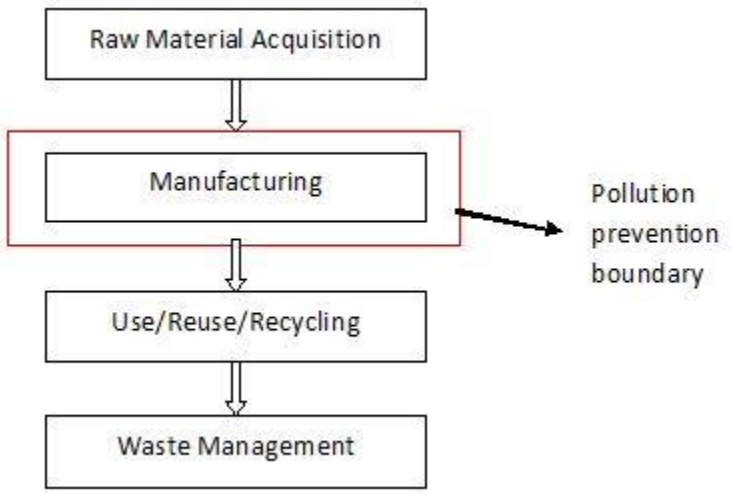

Figure 2.4 Pollution prevention assessment boundaries in the context of LCA [20]

Figure 2.4 identifies boundaries for pollution prevention assessments. Pollution prevention will benefit the facility but may not always achieve reduced impacts on the environment.

(B) The built environment

For example, building material and product suppliers, such as BHP Steel, used to deliver environmental impact assessments on their product. James Hardie and Pioneer study the life cycles of their product for one of the Olympic Games building in 2000. These companies had to study environmental impacts occurring in the production of their materials so that they could demonstrate their environmental credentials and thus be awarded contracts to supply materials in the construction phase[25].

(C) Waste management

LCA has had a prominent role in waste management. The Victorian government's Greenhouse Strategy 2002 identified waste as an important contributor to the green house effect through methane emission from landfills, as well as transport and processing of waste, and indirectly via lost savings that could be gained through recycling and valuable materials. The strategy considered waste from a several sources such as municipal, commercial and industrial, and construction and demolition waste.

EcoRecycle Victoria then commissioned two further LCAs: the first, to evaluate the environmental impacts of a range of waste management scenarios, and the second, to examine the

environmental benefits of recycling construction and demolition, and commercial and industrial waste[25].

(D) Greenhouse issues

The Commonwealth Australian Government's 1998 National Greenhouse Strategy, Measure 4.17 'Life cycle energy analysis', states[36]:

> *"Life cycle energy issues will be pursued through the following actions (a) governments, in consultation with industry, will develop a database and nationally accepted methodology for life cycle energy analysis and (b) based on these life cycle analysis, policies/programs will be developed and implemented to encourage producer responsibility for sourcing of materials, product design and manufacture, product operating efficiencies and product disposal, as a means of improving greenhouse outcomes."*

In 2003, the AGO developed the Greenhouse Friendly program, which certifies products and services as being 'carbon neutral'. This method involves burden of a greenhouse gas emission of a product or service and offsetting the greenhouse emissions with certified greenhouse gas deduction option.

(VIII) Future LCA

The future framework of the LCA is the LCSA [37] which broadens the scope of the current LCA. The LCA focuses only on environmental impacts. In contrast the LCSA covers all three dimensions of sustainability, namely people, planet and prosperity. It also widens the scope of LCA from product-related questions to questions related to sector and also economy-wide levels. The LCSA includes economic and behavioral relations. Discounting, weighting, and weak versus strong sustainability can be explicitly incorporated [38]. The LCSA is a trans-disciplinary integration framework of models. The broadening to economic and social impacts diverges from ISO's explicit restriction to environmental issues.

There are three important differences compared to the ISO 14040 framework.

(A) The combining of inventory analysis and impact assessment into a modeling phase.

After a decade of academic work on agricultural production, climate change, impacts of land use, rebound, etc., it is difficult to make a clear separation between behavior and technology. For example, the fuel that is used to drive 1 km

depends on many different factors, such as car, driver style, road, and traffic.

(B) The broadening of the object of analysis.

The LCSA can be performed at three different levels: product, meso, and economy-wide. The boundaries of these three levels are not sharply defined. Therefore, some questions may fall within the gray areas.

Products, (goods and services), are defined in the ISO 14040 standards. Product systems, which perform the same function, are compared, such as different milk packaging. Examples of methods and models for this level include process-LCA, hybrid LCA, and social LCA.

Mostly, meso level refers to a level in-between product and economy-wide. Meso level may consider groups of related products and technologies, baskets of commodities, a municipality etc. An example of this level is the conversion of biomass to a major car fuel. The appropriate methods and models for this level need further research[40]. In this specific aim, the focus is at this level.

“Economy-wide” refers to the economies of states or other geographical/political entities, and finally the world. As

stated in Eurostat report [41], economy-wide material flow accounts are consistent compilations of the overall material inputs into national economies, the changes of material stock within the economic system and the material outputs to other economies or to the environment. At this level one might consider the comparison of options for an emerging technologies such as large-scale introduction of wind energy or solar cells as strategy for phasing out fossil energy. Defining and finding appropriate methods and models for this level needs further research.

The boundaries of these three levels are not sharply defined. Therefore, some questions may fall within gray areas.

(C) The broadening of the scope of indicators.

There are three sustainability indicators, which need to be analyzed: environmental, economic and social indicators. A distinction is made between the LCA with just one set of sustainability indicators and the LCSA that includes all three indicators together[39].

(2) Literature review and background-LCC

(I) General introduction for LCC

Without government subsidies, renewable energy in the form of bio-oil from pyrolysis of biomass (such as switchgrass) can only exist when the production cost is lower or equal to that of fossil fuel energy. Therefore, in this specific aim, a total economic analysis is necessary in order to evaluate the economic viability.

Ravemark[40] defines LCC as the sum of costs (present values of investment, capital, installation, energy, operating, maintenance, and disposal) over the life-time of the project, product, or measure. Barringer[41] indicated that Life Cycle Costs (LCC) were cradle-to-grave costs summarized as an economics model of evaluating alternatives for equipment and projects.

Kawauchi and Rausand[42] stated that the main purpose of doing life cycle cost analysis was to find the total cost of production throughout its life cycle, which included research and development, construction, operation, maintenance, and disposal. Therefore, the LCC assesses the ability of using the switchgrass in the pyrolysis process to create an alternative

energy source that can finally be used in a power plant to create electricity.

Life cycle cost is the total ownership cost of a product over its useful life. It is the sum total of the direct, indirect, recurring, nonrecurring, and other related cost incurred, or estimated to be incurred, in design, research and development (R&D), investment, operations, maintenance, retirement, and other support of a product over its life cycle [43].

(II) History of Life cycle cost

Life cycle cost was incorporated into Life cycle assessment later in the late 1960s. Life cycle assessment was first documented for the Coca Cola study from 1969 [22]. The concept of exploring the life cycle of a product or function was initially developed in the United States in the 1950s and 1960s within the realm of public purchasing[30].

At that time, the use cost carried the main share of the total cost. Norvick[21] was the first person to mention of the life cycle concept which focused on life cycle analysis of cost. At that time, the main application of Life cycle cost was in the weapon systems. The costs covered purchasing cost, use cost, development and the cost of end-of-life operations.

Life cycle analysis then became the tool for improved budget management, which linked functionality to total cost of ownership. The federal government first used this concept. Many standardization questions soon emerged. For example, how is functionality defined? How should accidents and mistakes be considered?

Private firms quickly adopted the life cycle concept. They struggled with similar questions. Gupta and Chow[44] showed over six hundred life cycle studies that had been published by 1985. All these studies focused on cost to functionality. After several decades and plenty of studies, Life Cycle Analysis of Cost became Life Cycle Costing (LCC).

(III) Total Cost Assessment or total ownership cost

Total cost assessment (TCA) describes the long-term, comprehensive analysis of the full range of internal costs and saving resulting from pollution prevention projects and other environmental projects undertaken by the firm[20]. The TCA is different from conventional cost analysis. The TCA captures the full range of potential benefits of pollution prevention and other environmentally beneficial projects, which are not included in conventional practice. The failures result from the

misallocation of cost items, neglect of long-term costs and savings, and neglect of indirect costs or savings.

The application of the TCA involves four key elements designed to correct these shortcomings:

(A) A comprehensive costs and savings inventory

(B) More precise cost allocation

(C) Use of time horizons long enough to capture long-term costs and savings

(D) Use of profitability indicators, which account for the time value of money

These key elements will be explained in the following topic.

(A) Comprehensive cost inventory

A comprehensive cost inventory should include all costs and savings relevant to the analysis at hand. Cost can be separated into three main categories, which are direct conventional costs, indirect or hidden costs, probabilistic and less tangible costs as shown in Curran [20].

◊ Direct conventional costs

- Capital expenditures
- Buildings
- Equipment

- Utility connections
- Equipment installation
- Project engineering
- Operation and maintenance expense/revenues
- Raw materials
- Labor
- Waste disposal
- Utilities: energy, water, sewerage
- Revenue from recovered material

◊ Indirect or hidden Costs

- Compliance costs
- Permitting
- Reporting
- Tracking
- Monitoring
- Manifesting
- Training
- Waste handling
- Record keeping
- Labeling
- Testing
- Emergency preparedness
- Medical surveillance
- Waste storage
- Operation of on-site pollution control equipment
- Raw material costs linked to non product output (NPO)

- Environmental insurance (acute events, gradual impairment)

◊ Probabilistic and Less Tangible Costs

- Penalties and fines
- Personal injury and property damage
- Increased revenue from enhanced product quality
- Increased revenue from increased market share of "green products"
- Reduced worker compensation and absenteeism costs from improved employee health
- Increased productivity from improved employee relations
- Reduced staff burdens in dealing with community concerns.

The following table illustrates cost items that are more likely or less likely to be included in current practice

Table 2.2 more likely and less likely items to be included in current practice

More likely to be included	**Less likely to be included**
One-time, capital costs	Annual, recurring costs
Direct costs	Indirect, hidden costs
Certain costs	Uncertain, probabilistic costs
Short-term costs	Longer-term costs
Easily quantifiable costs	Difficult-to-quantify costs

Once a comprehensive project cost inventory has been developed, the corresponding cost data must be developed for the analysis.

(B) Appropriate Cost Allocation

Cost allocation procedures determine how production and other operating cost are assigned to specific processes and product lines within a firm. Overhead accounts often combine cost related to environmental management, such as waste storage, handling and treatment and environmental permitting. Sometimes overhead accounts also include materials, utilities, and salaries. Placing several costs in overhead accounts creates problems in two ways. First, costs that are lumped in overhead accounts are prone to omission from the project analysis cost inventory. Second, the lumped overhead costs are often misallocated to a process or product because of the inappropriateness of the chosen allocation basis.

Activity-based costing (ABC) is a term often used to describe systems which track costs back to the products and process whence they arose, rather than using simple, but often inaccurate, allocation bases such as product volume or manufacturing floor space[45]. With the ABC approach, costs are divided into broad categories. The categories can characterize

the type of activity that drives the cost. The activity categories will be shown in table below:

Table 2.3 Activity Categories for Cost Allocation [46]

Activity category	**Activity examples**
Facility-sustaining activities	Plant management, building and grounds
Product-sustaining activities	Process engineering, product specifications
Batch-level activities	Setups, material movements, inspections
Unit-level activities	Materials, labor, energy

An attempt to match each cost item with a correct category is to prevent misallocation of the costs.

(C) Time Horizon

This is another feature of the TCA. The TCA allows for a lengthy or shortened timing during project profitability analysis. In many situations, 2-5 years of time frame is necessary to capture the longer-term benefits characteristic of pollution prevention projects, liability, and recurrent savings due to waste avoidance. Some projects have longer time frame, which is 10-15 years resulting in more detail in project

analysis. However, the longer time frame is limited by many factors, such as financial capability for the project and competition for those funds by other projects. In this research, a longer time frame of 11 years is employed.

(D) Financial Indicators

The financial indicators should be set long enough to capture the long-term costs and savings characteristic of the pollution prevention projects. The financial indicators should be capable of incorporating those same costs and savings into a measure of long-term project profitability.

(IV) Life cycle costing

Life cycle costing is used to compare several options by identifying and assessing economic impacts over the life of each option [47].

Normally, ownership cost should be higher than acquisition costs. However, most of the time ownership cost is just 60-80% of total life cycle cost. Ownership cost can increase with time over the product's life cycle. It is crucial to minimize life cycle costs at the early phase of product's life cycle. Other than acquisition cost there are many hidden costs such as

maintenance, installation, training, testing, modifications, penalties cost, etc.

(A) Systems Life cycle costing

Since the acquisition is a small part in relation to the true or total cost associated with owning and operating the system, determining the LCC is crucial for systems.

There are four generally accepted methods for determining LCC.

- ◊ Engineering costs – direct estimation at the component level that lead to a detailed engineering build of the system
- ◊ Cost accounting – modern cost management systems to track and allocate expense
- ◊ Analogy – an estimate using historical results from similar products or components
- ◊ Parametric – based on mathematical relationships between costs and some product and process related parameters.

The combination of these four can be used to develop total ownership cost.

(B) Cost Estimation

Cost estimation techniques can be divided into three categories [43]:

◊ Parametric Cost Estimation

Parametric cost estimates are usually based on mathematical equations or models. Simple mathematical relationships such as linear and nonlinear regression are mainly utilized. Most of the time, they are based on historical data from like projects.

◊ Analogy Cost Estimating

Analogy estimates are performed on the basis of comparison and extrapolation using like items or efforts. In many cases, this cost estimating can be acquired by using simple relationship or equations with past projects.

◊ Engineering Buildup

The engineering buildup method rolls up individual estimates for each element, item, or component into the overall cost estimate. This is the most accurate means to develop a cost estimate. In the early stage, this method cannot be used since the systems have not been fully designed. However, most of the time, this estimate can be done based on experience of engineers in the project.

(C) Cost management

Engineering cost management is the process to identify, allocate, manage, and track resources needed to meet the stakeholder's requirements[43]. It is done to ensure that the most cost-effective solution is delivered. It consists of three steps:

- ◊ Define the requirements, level of quality desired, and the budget.
- ◊ Ensure that the risk, scope, and quality are aligned with the budget.
- ◊ Monitor and manage the balance of four components, which includes scope, risk, quality, and technical performance throughout the life of the project by using sound engineering techniques.

(D) Cost Analysis Goals

There are many possible applications of life cycle cost analysis. The following are samples [48].

- ◊ Alternative system/product operational scenarios and utilization approaches
- ◊ Alternative system maintenance concepts and logistic support policies
- ◊ Alternative system/product design configurations involving technology applications, equipment packaging schemes, diagnostic routines, built in test versus external test, manual functions versus

automation, hardware versus software approaches, component selection and standardization, reliability versus maintainability, levels of repair versus discard decisions, and so on.

- ◊ Alternative supplier sources for a given item.
- ◊ Alternative production approaches, such as continuous versus discontinuous production, quantity of production lines, number of inventory points and levels of inventory, levels of product quality, inspection and test alternatives and so on.
- ◊ Alternative product disposal and recycling methods.
- ◊ Alternative management policies and their impact on the system.

In brief, there is no single definition or protocol that exists for process and product life-cycle costing. This leads to inconsistency and confusion as which costs are included and which are excluded from the analysis. The best way to avoid this confusion is to make clear boundary conditions on every stages of the life cycle.

2.1.3. Literature review and background on Switchgrass

Switchgrass(*Panicumvirgatum L.*) is a perennial grass native to Central and North America. It is a promising bioenergy source for the following reasons: long life (more than 10 years), high productivity, adaptability, and high potential of integration

into conventional agricultural operation. There is a significant opportunity for using switchgrass in ethanol production and also combustion fuel source for power production due to its high cellulosic content. Switchgrass can be grown in many different regions including marginal land areas due to its highly adaptability and persistence. Moreover switchgrass is tolerant to cold weather and disease[49][50][51][52].

There are many environmental benefits from growing switchgrass such as increasing soil quality, reduced losses of soil nutrients, and recycling nutrients from municipal and agricultural wastes, soil carbon sequestration, and mitigating greenhouse gas emissions. There are 14 million hectare (ha) of Conservation Reserve Program (CRP) lands, which were created by the USA Food Security Act of 1985, in order to remove land from crop production and place a long term resource-conserving vegetation cover to prevent soil erosion, improve water quality, and enhance wildlife habitat. These lands have the potential to be used as areas for biomass production[52][53].

Switchgrass can be separated into two categories, namely upland and lowland types. The upland types are suited to drier soils and are better in semi-arid climates. On the other hand, the lowland types grow better in heavier soils and require more

water. However, the lowland types have a higher dry mass production than the upland type. The upland types include Trailblazer, Blackwell, Cave-in-Rock, Pathfinder and Caddo. Alamo and Kanlow are the lowland types[49].

Lemus et al. [54] state that the mean yield of 20 switchgrass cultivars grown in southern Iowa and harvested in autumn 1998 through 2001 was 9.0 Mg ha^{-1}. Fikeet al. [55] reported that because of the Lowland switchgrass greater productivity, they appeared better suited to biomass production in the upper southeastern USA. For the upland switchgrass, two cuts per year may be benefit dependent on production cost and feed stock quality. On the other hand, for the lowland switchgrass, two harvests per year may not have adequate biomass yield.

Table 2.4 Switchgrass cultivars and characteristics for upland varieties [49]

Upland Varieties	Characteristics
Trailblazer	Developed by USDA-ARS and Nebraska Agricultural Research Division, Dept. of Agronomy, Univ. of Nebraska. Released 1984. Collections from natural grasslands in Nebraska and Kansas. Adapted to Central Great Plains and adjacent Midwestern states.

Upland Varieties	Characteristics
Blackwell	Developed by Plant Materials Center, NRCS, Manhattan, Kansas. Released 1944. Upland-type switchgrass. Widely adapted to Kansas, Oklahoma, southern Nebraska, and northern Texas in areas with 20 inches or more of annual precipitation.
Cave-in-Rock	Plant Materials Center, NRCS in cooperation with the Missouri AES. Released 1973. Tolerant to flooding. Adapted to Midwest
Pathfinder	Selected at Nebraska AES, Lincoln, ARS cooperating. Released 1967. Winter-hardy, late maturing.
Caddo	Selected at Oklahoma AES, Stillwater, ARS cooperating. Released 1955. Forage yield under irrigation outstanding for native grass; recovers well after mowing.

Table 2.5 Switchgrass cultivars and characteristics for lowland varieties [95]

Lowland Varieties	
Alamo	Developed by Texas Agricultural Experiment Station and NRCS, Knox City, Texas. Released 1978. A premier lowland variety, heavy yields especially in the south.
Kanlow	Developed at Kansas AES and ARS, Manhattan. Released 1963. Developed for soil conservation in poorly drained or frequently flooded sites.

The switchgrass cultivars and characteristics for upland and lowland varieties are shown in Table 2.4 and Table 2.5 respectively.

Table 2.6 Biomass yield of several switchgrass varieties cultivars grown in southern Iowa from 1998 to 2001[54]

Varieties	**Yield (Mg ha^{-1})**
Trailblazer	7.9
Blackwell	8.3
Cave-in-Rock	9.3
Pathfinder	7.3
Caddo	7.8
Alamo	12.1
Kanlow	13.1

Table 2.6 shows biomass yield of several switchgrass including both lowland and upland switchgrass. As stated earlier, lowland is more productive than upland switchgrass.

2.2. Model development

In this specific aim, we study LCC and LCA for harvesting, conversion and the use of switchgrass to produce electricity. The model system is defined in Figure 2.5.

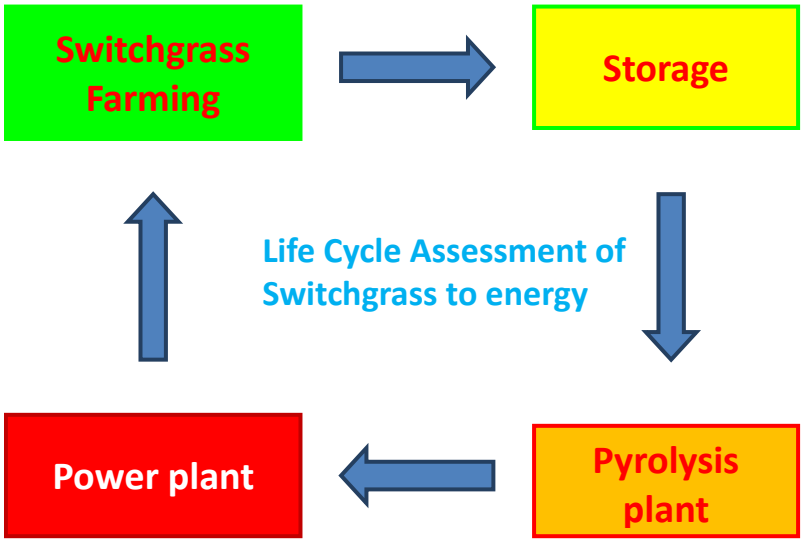

Figure 2.5 Life Cycle Assessment of switchgrass to energy

In Figure 2.5, the process begins with the cultivation and harvesting in switchgrass farming. Subsequently, all the switchgrass is transported to storage. In the next step, switchgrass is transported to the pyrolysis plant to be converted to pyrolysis oil. Next, the pyrolysis oil is transported to the power plant for electricity generation. In this work zero net carbon emission is assumed. All of the GHG emission created at this stage is adsorbed and used in the photosynthesis of switchgrass in switchgrass field.

2.2.1. LCA model

Mass balances are employed as follows.

$$\begin{aligned} &Total\ emission\ for\ LCA\ mode \\ &= (total\ emission\ from\ switchgrass\ field) \\ &+ (total\ emission\ from\ transportation\ of\ switchgrass \\ &+ (total\ emission\ from\ storage\ process) \\ &+ (total\ emission\ from\ pyrolysis\ plant) \\ &+ (total\ emission\ from\ transport\ pyrolysis\ oil) \\ &+ (total\ emission\ from\ power\ plant) \end{aligned} \quad (2.1)$$

$$\begin{aligned} &Total\ emission\ from\ switchgrass\ field \\ &= (total\ emission\ from\ fuel\ used\ in\ the\ field) \\ &+ (total\ emission\ from\ fertilizer\ and\ herbicide) \end{aligned} \quad (2.2)$$

$$\begin{aligned} &Total\ emission\ from\ transportation\ of\ switchgrass \\ &= (total\ emission\ of\ fuel\ used\ in\ transportation) \end{aligned} \quad (2.3)$$

$$\begin{aligned} &Total\ emission\ from\ storage\ process \\ &= (total\ emission\ of\ fuel\ used\ in\ the\ storage\ system) \\ &+ (total\ emission\ from\ the\ mass\ loss\ during\ keeping) \end{aligned} \quad (2.4)$$

$$\begin{aligned} &Total\ emission\ from\ transportation\ of\ pyrolysis\ oil \\ &= (total\ emission\ of\ fuel\ used\ in\ transportation) \end{aligned} \quad (2.5)$$

2.2.2. LCC model

The total cost of the whole process is broken down as follows.

$$\begin{aligned} &Total\ cost\ for\ LCC\ model \\ &= (total\ cost\ from\ switchgrass\ field) \\ &+ (total\ cost\ of\ transportation\ of\ switchgrass \\ &+ (total\ cost\ from\ storage \\ &+ total\ cost\ from\ pyrolysis\ process) \\ &+ (total\ cost\ from\ transportation\ of\ pyrolysis \\ &+ (total\ cost\ from\ power\ plant) \end{aligned} \tag{2.6}$$

$$\begin{aligned} &Total\ cost\ from\ switchgrass\ field \\ &= (total\ cost\ of\ machinery) \\ &+ (total\ cost\ of\ fuel) \\ &+ (total\ cost\ of\ fertilizer\ and\ herbicide) \\ &+ (loan\ interest) \end{aligned} \tag{2.7}$$

$$\begin{aligned} &Total\ cost\ of\ transportation\ of\ switchgrass \\ &= (total\ cost\ of\ fuel\ and\ labor) \end{aligned} \tag{2.8}$$

$$\begin{aligned} &Total\ cost\ from\ storage \\ &= (total\ cost\ of\ construction\ of\ storage) \\ &+ (total\ cost\ of\ fuel\ and\ labor) \\ &+ (total\ cost\ of\ switchgrass\ lost\ during\ storag \end{aligned} \tag{2.9}$$

$$\begin{aligned} &Total\ cost\ from\ pyrolysis\ process \\ &= (total\ cost\ of\ establishing\ pyrolysis\ plant) \\ &+ (operating\ cost) + (switchgrass\ cost) \\ &+ (maintenance\ cost) + (loan\ interest) \end{aligned} \tag{2.10}$$

$$\begin{aligned} &Total\ cost\ of\ transportation\ of\ pyrolysis\ oil \\ &= (total\ fuel\ cost\ and\ labor) \end{aligned} \tag{2.11}$$

$$\begin{aligned} &Total\ cost\ from\ power\ plant \\ &= (capital\ cost) \\ &+ (operation\ cost) \\ &+ (maintenance\ cost) \end{aligned} \tag{2.12}$$

We employed a Dell computer workstation with Intel(R) Xeon(R) CPU E5405 2.00GHz and the Matlab software environment [56]to perform the calculations.

2.2.3. Cost of establishing, reseeding, and producing switchgrass

Table 2.7 The estimated costs of pre-harvest machinery in establishing per hectare [57][58][59][60]

Pre-harvest machinery operations	**Cost without fuel ($/ha)**	**Diesel(gal/ha)**	**Diesel cost ($/ha)**
Disk	31.01	3.46 (13.10 l/ha)	12.97
Harrow	19.10	1.24 (4.69 l/ha)	4.63
Airflow spreader (seed and fertilizers)	31.26	1.48 (5.60 l/ha)	5.56
Spraying chemicals	8.28	0.49 (1.85 l/ha)	1.85
Total	89.65	6.67 (25.25 l/ha)	25.02

Table 2.8 The operating expense in establishing per hectare [57][58][59][60]

Operating Expense	**Price $/unit**	**Unit/ ha**	**$/ha**
Seed	$7.5 /lb ($16.5/kg)	14.83 lb (6.74 kg)	111.20
Fertilizer			
N	$0.31 /lb ($0.68/kg)	264.55 lb (120.25 kg)	82.01
P	$0.37 /lb ($0.81/kg)	74.13 lb (33.70 kg)	27.43
K	$0.23 /lb ($0.51/kg)	98.84 lb (44.93 kg)	22.73
Lime	$21 /ton	7.41 ton	155.68
Herbicides			
Pursuit +	$53/gal ($14.00/l)	7.41oz(0.22 l)	3.06
MSO	$1.75/pt ($3.70/l)	79.07oz (2.34 l)	8.65

Operating Expense	Price $/unit	Unit/ ha	$/ha
2,4D	$16/gal ($4.23/l)	3.71pts (1.76 l)	7.41
Total operating costs			418.17

Table 2.9 Total cost and prorated yearly in establishing per hectare

Total cost and prorated yearly	$/ha
Total Pre-harvest machinery	89.65
Total operating costs	418.17
Total establishment(11 years at 8% amortization (.14008 factor))	532.84
Prorated yearly establishment Cost per ha	72.99

Table 2.10 The estimated GHG emission for establishing switchgrass per hectare [57][58][59][61][60]

Pre-harvest machinery operations, fertilizer and herbicides	CO_2 (kg/ha)	N_2O (kg/ha)	CH_4 (kg/ha)	Estimate CO_2 equivalent/ ha
Disk	37.10	0.0152	0.0020	41.85
Harrow	13.25	0.0054	0.0007	14.95
Airflow spreader (seed and fertilizers)	15.90	0.0065	0.0009	17.93
Spraying chemicals	5.30	0.0022	0.0003	5.98
Fertilizer (N)		5.050	1.20	1590.94
Herbicides				79.8
Total	71.56	5.079	1.204	1751.44

Table 2.11 The estimated pre-harvest machinery operations cost in reseeding per hectare [57][58][59][60]

Pre-harvest machinery operations	Cost without fuel ($/ha)	gal of diesel/ha	diesel cost ($/ha)
Airflow spreader (seed and fertilizer)	31.26	1.48 (0.70 l/ha)	5.56
Spraying chemicals	8.28	0.49 (0.23 l/ha)	1.85
Total	39.54	1.97 (0.93 l/ha)	7.41

Table 2.12 The estimated operating expense in reseeding year per hectare [57][58][59][60]

Operating Expense	Price/unit	Unit/ha	$/ha
Seed	$7.5 /lb ($16.5/kg)	3.71 lb (1.69 kg)	27.80
Fertilizer			
N	$0.31 /lb ($0.68/kg)	264.55 lb (120 kg)	82.01
P	$0.37 /lb ($0.81/kg)	74.13 lb (32.62 kg)	27.43
K	$0.23 /lb ($0.51/kg)	98.84 lb (44.83 kg)	22.73
Herbicides			$/ha
Pursuit +	$53/gal ($14.00/l)	7.41oz (0.22 l)	3.06
MSO	$1.75/pt ($3.70/l)	79.07oz (2.34 l)	8.65
2,4D	$16/gal ($4.23/l)	3.71pts (1.76 l)	7.41
Total operating costs			179.09

Table 2.13 Total cost and prorated yearly in reseeding per hectare

Total cost and prorated yearly	**$/ha**
Total Pre-harvest machinery	46.95
Total operating costs	179.09
Total reseeding costs (10 years at 8% amortization (.14903 factor))	226.04
Prorated yearly reseed Cost per ha	32.91

Table 2.14 The estimated GHG emission for reseeding switchgrass per hectare [57][58][59][61][60]

Pre-harvest machinery operations ,fertilizer and herbicides	**CO_2 (kg/ha)**	**N_2O (kg/ha)**	**CH_4 (kg/ha)**	**Estimates CO_2 equivalent /ha**
Airflow spreader (seed and fertilizer)	15.90	0.0065	0.0009	17.93
Spraying chemicals	5.30	0.0022	0.0003	5.98
Fertilizer (N)		5.0500	1.20	1590.94
Herbicides				79.8
Total	21.20	5.0587	1.2012	1694.65

Switchgrass field is assumed to deliver 9 tons of switchgrass per hectare.

Table 2.15 The estimated costs per hectare of pre-harvesting machinery operations for production year per hectare [57][58][59][60]

Pre-harvest machinery operations	**Cost without fuel ($/ha)**	**gal of diesel/ha**	**diesel cost ($/ha)**
Bulk fertilizer spreader	8.28	0.49 (1.85 l/ha)	1.85
Liquid N application and Sprayer	17.42	1.48 (5.60 l/ha)	5.56
Total	25.70	1.97 (7.46 l/ha)	7.41

Table 2.16 The estimated operating expense in production year per hectare [57][58][59][60]

Operating Expense	**Price $/unit**	**Unit/ha**	**$/ha**
Fertilizer			
N	$0.31/lb ($0.68/kg)	247.11 lb (112.09 kg)	76.60
P	$0.37/lb ($0.81/kg)	4.79 lb (2.17 kg)	1.77
K	$0.23/lb ($0.51/kg)	56.34 lb (25.56 kg)	12.96
Herbicides			
Pursuit +	$53/gal ($14.00/l)	7.41oz (0.22 l)	3.06
MSO	$1.75/pt ($3.70/l)	79.07oz (2.34 l)	8.65
2,4D	$16/gal ($4.23/l)	3.71pts (1.76 l)	7.41
Total			110.45

Table 2.17 The estimated cost of harvest machinery operation in production year per hectare [57][58][59][60]

Harvest machinery operations	**Cost without fuel ($/ha)**	**gal of diesel/ha**	**diesel cost ($/ha)**
Mow/conditioning	36.37	2.792 (10.57 l/ha)	10.47
Rake	13.81	0.766 (2.90 l/ha)	2.87
Baling: large square	45.22	2.644 (10.01 l/ha)	9.92
Staging	49.42	2.471 (9.35 l/ha)	9.27
Total	144.83	8.67 (32.82 l/ha)	32.53

Table 2.18 The total cost and prorated yearly in production year per hectare

Total cost in production year	**$/ha**
Total Pre-harvest machinery operations	33.11
Total operating expense	110.45
Total Harvest machinery operations	177.36
Yearly production Costs per ha	320.92
Prorated establishment cost	72.99
Prorated reseeding cost	32.91
Total Production costs	426.82
Production costs per ton	47.42

Table 2.19 estimated GHG emission for pre-harvest machinery operations, fertilizer, and herbicide per hectare [57][58][59][60][61]

Pre-harvest machinery operations, fertilizer, and herbicide	**CO_2 (kg/ha)**	**N_2O (kg/ha)**	**CH_4 (kg/ha)**	**Estimate CO_2 equivalent /ha**
Bulk fertilizer spreader	5.30	0.0022	0.0003	5.978
Liquid N application and Sprayer	15.90	0.0065	0.0009	17.93
Fertilizer (N)		4.72	1.12	1486.00
Herbicides				79.8
Total	21.20	4.7287	1.1212	1589.71

Table 2.20 estimated GHG emission for harvest machinery operations per hectare [57][58][59][61][60]

Harvest machinery operations	**CO_2 (kg/ha)**	**N_2O (kg/ha)**	**CH_4 (kg/ha)**	**Estimate CO_2 equivalent /ha**
Mow/conditioning	29.95	0.012	0.0016	33.76
Rake	8.216	0.003	0.0004	9.27
Baling: large square	28.36	0.012	0.0015	31.98
Staging	26.50	0.011	0.0014	29.89

Table 2.7 to Table 2.10 show the estimated costs of establishing the switchgrass and GHG while Table 2.11 to Table 2.14 show the estimated reseeding costs per ha and GHG. Table

2.15 to Table 2.20 shows the estimated yearly production costs per ha and GHG.

2.2.4. Biomass transportation

In this work, we assumed that switchgrass was collected from the field to the pyrolysis plant located in the center of the circle with radius R_{circle} . Overend[62] developed a model to compute the transportation distance between the point of harvesting biomass and the central processing plant.

$$R_{circle} = 0.6833\tau\sqrt{\frac{n}{\phi}}\sqrt{\frac{P}{M}} \tag{2.13}$$

τ is the tortuosity factor of the road; this is a function of the terrain and can range from 1.27 where a regular rectangular road grid is superimposed over a flat terrain to in excess of 3 for a complex or hilly terrain constrained by geographical features such as lakes and swamps. n is the number of sectors to complete a circle. ϕ is the fraction of terrain devoted to switchgrass. P is the pyrolysis plant scale in ton/day. M is the switchgrass productivity in ton/(ha*year). It is assumed that switchgrass is transported by 20 tons semi-trucks.

$$A = \frac{P \times 330\, days}{M\phi}(ha) \tag{2.14}$$

A is the area of switchgrass field in ha units. The switchgrass is assumed to be grown by farmers around the pyrolysis plant.

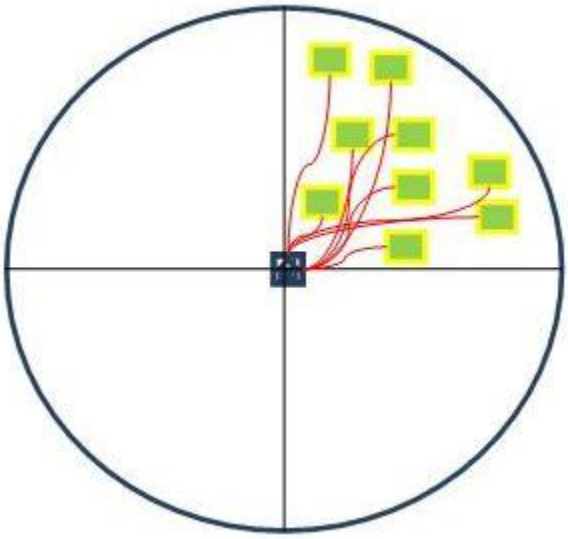

Figure 2.6 Calculating harvesting distance from farm to central pyrolysis plant

In Figure 2.6, switchgrass is grown in different farms in the upper right quadrant. The number of sectors to complete a circle is four since the circle separated into four pieces. The fraction of terrain devoted to switchgrass is total area of every farm per area of the upper right quadrant. The red line is the road between a farm and a pyrolysis plant.

We assume that 20 tons of switchgrass is transported per truck. The truck mileage is assumed to be 2.4 km/l [63]. The

driver cost is assumed to be $0.6/mile ($0.38/km). We assume that 4% of switchgrass is lost during transportation.

2.2.5. Land use change effect

There are many studies that have reported on the amount of carbon deposited into the soil after growing switchgrass. Planting switchgrass can increase the carbon deposit rate by 0.2 to 1.1 tons of carbon per hectare per year [64]. Carbon dioxide was reported to be sequestered into the soil at a rate of 1.79 tons of carbon per hectare per year[65]. Francesco et al. [66] assumed a C sequestration rate of 0.6 tons of carbon per hectare per year. In this specific aim, the value of soil organic compound at 0.49 tons of carbon per hectare per year is assumed for the first two years of establishment; thereafter 1.5 tons of carbon per hectare per year is assumed for mature crop[67].

2.2.6. Storage

Table 2.21 Initial construction costs of the selected storage systems (storage losses are not included)[68]

Storage system for square bales (950lb/bale)	**Cost per m^2 ($)**	**Life years**	**Annual costs ($/$m^2$)**	**Cost per bale ($/bale)**
				10 bales high
Collective storage facility	107.64	15	12.58	3.77

Storage system for square bales (950lb/bale)	Cost per m^2 ($)	Life years	Annual costs ($/$m^2$)	Cost per bale ($/bale)	
				5 bales high	6 bales high
Pole frame structure-enclosed on crushed rock	70.39-107.64	15	8.22-12.58	4.93-7.55	4.11-6.29
				4 bales high	
Reusable tarp on crushed rock (19.8 sq. ft/bale i.e. 1.84 m^2/bale)	1.47	5	0.37	1.39	
Outside Unprotectected on crushed rock	2.70	5	0.68	0.51	
Outside and Unprotected on ground	0.00	-	0.00	0.00	

Table 2.22 Storage systems and expected dry matter loss[68]

Storage system for square bales (950lb/bale)	Average DM loss (%)
Pole frame structure-enclosed on crushed rock	2
Pole frame structure-open sides on crushed rock	4
Reusable tarp on crushed rock	7
Outside Unprotected on crushed rock	15
Outside and Unprotected on ground	25

Table 2.21 shows Initial construction costs of the selected storage systems (storage losses are not included). From Table 2.22, the pole frame structure-enclosed on crushed rock (used in our work) loses the least amount of switchgrass compared with other storage types. We assume that the labor cost is $12/hour and the tractor cost is $20/hour. The unloading time and storage time for one truck is half hour. The unloading time from storage is 20 min. Emission from the storage process is 0.92 kg CO2 eq. per ton of switchgrass.

2.2.7. Pyrolysis oil production

In this dissertation we have chosen pyrolysis for producing bio-oil. Boateng et al. [15] designed a bench-scale pyrolysis reactor to convert switchgrass to bio-oil. We assumed a pyrolysis plant based on the authors' work. Results from the authors show that switchgrass pyrolysis could yield over 85% of mass basis. The product consists of bio-oil 60.7%, bio-char 11.3% and non-condensable gas 12.9% in mass basis. The non-condensable gas consists of CO_2 29%, CO 57.6%, H_2 5.1%, and CH_4 7.8% by volume. In this work, the bio-oil product is assumed to be 60.7%wt as the lowest yield for switchgrass that author suggested. The pyrolysis oil is assumed to be transported by a tank truck capacity of 11600 US gallons. The mileage of the tank

truck is 2.4 km/l[63]. Emission from the storage process is 6.2×10^{-3}kg CO_2 eq. per ton of switchgrass.

Table 2.23 Biorefinery capital cost components based on the reference plant size[69]

Capital cost for fast pyrolysis (28mmgpy bio-oil)	**Cost(millions)**
handling and drying	5.57
pyrolysis reactor	3.92
Quench	1.94
heat recovery	1.14
product recovery and storage	0.8
recycle	1.38
steam and power production	3.16
utilities	3.13
contingency	7.37
total	28.41

Table 2.24 Biomass fast pyrolysis annual operating cost components based on the reference plant size[69]

Fast pyrolysis operation cost	**cost**	**explanation**
water treatment	1	linear scaling
electricity	0.21	linear scaling
labor	1.34	0.6 power law scaling
overhead	0.8	60% labor
maintenance	0.57	2% equip
insurance/taxes	0.72	1.5% TCI
charcoal (credit)	1.92	50/ton

Table 2.25 Production from switchgrass pyrolysis[15]

Product	**% wt**
bio-oil	60.7%
bio-char	11.3%
non-condensable gas	12.9%

Table 2.26 Properties of pyrolysis oil [15]

Property	
Density at 15°C, kg/l	1.25
kinematic viscosity at 50 °C, cSt	13.11
kinematic viscosity at 100 °C, cSt	2.54
heat of combustion, MJ/kg	16.02
ash at 775 °C, wt %	0.01

Table 2.23 shows the biorefinery capital cost while Table 2.24 shows the operating cost for the plant. Table 2.25 shows production from switchgrass pyrolysis. Properties of pyrolysis oil are shown in Table 2.26.

2.2.8. Power generation

Power generation from fossil fuels is one of the major green house gas producers; an estimated one third of the carbon dioxide emission is from Europe. The pyrolysis oil can be used as a substitute for fossil fuels in conventional power plants such as gas engines, gas turbines, and coal fired plants in order to reduce green house gas emissions. Pyrolysis oil is acidic, unstable, contains solid residue, and many chemicals in bio-oil dissolve in water. The heating value, density, and viscosity of bio-oil depend on water and additives in the bio-oil, which also differs from fossil fuels. These factors are problematic in using pyrolysis oil in conventional power plants. Despite these problems, bio-oil still can be used in the

conventional power plants by modifying the engines as many studies suggest[7][13].Balat et al. [70] also suggested the main route of using the bio-oil in boilers, diesel engines or gas turbines for heat and electricity generation. In this work, the power plant is assumed to operate 8760 hour/year. The main power technologies we considerare:

Table 2.27 Power plant efficiency

Power plant	Efficiency
Diesel Engine	32.4% [13]
Gas turbines	42% [71]
Steam turbine coal-fired power plant	33% [71]
Steam turbine fuel-oil power plant	34% [72]

Table 2.28 Specification on wt% of pyrolysis liquid component (to be able to use as fuel in boilers, engines and turbines)[73]

Component	Specification to be met	Pyrolysis oil from reference switchgrass[15]
Water	<27 wt%	23 wt%
Total solids	<0.01 wt%	0.01 wt%*
Inorganics	<0.01 wt%	0.01 wt%*

*ash content

Table 2.27 shows power plant efficiencies. Table 2.28 shows specification on wt% of pyrolysis liquid component (to be able to use as fuel in boilers, engines and turbines). Comparing specification pyrolysis oil from Oasmaa et al. with pyrolysis

oil from switchgrass, we assume that the pyrolysis oil from switchgrass can be used boilers, engines and turbines.

(1) Diesel Engine power plant

Yoshikawa[74] studied the efficiency of the diesel engine in power plants when using low-BTU fuel gas which was produced by pyrolized solid fuel. The result showed that the efficiency of diesel engines was about 30%. Solantausta et al. [75] reported the efficiency of 34% using pyrolysis oil in diesel. In this dissertation, the thermal efficiency of diesel engines which use pyrolysis oil is assumed to be 32.4% [13].

(2) Pyrolysis oil substituting natural gas in gas turbines

In order to use pyrolysis oil in gas turbines, the gas turbine engine must be modified and pyrolysis oil needs to be upgraded. The gas turbine engine must be able to resist low pH substance, which is pyrolysis oil. The nozzles must be modified for higher flow cause by lower heating value and higher viscosity of pyrolysis oil. The pre-heating unit to heat the pyrolysis oil to 70-90°C is necessary to reduce the viscosity of pyrolysis oil to less than 10 cSt[13]. However, Wagenaar et al. [76] reported the use of bio-oil to substitute the natural gas in the real power plant. The experiment showed the possible of using pyrolysis oil in the gas turbine power plant. Herdin et

al. [77] reported the efficiency of gas turbine for electric generation using natural gas was 45%. In this dissertation, the efficiency of pyrolysis oil in gas turbines engine is assumed to be 42% which is the same as Jaramillo's dissertation.

(3) Steam turbine generator

In this work, pyrolysis oil is being used as a replacement for coal and fuel oil in a steam turbine generator. Steam turbine generators use fuel combustion in a boiler to produce steam. Next, steam is injected into steam turbine to generate electricity. Normally, steam turbines have a lower efficiency compared to a reciprocating engine such as diesel engine or gas turbines but overall efficiency can be higher[78]. In order to operate the boiler with pyrolysis oil, some modification is needed to improve combustion stability. A support fuel is needed to start up the boiler. In case of low quality pyrolysis oil, support fuel is needed during operation. Pyrolysis oil has a longer flame than standard fuel oil. Schreiner et al.[79]investigated the use of biomass pyrolysis in the coal power plant. Their work showed promising result. The combustion of pyrolysis oil in the boiler is clean and efficient[80]. In this work, we assume that operating a coal power plant by using pyrolysis oil is going to give the same 33% efficiency as using

coal in the operation [71]. Pyrolysis oil (as a substitute for fuel oil) is assumed to have an efficiency of 34% [72].

Table 2.29 Power Generation capital, operation and maintenance cost per kWyr for different power plants[81]

System	Annual fixed capital cost, $/kWyr	Annual fixed operation and maintenance cost, $/kWyr
Diesel engine	75.00	3.00
Natural-gas-fired combustion turbine	32.00	3.25
Coal-fired steam cycle	120.00	6.25
Oil-fired steam cycle	96.00	5.50

Annual capital, operation and maintenance cost per kilo-watt year for different power plants are shown in Table 2.29.

2.3. Result, discussion, and conclusion

This work views the switchgrass as a source of energy for different power plants. The LCA and LCC are used for understanding total emission and economics over the switchgrass pyrolysis from cradle-to-grave. We started by calculating all impacts from growing switchgrass in an empty field to a final user, which is a power plant. The mass and energy balance is applied in this work to calculate the life cycle assessment.

2.3.1. Pyrolysis plant capacity effect

The different capacities of pyrolysis plant from 100 ton per day to 5000 ton per day of switchgrass are assumed to be used to produce pyrolysis oil. The effect of the pyrolysis plant capacity will be shown in both the LCA and LCC. The total GHG emission, area used to grow switchgrass, switchgrass price, pyrolysis oil price and electric price are affected by the capacity of pyrolysis plants. We assume that the distance from the pyrolysis plant to the power plant is 60 km.

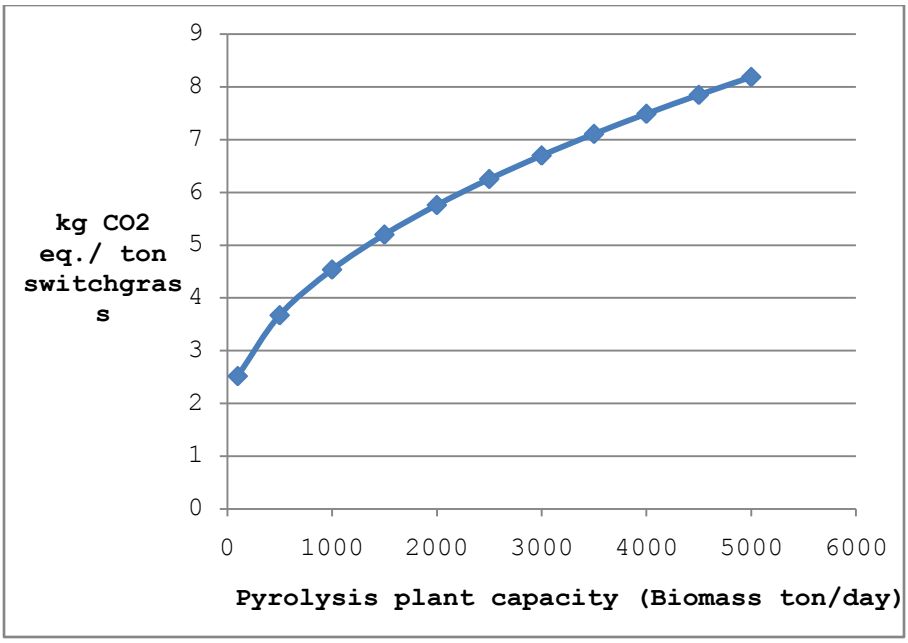

Figure 2.7 dependence of emission from switchgrass transportation on pyrolysis plant capacity

In Figure 2.7, emission from transportation of switchgrass to storage depends on the distance from the field to storage that means emission per ton of switchgrass increasing as the plant capacity increasing.

2.3.2. Switchgrass production

The switchgrass price per ton is considered by two life cycle stages:

(1) switchgrass cultivation and harvesting

(2) transportation

In this analysis, the switchgrass is grown in a circular field, which has a land fraction of 0.441. This land faction is

the same as the average agriculture land fraction for the USA[82].

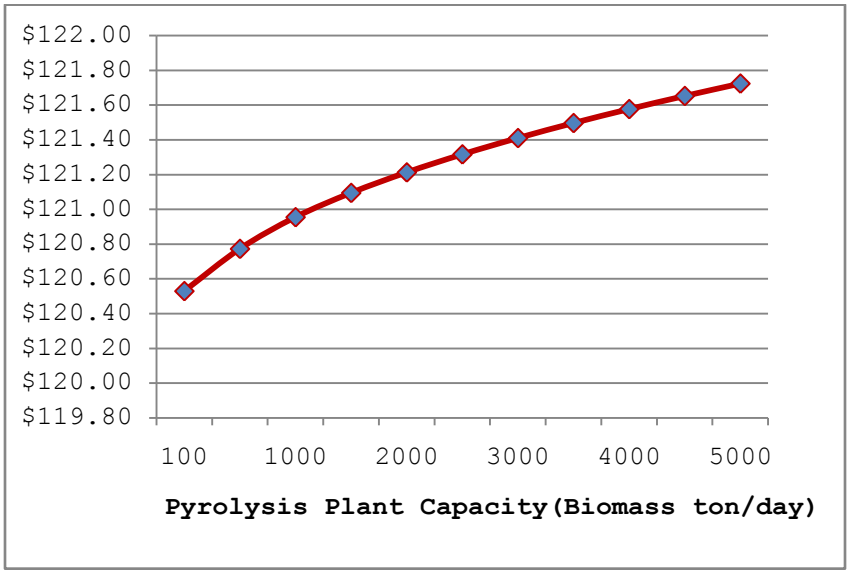

Figure 2.8 Switchgrass price versus Pyrolysis plant capacity

Figure 2.8 shows that the price of switchgrass is increased by increasing the capacity of the pyrolysis plant. For example, if the pyrolysis plant capacity increases from 100 tons per day to 5000 tons per day, the switchgrass price increases more than one dollar per ton from $120.53 to $121.72 per ton. The price increase is due to the longer delivery distance for the switchgrass and the bigger area needed for switchgrass harvesting.

2.3.3. Area of switchgrass field

Normally, the area to grow switchgrass gets larger as the capacity of the pyrolysis plant increases. In this study, the

loss of the switchgrass in transportation and processing is approximately 4% weight[83]. We choose a pole frame structure-enclosed on crushed rock as a storage system because it loses only 2%[68] weight of the switchgrass in storage. Even if the price of building storage in the pole frame is high, we lose less switchgrass from this storage. As a result, we need less area to grow it. The land fraction used for switchgrass was 0.441 in a circular shape field.

The relationship between pyrolysis plant capacity and area of switchgrass field is a simple linear equation, namely $y = 88.38x$ .From this equation we conclude that one ton of pyrolysis plant capacity needs 88.38 ha of switchgrass field, a rather large area. To put this in perspective, for 5000 tons per day of pyrolysis plant capacity, the corresponding land area of 441880 Ha (1034 square miles) is bigger than the land area of Rhode Island.

2.3.4. Pyrolysis oil production

In order to produce pyrolysis oil from switchgrass, there are three life cycle stages:

(1) switchgrass cultivation and harvesting

(2) transportation

(3) storage

The pyrolysis plant produces three products: NCG, pyrolysis oil and bio-char. The ratio of pyrolysis oil produced is 60.7% w/w. NCG is 12.9% w/w and bio-char is 11.3%w/w. The NCG and bio-char are used in the pyrolysis plant as an energy source to operate the pyrolysis plant. Therefore, the net product from this plant is only pyrolysis oil, which is assumed to be sold to different power plants as a substituted energy source.

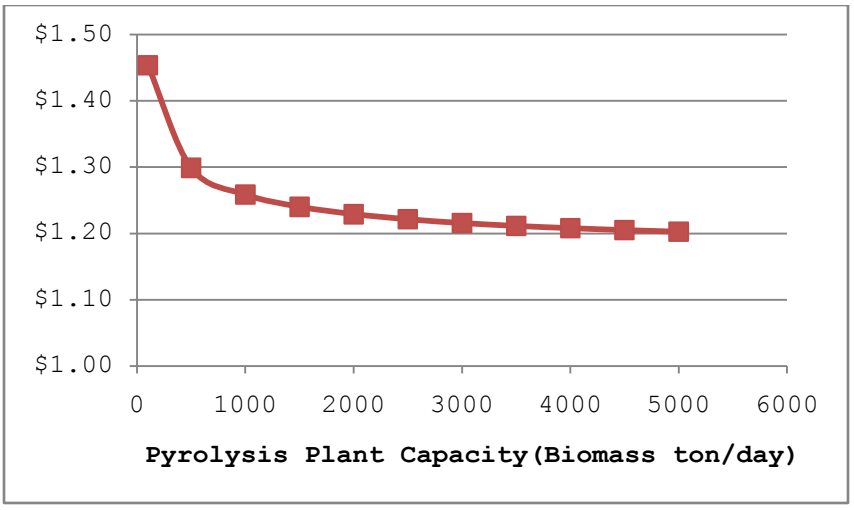

Figure 2.9 Pyrolysis oil price versus Pyrolysis plant capacity

From Figure 2.9, the pyrolysis oil price decreases, while the pyrolysis plant size increases. The price of pyrolysis oil is $1.45 per gal at a capacity of 100 tons per day, while

pyrolysis oil price reduces to $1.20 per gal at a capacity of 5000 tons per day.

2.3.5. Electricity produced by pyrolysis oil in different power plants

In order to produce electricity from switchgrass, we considered four life cycle stages:

(1) switchgrass cultivation and harvesting

(2) transportation and storage

(3) pyrolysis production and transportation

(4) electric generator

There are four kinds of power plants:

(1) Diesel engine power plant

(2) Natural-gas-fired combustion turbine power plant

(3) Coal-fired steam cycle power plant

(4) Oil-fired steam cycle power plant.

The Natural-gas-fired combustion turbine power plant is the most efficient plant having an efficiency of 42%, while the diesel engine power plant is the lowest efficiency at 32.4%. The Coal-fired steam cycle power plant and Oil-fired steam cycle power plant have an efficiency of 33% and 34% respectively.

(1) Amount of electricity produced by different power plants vary with pyrolysis plant capacity

Table 2.30 Slope of electricity produced by different power plants vary with pyrolysis plant capacity

$y = mx$	**Slope** (m)
Natural-gas-fired combustion turbine	0.114
Oil-fired steam cycle	0.093
Coal-fired steam cycle	0.090
Diesel engine power plant	0.088

Electricity produced by different power plants varies with pyrolysis plant capacity in a linear fashion as $y = mx$. The slopes for different power plant are shown in the table above. The slope for natural-gas fired combustion turbine power plant is the largest while the slope for diesel engine power plant is the smallest.

It can be concluded that the natural-gas fired combustion turbine will produce a higher amount of electricity (11.44 Mw) than the diesel engine (8.83 Mw), when both are supplied with equal amounts of pyrolysis oil from a plant of capacity 100 tons per day. At a plant capacity of 5000 tons per day, the natural-gas-fired combustion turbine produces 572.13 Mw, while the diesel engine could produce 441.36 Mw. With 572.13 Mw of electricity or 5011.86 million kilowatt-hours, it can provide

enough electricity for the entire state of Hawaii. From the report of the U.S. Energy Information Administration in 2012 [84], Hawaii consumed 4723 million kilowatt-hours.

(2) Price of electricity per kwh produced from different power plants

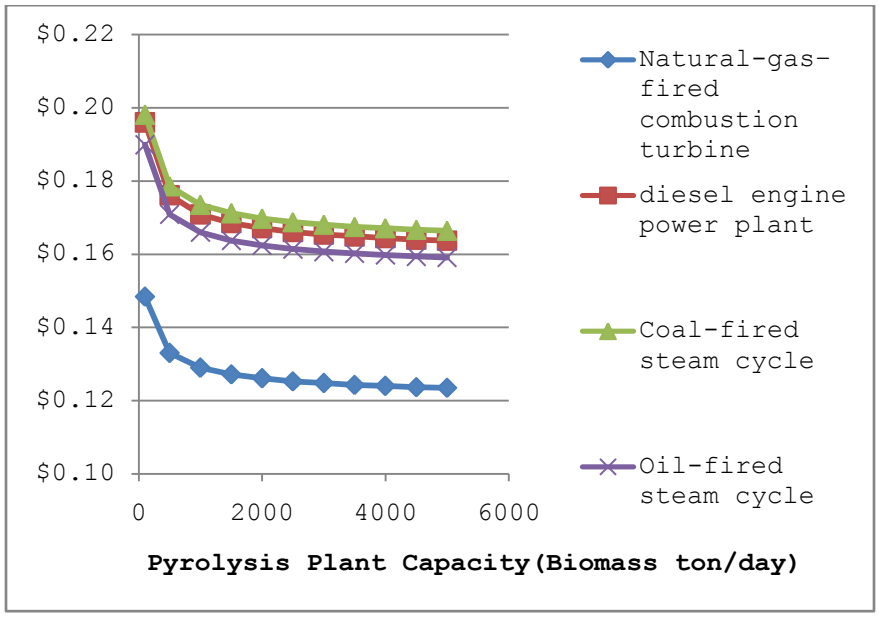

Figure 2.10 Price of electricity in different power plants versus pyrolysis plant capacity

From Figure 2.10, it can be concluded that because the natural-gas-fired combustion turbine is the most efficient power plant compared with others, it produces the cheapest electricity. The pyrolysis plant capacity of 100 tons of switchgrass can supply the natural-gas-fired combustion turbine to produce electricity at a price of $0.15 per kwh. The price could drop to $0.12 per kwh with the pyrolysis plant at a

capacity of 5000 tons per day. The highest electric price was produced by the coal-fired steam cycle since the capital cost and maintenance cost is the highest. The electric cost was $0.20 per kwh for the pyrolysis plant at capacity of 100 tons per day. The price could drop to $0.17 per kwh for the pyrolysis plant at capacity of 5000 tons per day. From the U.S. Energy Information Administration [85], the average electricity cost in the United States in 2011 was $0.10 per kwh. From the analysis, the cost of electricity from combustion of bio-oil is higher than the normal average electricity cost in the United States.

2.3.6. GHG emission per kwh

Because the average agricultural land in the US is about 44.1% [82] of the entire US land, we assume that the average percentage of land use to grow switchgrass is 44.1% (land fraction). The land shape was assumed to be circular. The total GHG emission per kwh of using pyrolysis oil from switchgrass is negative because carbon dioxide is sequestrated into the soil while growing switchgrass. The value of soil organic compound increasing at the rate of 0.49 tons of carbon per hectare per year is used for the first two years of establishment and reseeding case [67] and 1.5 tons of carbon per hectare per year is used for mature crop case. The natural-gas-fired combustion turbine seems to have higher GHG emission per kwh because this

power plant was assumed to have highest efficiency at 42% while others have efficiency around 32-34%. In order to calculate GHG emission per kwh, firstly we calculate an accumulation of GHG emission from starting of seeding year through the end of switchgrass live cycle at the eleventh year. Secondly, we average the total GHG emission per kwh, which is produced during nine years of operation of the power plant.

Table 2.31 variation of total emission (of different power plants) with pyrolysis plant capacity

$y = mx + c$	**Slope** (m)	**Intercept** (c)
Natural-gas-fired combustion turbine	1.428×10^{-7}	-0.485
Oil-fired steam cycle	1.8×10^{-7}	-0.599
Coal-fired steam cycle	1.8×10^{-7}	-0.617
Diesel engine power plant	1.8×10^{-7}	-0.626

The relationship of total emission (of different power plants) with pyrolysis plant capacity can be expressed as $y = mx + c$. The slopes and intercepts are shown in Table 2.31.

Because the natural-gas-fired combustion turbine is the most efficient power plant, which generated most electricity, its GHG emission per kwh is the highest. However, all the GHG results are negative which mean the GHG is adsorbed to the system. Results from Table 2.31 show that the pyrolysis plant

capacity almost has either no effect, or only a small effect on GHG emission as the capacity increases. From the results of LCA, switchgrass pyrolysis leads to clean energy, which can reduce the GHG emission.

2.3.7. Distance from pyrolysis plant to power plant effect on pyrolysis oil price

The relationship of dependence of price of pyrolysis oil on distance from pyrolysis plant to power plant is linear as:

$$y = 1.23 \times 10^{-4} x + 1.251$$

From the equation above, the price of pyrolysis oil is higher if the distance between the pyrolysis plant and the power plant is larger. However, since the slope is close to zero, the pyrolysis oil price only varies slightly with the distance. At zero distance, (the pyrolysis plant and the power plant are at the same location), pyrolysis oil price is $1.251 per gal. When the distance between the pyrolysis plant and the power plant is 120 km, the pyrolysis oil price is $1.266 per gal.

The relationship of dependence of electric cost on distance between pyrolysis plant and power plant is also linear. The slope and intercept are shown in the table below:

Table 2.32 Slope and intercept in linear relation for dependence of electric cost on distance between pyrolysis plant and power plant

$y = mx + c$	**Slope** (m)	**Intercept** (c)
Natural-gas-fired combustion turbine	9.33×10^{-6}	0.128
Oil-fired steam cycle	1.20×10^{-5}	0.165
Coal-fired steam cycle	1.20×10^{-5}	0.173
Diesel engine power plant	1.27×10^{-5}	0.170

Since the slope is close to zero, the distance from the pyrolysis plant and the power plant had a minor effect on the electricity cost. The type of power plant is the determining factor for decreasing electricity cost. The natural gas turbine power plant produces the cheapest electricity. At zero distance, the electricity cost was 12.83 cent per kwh. At 120 km, the electricity cost is 12.97 cent per kwh. The most expensive electricity comes from substituting pyrolysis oil into the coal-fired, steam-cycle power plant. At zero distance, the electricity cost is 17.26 cent per kwh. At 120 km, the electricity cost increases to 17.44 cent per kwh. At these electricity costs, substituting pyrolysis oil in the power plant is not competitively priced compared to fossil fuel.

The relationship of the dependence of total GHG emission on distance between pyrolysis plant and power plant is also linear. The slopes and intercepts are shown in table below:

Table 2.33 Slope and intercept for dependence of total GHG emission on distance between pyrolysis plant and power plant

$y = mx + c$	**Slope** (m)	**Intercept** (c)
Natural-gas-fired combustion turbine	3.92×10^{-5}	-0.487
Oil-fired steam cycle	4.83×10^{-5}	-0.602
Coal-fired steam cycle	5.00×10^{-5}	-0.620
Diesel engine power plant	5.08×10^{-5}	-0.6312

Since the slope is close to zero, the distance between the pyrolysis plant and the power plant has a minor effect on GHG emission per kwh. The type of power plant has affected GHG emission per kwh more so than the distance. All of the power plants, which used pyrolysis oil substituted for fossil fuel, had negative GHG emission. The most negative GHG emission per kwh comes from the diesel engine power plant. At zero distance, the GHG emission per kwh of the diesel engine power plant is -0.6251 kg CO_2 eq./kwh. At 120 km, the GHG emission per kwh is -0.6312. The natural gas turbine power plant has less negative GHG emission compared to other power plants. At zero distance,

the GHG emission per kwh is -0.4869 kg CO_2 eq. per kwh. At 120 km, the GHG emission per kwh is -0.4822 kg CO_2 eq. per kwh.

Table 2.34 Life-cycle assessment of green house gas emissions (kt eq. CO_2 per Twh)[86]

	emission rate kt CO_2eq. per TWh
Diesel engine power plant	649
Natural gas turbine power plant	422
Oil-fired steam-cycle power plant	841
Coal-fired steam-cycle power plant	941

Comparing the GHG emission of pyrolysis oil from switchgrass to that of conventional fossil fuels (reported in Table 2.34), the GHG emission from pyrolysis oil was desired. All of the power plants that used pyrolysis oil from switchgrass were environmentally friendly since total GHG emission from the process was negative. Based on this analysis, the switchgrass field adsorbed more GHG than was emitted from other processes.

2.3.8. Land fraction and field shape effect

In this study, the land fraction and field shape effect has been analyzed. The land fraction and field shape have an effect on switchgrass price, pyrolysis oil price, electricity cost, and GHG emission per kwh. The field was divided into numbered

sectors to complete a circle (n). The $n=1$ represented a complete circles-like shape. The n =10 to 16 represented the long, narrow shapes of the divided sectors.

Land fraction and field shape effect many parameters.

(1) Land fraction and field shape effect on switchgrass price

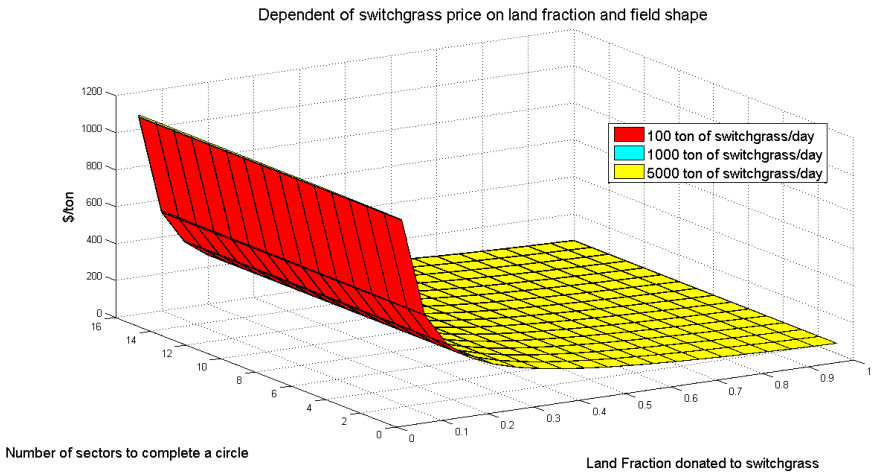

Figure 2.11 Dependency shape of switchgrass price on land fraction and field

From Figure 2.11, the land fraction used for switchgrass and the number of sectors to complete a circle affect switchgrass price. The capacity of the pyrolysis plant has a small effect compared to the land fraction used for switchgrass. The capacity of the pyrolysis plant at 1000 tons per day is chosen as a representative of this calculation. If all the land is used for switchgrass (100%) and the field shape is circular, the switchgrass price can reduce to $53.48 per ton. From this

information, the most important parameter is land fraction used for switchgrass. The switchgrass should be grown in an isolated empty field, separated from other plant species. This can lower the price of switchgrass.

(2) Land fraction and field shape effect to pyrolysis price

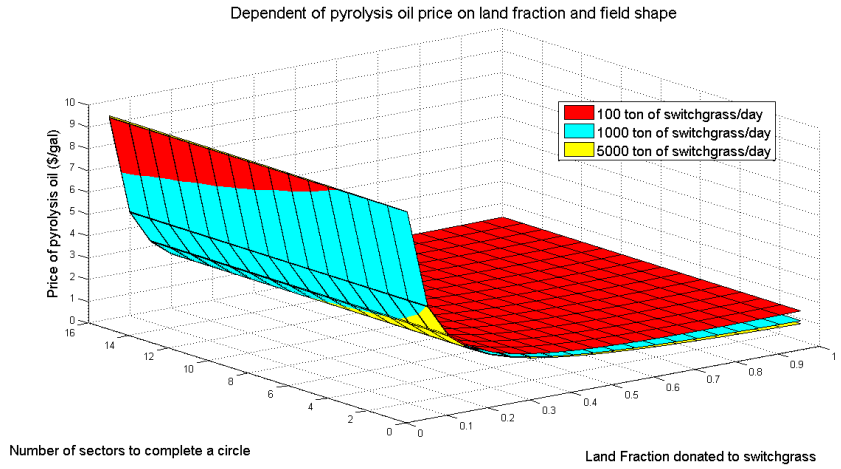

Figure 2.12 Dependency of pyrolysis oil price on land fraction and field shape

From Figure 2.12, the land fraction used for switchgrass and number of sectors in a circle affects pyrolysis price. The capacity of the pyrolysis plant has some effect on the pyrolysis oil price. If pyrolysis plant capacity is 5,000 tons per day, pyrolysis oil price can be as low as $0.734 per gallon if the land fraction used for switchgrass is 1 and the number of sectors to complete a circle, which is 1.

(3) Land fraction and field shape effect electricity cost

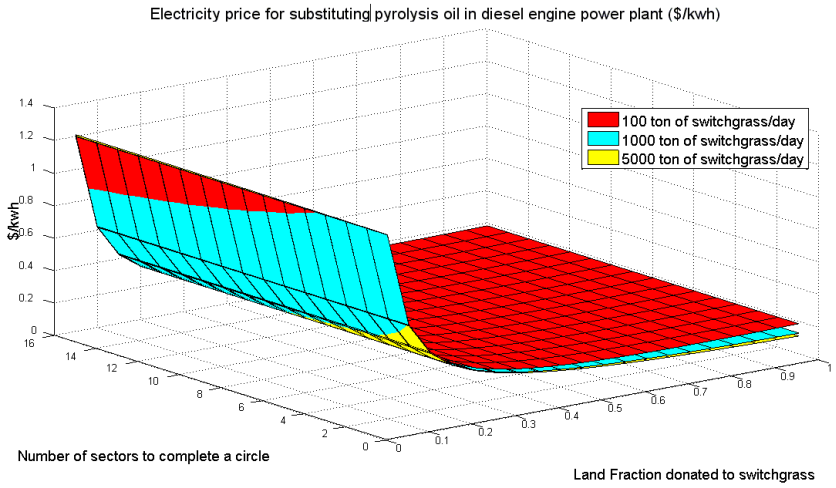

Figure 2.13 Electricity price for substituting pyrolysis oil in diesel engine power plant vary with land fraction and land shape

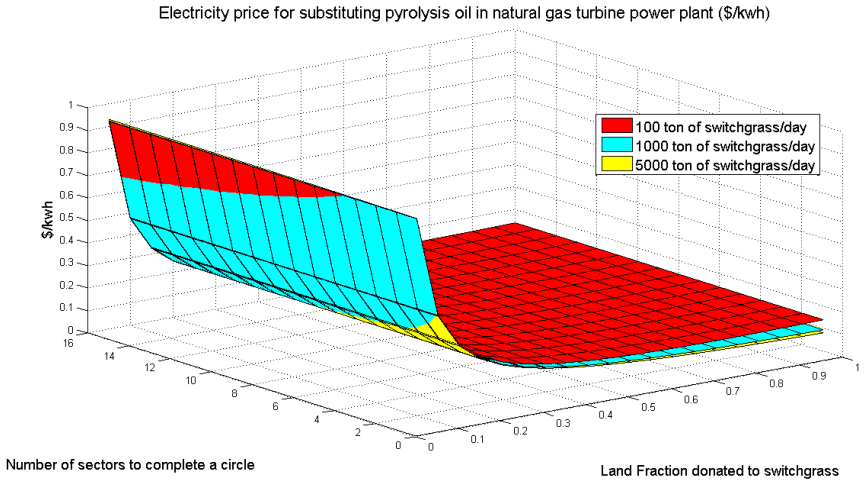

Figure 2.14 Electricity price for substituting pyrolysis oil in natural gas turbine power plant vary with land fraction and land shape

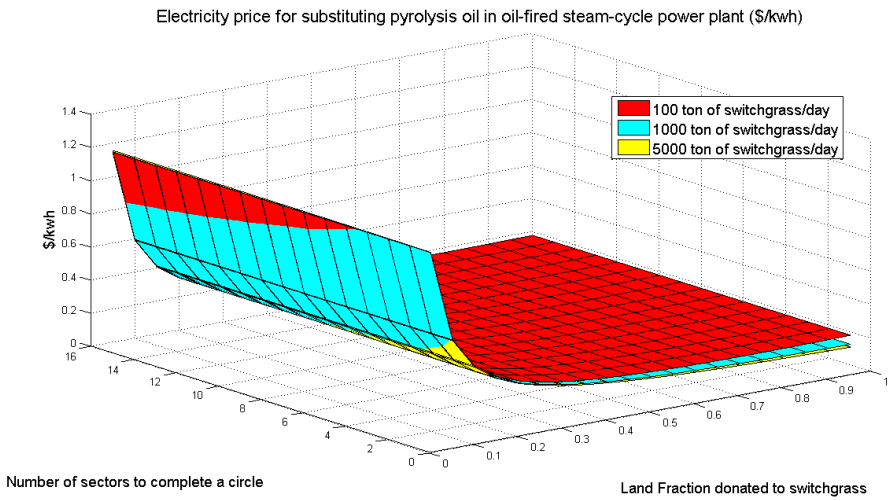

Figure 2.15 Electricity price for substituting pyrolysis oil in oil-fired steam-cycle power plant vary with land fraction and land shape

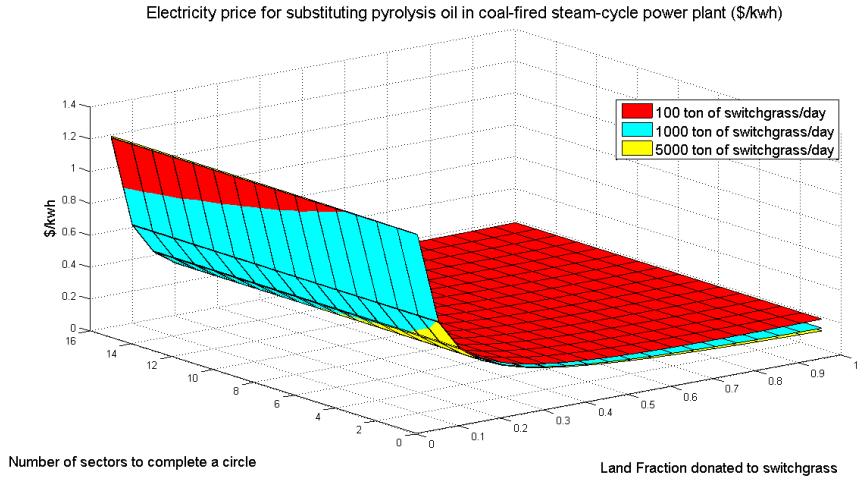

Figure 2.16 Electricity price for substituting pyrolysis oil in coal-fired steam-cycle power plant vary with land fraction and land shape

In Figure 2.13 to Figure 2.16, the land fraction utilized to grow switchgrass and the number of sectors in a circle affect pyrolysis price. The capacity of pyrolysis plant also has an effect on the pyrolysis price.

The coal-fired steam-cycle power plant produces the most expensive electricity cost per kwh. If pyrolysis plant capacity is 5000 tons per day, the electricity cost will drop to $0.102 per kwh, when the entire land area is utilized to grow switchgrass (land fraction=1) and the field shape is circular $(n=1)$.

The natural gas turbine power plant produces cheapest electricity cost per kwh. If pyrolysis plant capacity is 5000 tons per day, the electricity cost will be dropped to $0.077 per kwh, when the entire land area is utilized to grow switchgrass (land fraction=1) and the field is circular $(n=1)$.

The oil-fired steam-cycle power plant produces a cheaper electricity cost than the diesel engine power plant. Based on this analysis, the natural gas turbine power plant is the most promising plant to utilize pyrolysis oil since it produces cheapest electricity cost. The electricity cost at 7.70 cent per kwh is preferable since it is a competitive cost to conventional energy resources. According to the U.S. Energy Information Administration [85], the average electricity cost in the United State in 2011 was $0.10 per kwh. The electricity cost at 7.70 cent per kwh can be obtained only if the entire field is utilized to grow switchgrass. However, it is impossible to fill

such a huge area (441880 Ha) with a sea of switchgrass. The efficient management of growing, transportation, storage and pyrolysis, and choosing a suitable power plant are all required in order to make switchgrass energy sustainable and competitive with conventional energy sources.

(4) Land fraction and field shape effect to the total GHG emission

The relationships of total Emission of switchgrass pyrolysis oil substituting in power plant that vary with land fraction and field shape are linear. The equation is in form $ax+by+cz=r$. The parameters are shown in the table below.

Table 2.35 parameters for Land fraction and field shape effect to the total GHG emission equation

$ax+by+cz=r$	a	b	c	r
Natural-gas-fired combustion turbine	7.76	-0.54	-7.00	12.31
Oil-fired steam cycle	-6.58	3.20×10^{-4}	-4.80	-5.89
Coal-fired steam cycle	-7.41	2.30×10^{-4}	-5.24	2.82×10^{-2}
Diesel engine power plant	-7.47	-4.53×10^{-3}	-5.12	1.50×10^{-1}

The land fraction used for switchgrass, number of sectors in a circle, and type of power plant have effects on the GHG emission. The pyrolysis plant capacity has a small effect on the GHG emission. In Table 2.35, parameters for Land fraction and

field shape effect to the total GHG emission equation for four power plants are shown. Operating all of the power plants with pyrolysis oil from switchgrass has negative GHG emissions. The most negative GHG emission per kwh comes from the diesel engine power plant. The least negative GHG emission per kwh comes from the natural gas turbine power plant.

For the diesel engine power plant, if all the land is used to grow switchgrass (land fraction=1) and the field is circular $(n=1)$, the GHG emission is -1.4321kg CO_2 eq. per kwh–the lowest GHG emission. For the natural gas turbine power plant, if all the land is used to grow switchgrass (land fraction=1) and the field is circular $(n=1)$, the GHG emission is -1.1037kg CO_2 eq. per kwh.

2.3.9. Conclusion and future work

This study is based on bio-oil produced through fast pyrolysis. The switchgrass was grown in fields of different shapes and land fractions. Life cycle assessment analysis and Life cycle cost analysis were performed on a system which consisted of cultivating and harvesting, transportation and storage, pyrolysis, transportation and power generation. The GHG emission from the system was negative. Based on life cycle assessment, the power generation using pyrolysis oil is

environmentally friendly since it reduces GHG emissions. On the other hand, life cycle cost analysis reveals that the electricity cost per kwh is higher than the conventional technology which uses fossil fuels. However, based on the analysis, the electricity cost from pyrolysis oil could be competitive if we can utilize the system with the cheapest scenarios. A circular field entirely filled with switchgrass is optimal for reducing electricity cost because of lower cost of cultivation, harvesting and transport. A circular field with a pyrolysis plant capacity of 5000 tons per day using the natural gas turbine power plant could have an electricity cost as low as 7.70cent/kwh. However, power generation from switchgrass requires a huge amount of land. We assumed that the land fraction utilized to grow switchgrass is the same as the average agriculture land fraction in the US, which is 44.1%. In order to provide enough switchgrass for a pyrolysis plant capacity of 5000 tons per day, a large land area size of 1706.11 square miles, which is even bigger than Rhode Island, is required. In the future, when carbon credit is fully utilized, pyrolysis oil could be more competitive for the benefit of carbon credit.

For future work, we can expand the use of this model to other biomass sources that are available at different places. For example, rice hulk is plentiful in Thailand as agriculture

wastes; typically these are burned after harvest. This is wasteful and leads to pollution. We can use our modeling approach to verify whether the rice hulk can be converted to clean energy.

Reference

[1] International Energy Agency. Climate and Electricity Annual 2011. OECD Publishing; 2011.

[2] Goswami DY. A Review and Future Prospects of Renewable Energy in the Global Energy System. In: Goswami DY, Zhao Y, editors. Proc. ISES World Congr. 2007, Springer Berlin Heidelberg; 2008, p. 3–10.

[3] Faaij A. Modern Biomass Conversion Technologies. Mitig Adapt Strateg Glob Chang 2006;11:335 – 367.

[4] Roland K. Petroleum in the Next Century - Conclusion: Global Warming Is Dire Oil Industry Issue. Oil Gas J 1998;96:61 – 64.

[5] Richard A, Berntsen T, Bindoff NL, Chen Z, Chidthaisong A, Friedlingstein P, et al. Climate Change 2007: The Physical Science Basis. Paris: 2007.

[6] Hofmann DJ, Butler JH, Tans PP. A New Look at Atmospheric Carbon Dioxide. Atmos Environ 2009;43:2084 – 2086.

[7] Hammons TJ. Impact of Electric Power Generation on Green House Gas Emissions in Europe: Russia, Greece, Italy and Views of the EU Power Plant Supply Industry – A Critical Analysis. Int J Electr Power Energy Syst 2006;28:548 – 564.

[8] AEO2012 Early Release Overview. vol. 2012. 2012.

[9] Brammer JG, Lauer M, Bridgwater AV. Opportunities for Biomass-Derived “Bio-Oil” in European Heat and Power Markets. Energy Policy 2006;34:2871 – 2880.

[10] Fan JQ, Kalnes TN, Alward M, Klinger J, Sadehvandi A, Shonnard DR. Life Cycle Assessment of Electricity Generation Using Fast Pyrolysis Bio-Oil. Renew Energy 2011;36:632 – 641.

[11] Solantausta Y, Nylund N, Gust S. Use of Pyrolysis Oil in a Test Diesel Engine to Study the Feasibility of a Diesel Power Plant Concept. Biomass and Bioenergy 1994;7:297 – 306.

[12] Arbon IM. Worldwide Use of Biomass in Power Generation and Combined Heat and Power Schemes. Proc Inst Mech Eng Part A J Power Energy 2002;216:41 – 57.

[13] Chiaramonti D, Oasmaa A, Solantausta Y. Power Generation Using Fast Pyrolysis Liquids from Biomass. Renew Sustain Energy Rev 2007;11:1056 – 1086.

[14] Arbogast S, Bellman D, Paynter JD, Wykowski J. Advanced Bio-Fuels from Pyrolysis Oil: The Impact of Economies of Scale and Use of Existing Logistic and Processing Capabilities. Fuel Process Technol 2012:1–7.

[15] Boateng AA, Daugaard DE, Goldberg NM, Hicks KB. Bench-Scale Fluidized-Bed Pyrolysis of Switchgrass for Bio-Oil Production. Ind Eng Chem Res 2007;46:1891 – 1897.

[16] Eco Smes. LCA Definition According to SETAC n.d.

[17] Finkbeiner M, Inaba A, Tan RBH, Christiansen K, Klüppel H-J. The New International Standards for Life Cycle Assessment: ISO 14040 and ISO 14044. Int J Life Cycle Assess 2006;11:80 – 85.

[18] Frankl P, Rubik F. Life Cycle Assessment in Industry and Business: Adoption Patterns, Applications and Implications. Bus Strateg Environ 2001;10:253 – 254.

[19] Rebitzer G, Ekvall T, Frischknecht R, Hunkeler D, Norris G, Rydberg T, et al. Life Cycle Assessment Part 1: Framework, Goal and Scope Definition, Inventory Analysis, and Applications. Environ Int 2004;30:701 – 720.

[20] Curran MA. Environmental Life-Cycle Assessment. New York: McGraw-Hill; 1996.

[21] Novick D. The Federal Budget as an Indicator of Government Intentions and the Implications of Intentions. Defense Technical Information Center; 1959.

[22] Hunt RG, Franklin WE, Hunt RG. LCA — How It Came about: Personal Reflections on the Origin and the Development of LCA in the USA. Int J Life Cycle Assess 1996;1:4–7.

[23] Boustead I, Hancock GF. Handbook of Industrial Energy Analysis. New York: E. Horwood; 1979.

[24] Fava JA. A Technical Framework for Life-Cycle Assessments. Society of Environmental Toxicology and Chemistry and SETAC Foundation for Environmental Education; 1991.

[25] Horne R, Grant T, Verghese K. Life Cycle Assessment: Principles, Practice, and Prospects. Collingwood, Vic: CSIRO PUBLISHING; 2009.

[26] Winsemius P. Guests in Our Own Home. McKinsey & Co.; 1990.

[27] Liefferink D. The Netherlands: A Net Exporter of Environmental Policy Concepts. Eur Environ Policy Pioneers, Manchester Univ Press Manchester 1997.

[28] ISO. 14040: Environmental Management–Life Cycle Assessment–Principles and Framework. London Br Stand Inst 2006.

[29] ISO. 14044: Environmental Management—Life Cycle Assessment—Requirements and Guidelines. Int Organ Stand 2006.

[30] Curran MA. Life Cycle Assessment Handbook: A Guide for Environmentally Sustainable Products. Wiley; 2012.

[31] Fava JA. Life Cycle Initiative: A Joint UNEP/SETAC Partnership to Advance the Life-Cycle Economy. Int J Life Cycle Assess 2002;7:196 – 198.

[32] Consoli F. Guidelines for Life-Cycle Assessment: A "Code of Practice": from the SETAC Workshop Held at Seimbra, Portugal, 31 March-3 April 1993. Society of Environmental Toxicology and Chemistry; 1993.

[33] Vigon BW, Tolle DA, Cornaby BW. Life-Cycle Assessment: Inventory Guidelines and Principles. Life-cycle Assess. Invent. Guidel. Princ., EPA; 1993.

[34] Fava JA. A Conceptual Framework for Life-Cycle Impact Assessment. Society of Environmental Toxicology and Chemistry and SETAC Foundation for Environmental Education; 1993.

[35] Allen DT, Shonnard DR. Green Engineering: Environmentally Conscious Design of Chemical Processes. Pearson Education; 2001.

[36] AGO. National Greenhouse Strategy Strategic Framework for Advancing Australia's Greenhouse Response. Canberra: 1998.

[37] Zamagni A, Buttol P, Buonamici R, Masoni P, Guinée JB, Huppes G, et al. Blue Paper on Life Cycle Sustainability Analysis. 2009.

[38] Heijungs R, Huppes G, Guinée JB. Life Cycle Assessment and Sustainability Analysis of Products, Materials and Technologies. Toward a Scientific Framework for Sustainability Life Cycle Analysis. Polym Degrad Stab 2010;95:422 – 428.

[39] Foran B, Lenzen M, Dey C. Balancing Act: A Triple Bottom Line Analysis of the Australian Economy. Canberra: 2005.

[40] Ravemark D. State of the Art Study of LCA and LCC Tools 2003.

[41] Barringer HP. A Life Cycle Cost Summary. Int. Conf. Mainte, 2003, p. 1–10.

[42] Kawauchi Y, Rausand M. Life Cycle Cost (LCC) Analysis in Oil and Chemical Process Industries. Chiba: 1999.

[43] Farr JV. Systems Life Cycle Costing: Economic Analysis, Estimation, and Management. CRC Press Inc; 2011.

[44] Gupta Y, Chow WS. Twenty-Five Years of Life Cycle Costing—Theory and Applications: A Survey. Int J Qual Reliab Manag 1985;2:51–76.

[45] Cooper R, Kaplan RS. How Cost Accounting Systematically Distorts Product Costs. Account. Manag. F. study Perspect., Boston: Harvard Business School Press; 1987, p. 204 – 228.

[46] Kreuze JG, Newell GE. ABC and Life-Cycle Costing for Environmental Expenditures. Manag Account 1994;75:38 – 42.

[47] Dell'Isola AJ, Kirk SJ. Life Cycle Costing for Facilities: Economic Analysis for Owners and Professionals in Planning,

Programming, and Real Estate Development: Designing, Specifying, and Construction, Maintenance, Operations, and Procurement. Robert s Means Co; 2003.

[48] Fabrycky WJ, Blanchard BS. Life-Cycle Cost and Economic Analysis. Englewood Cliffs, NJ: Prentice Hall; 1991.

[49] Rinehart L. Switchgrass as a Bioenergy Crop. 2006.

[50] David K, Ragauskas AJ. Switchgrass as an Energy Crop for Biofuel Production: A Review of Its Ligno-Cellulosic Chemical Properties. Energy Environ Sci 2010;3:1182 – 1190.

[51] Evanylo GK, Abaye a O, Dundas C, Zipper CE, Lemus R, Sukkariyah B, et al. Herbaceous Vegetation Productivity, Persistence, and Metals Uptake on a Biosolids-Amended Mine Soil. J Environ Qual 2005;34:1811 – 1819.

[52] Mclaughlin SB, Adamskszos L, Adams Kszos L. Development of Switchgrass (Panicum Virgatum) as a Bioenergy Feedstock in the United States. Biomass and Bioenergy 2005;28:515 – 535.

[53] Sanderson M a., Adler PR, Boateng a. a., Casler MD, Sarath G. Switchgrass as a Biofuels Feedstock in the USA. Can J Plant Sci 2006;86:1315 – 1325.

[54] Lemus R, Brummer EC, Moore KJ, Molstad NE, Burras CL, Barker MF. Biomass Yield and Quality of 20 Switchgrass Populations in Southern Iowa, USA. Biomass and Bioenergy 2002;23:433 – 442.

[55] Fike JH, Parrish DJ, Wolf DD, Balasko J a., Green Jr JT, Rasnake M, et al. Switchgrass Production for the Upper Southeastern USA: Influence of Cultivar and Cutting Frequency on Biomass Yields. Biomass and Bioenergy 2006;30:207 – 213.

[56] MATLAB 2009.

[57] Duffy M. Estimated Costs for Production, Storage, and Transportation of Switchgrass. Iowa State University, Department of Economics; 2007.

[58] Schnitkey G, Lattz D. Machinery Cost Estimates: Field Operations. 2008.

[59] Schnitkey G, Lattz D. Machinery Cost Estimates: Forage Field Operations. 2010.

[60] Duffy MM, Nanhou VY. Costs of Producing Switchgrass for Biomass in Southern Iowa. In: Janick J, Whipkey A, editors. Proc. fifth Natl. Symp. New Crop. New Uses Strength Divers., vol. 1998, ASHS Press; 2002, p. 267 – 275.

[61] Maraseni TNTN, Cockfield G, Apan A. A Comparison of Greenhouse Gas Emissions from Inputs into Farm Enterprises in Southeast Queensland, Australia. J Environ Sci Heal Part A Toxic/Hazardous Subst Environ Eng 2007;42:11 – 18.

[62] Overend R. The Average Haul Distance and Transportation Work Factors for Biomass Delivered to a Central Plant. Biomass 1982;2:75 – 79.

[63] Brazil Green Freight Transport Report. 2011.

[64] Paustian K, Antle J, Sheehan J, Paul E. Agriculture's Role in Greenhouse Gas Mitigation. Prepared for the Pew Center on Global Climate Change; 2006.

[65] Ney RA, Schnoor JL. Greenhouse Gas Emission Impacts of Substituting Switchgrass for Coal in Electric Generation: the Chariton Valley Biomass Project. vol. 20. 2002.

[66] Cherubini F, Jungmeier G. LCA of a Biorefinery Concept Producing Bioethanol, Bioenergy, and Chemicals from Switchgrass. Int J Life Cycle Assess 2010;15:53–66.

[67] McLaughlin SB, Walsh ME, Aughlin SBMCL, Alsh MEW. Evaluating Environmental Consequences of Producing Herbaceous Crops for Bioenergy. Biomass and Bioenergy 1998;14:317 – 324.

[68] Brummer EC, Burras CL, Duffy MD, Moore KJ. Switchgrass Production in Iowa: Economic Analysis, Soil Suitability, and Varietal Performance. Oak Ridge, Tennessee: 2002.

[69] Wright MM, Brown RC, Boateng AA. Distributed Processing of Biomass to Bio-Oil for Subsequent Production of Fischer Tropsch Liquids. Biofuels, Bioprod Biorefining 2008;2:229 – 238.

[70] Balat M, Kırtay E, Balat H. Main Routes for the Thermo-Conversion of Biomass into Fuels and Chemicals. Part 1: Pyrolysis Systems. Energy Convers Manag 2009;50:3147 – 3157.

[71] Jaramillo P. A Life Cycle Comparison of Coal and Natural Gas for Electricity Generation and the Production of Transportation Fuels. Carnegie Mellon University, 2007.

[72] GHGenius model n.d.

[73] Oasmaa A, Peacocke C, Gust S, Meier D, McLellan R. Norms and Standards for Pyrolysis Liquids. End-User Requirements and Specifications. Energy & Fuels 2005;19:2155 – 2163.

[74] Yoshikawa K. R&D (Research and Development) on Distributed Power Generation from Solid Fuels. Energy 2006;31:1656 – 1665.

[75] Solantausta Y, Bridgwater A, Beckman D. Feasibility of Power Production with Pyrolysis and Gasification Systems. Biomass and Bioenergy 1995;9:257 – 269.

[76] Wagenaar BM, Gansekoele E, Florijn J, Venderbosch RH, Penninks FWM, Stellingwerf A. Bio-Oil as Natural Gas Substitute in a 350 MW Power Station. Biomass energy Ind. Clim. Prot., Florence: World biomass conference; 2004, p. 10 – 14.

[77] Herdin GR, Gruber F, Plohberger D, Wagner M. Experience with Gas Engines Optimized for H2-rich Fuels. Intern. Combust. Engine Div. Spring Tech. Conf., Salzburg, Austria: American Society of Mechanical Engineers; 2003, p. 679 – 690.

[78] RESTMAC. Creating Markets for Renewable Energy Technologies EU RES Technology Marketing Campaign. European Biomass Industry Association; n.d.

[79] Schreiner M, Kampichler G, Krzack S, Meyer B. Thermodynamic Modelling of Co-Firing Coal and Biomass Pyrolysis Gas in a Power Plant. Fuel Process Technol 2011;92:787 – 792.

[80] Czernik S, Bridgwater A V. Overview of Applications of Biomass Fast Pyrolysis Oil. Energy & Fuels 2004;18:590 – 598.

[81] Beaty HW. Handbook of Electric Power Calculations. New York: McGraw-Hill; 2001.

[82] The World Bank. Agricultural land (% of land area) 2009.

[83] Qin X, Mohan T, El-Halwagi M, Cornforth G, McCarl B a. Switchgrass as an Alternate Feedstock for Power Generation: an Integrated Environmental, Energy and Economic Life-Cycle Assessment. Clean Technol Environ Policy 2006;8:233 – 249.

[84] U.S. Energy Information Administration. Electric Power Monthly with Data for June 2012. Washington, DC: 2012.

[85] U.S. Energy Information Administration. Electricity Explained Factors Affecting Electricity Price 2010.

[86] Gagnon L. Comparing Power Generation Options. Quebec: 2003.

Chapter 3 Specific Aim 3

Fuzzy Modeling of Biomass Pyrolysis

Lerkkasemsan N, Achenie LEK. Pyrolysis of biomass – fuzzy modeling. Renewable Energy 2014;66:747 – 758.

3. Chapter 3 - Fuzzy Modeling of Biomass Pyrolysis

In this specific aim, we find a new way to model the kinetic of biomass in pyrolysis process. Since the pyrolysis of biomass is hard to model with a conventional power law model, the new model with more accurate result should make a better contribution of modeling for predicting pyrolysis of biomass yield. In our work, instead of modeling the pyrolysis of biomass which is full of uncertainty with a deterministic model, we use a tool that suitable for handling the uncertainty in the system. We use ANFIS (adaptive neural fuzzy inference system) to build a model for pyrolysis of biomass.

3.1. Introduction and literature review

3.1.1. Introduction

Energy consumption by humans is increasing rapidly every year. As such our dependence on fossil fuel as a primary energy source is increasing. From a report of the U.S. Department of energy[1], transportation energy demand is expected to increase at an annual rate of 0.2 percent from year 2010 to 2035. Total electricity consumption is expected to increase at an annual rate of 0.8 percent from 3879 billion kilowatt-hours in 2010 to 4775 billion kilowatt-hours in 2035. However, fossil fuel reserves are decreasing. From BP Oil's estimate [2], world oil production has already reached its maximum and is starting to drop. Alternative energy sources such as bio-oil can help make up for the reduction of fossil fuel production. Faaij[3]reported that fossil fuel dominated the world's energy uses, supplying 80% of the total energy requirement. However, 10-15% of this demand could be covered by biomass resource. Biomass is an important energy resource for developing countries accounting for 50-90% of their total energy requirement. Advantages of biomass energy include the potential to reduce Greenhouse gases (GHG) emissions, substitution for depleting global crude oil reservoir, potential impacts on waste management, and the conversion of waste resources into clean energy. Waste resources

include natural forests wood, forestry residues, agricultural residues, industrial wastes, food processing wastes and municipal solid wastes.

There are many ways to convert biomass to an easy-to-use form. The thermochemical conversion of biomass processes (namely pyrolysis, gasification, and combustion) is a promising process for future energy supply. The process is easy to scale up to industry size. Pyrolysis is the thermal degradation of biomass in the absence of oxygen. The three main products from pyrolysis of biomass are charcoal, bio-oil and gaseous product; these are more useful energy holders. Bio-oil and gaseous product are chemical resources for the refinery plant. In order to develop an efficient pyrolysis process, a determination of key pyrolysis parameters and their effect on the process is essential. In many studies, pyrolysis kinetic models are relatively simple but useful. The models in those cases only predict the overall yield of pyrolysis process without considering the physicochemical mechanism of the process.

Although there are many studies on biomass pyrolysis, there is a severe lack of models for predicting the pyrolysis rate and final conversion under a wide range of process conditions and biomass feedstock compositions. Modeling the biomass pyrolysis

is complicated by many factors. Biomass is a complex mixture of several organic compounds and polymers. Thus it is a challenge to identify all the molecular species as well as quantify the composition of the known molecular species. Moreover, there are hundreds of reactions that take place during pyrolysis reactions. Most of the existing models are specific to a particular biomass source – this limits the range of applicability of the model. Li[4] studied the pyrolysis of corn straw. For example Chiang[5]considered the kinetics of rice hulk pyrolysis. Gašparoviè[6]proposed a distribution activation energy model (DAEM) to describe the pyrolysis decomposition of wood. The model is able to describe an integral decomposition curve for wood but fails to describe the differential curve. In general, DAEM does not accurately describe biomass pyrolysis.

On the other hand, there is a limited number of models that account for uncertainty in other systems. For example Sohpal[7]developed a fuzzy model for predicting the optimal temperature for biodiesel produced from transesterification of JatrophaCurcas oil with butanol. The authors employed an adaptive neuro-fuzzy inference system (ANFIS), which compared favorably with batch kinetics experimental data. Fazilat[8]employed ANFIS to predict the thermal degradation kinetics of NY6/FK blend films. Lertworasirikul[9]used ANFIS to

estimate the dynamic drying behavior of semi-finished cassava crackers.

We propose the use of ANFIS to model biomass pyrolysis considering the modeling challenges discussed earlier. We employ ANFIS to relate the raw materials (Reed Canary grass and wood) to product. The Reed Canary grass is a tall perennial grass, which is widely grown across the northern states of the US. It is adaptable to diverse soils and climates. Moreover it can tolerate a soil PH range of 4.9 to 8.2, and it can be grown in poorly drained soils and it is winter hardy. In order to validate our model, we also employ the ANFIS model to the pyrolysis of wood, which is another biomass source.

3.1.2. Literature review

Since biomass is an abundant source in the world, it is possible to be a great raw material source to supply to an energy unit. Biomass is a clean, renewable energy source that can improve the environment. Farming bioenergy crops also reduces Greenhouse gases in atmospheres [10].

Pyrolysis is one of the thermochemical biomass conversion processes where thermal destruction of organics occurs in the absence of oxygen. Products contain several organic chemicals and high-energy contents. These products can be extracted as a raw material for chemical industries. They can be used as an energy source as well. The products can be separated into three main components: char, bio-oil, and gases.

Biomass pyrolysis involves numerous extremely complex reactions that result in a large number of intermediates and end products. Therefore, deriving an exact reaction mechanism and kinetic model for biomass pyrolysis is difficult. The mechanisms for pyrolysis of biomass are mostly developed under a general approach: biomass is the raw material and gas/ volatiles, bio-oil, char are the products.

Several kinetic models have been delivered.

(1) Literature review - Kinetic study of pyrolysis of biomass

(I) Power law model

In the literature, the decomposition of material is conventionally modeled using the following equations.[11]

$$\frac{da}{dt} = k f(a) \tag{3.1}$$

$$k = A\exp(-E/RT) \tag{3.2}$$

$$T = T_0 + bt \tag{3.3}$$

Here α is the fraction decomposed; k is the rate constant at temperature T (K); A is the pre-exponential factor; E is the activation energy; R is the gas constant; b is the heating rate; T_0 is the starting temperature; and $\frac{d\alpha}{dt}$ can be expressed as:

$$\left(\frac{d\alpha}{dt}\right)_T = -\frac{1}{m_0}\left(\frac{dm}{dt}\right)_T \tag{3.4}$$

$\frac{dm}{dt}$ is the rate of change of mass used in the DTG (differential thermo gravimetric) curve; the latter shows the weight loss as the pyrolysis proceeds. An example of this method is from Coats

[12]where the form of the kinetic expression is power law as follows

$$\frac{d\alpha}{dt} = k(1-\alpha)^n \tag{3.5}$$

To determine the kinetic data from the pyrolysis of biomass, one considers a series of pyrolysis runs under different temperatures. To construct the Arrhenius-type plot and estimate the activation energy, the experiment needs to be repeatable and be isokinetic[11]; this meansthat there is a linear relation between the activation enthalpies and activation entropies in a series of related reactions.

$$\Delta H_n = \beta \Delta S_n + \Delta H_0 \tag{3.6}$$

The slope β represents the isokinetic temperature at which all the reactions of the series react at the same rate.

Since biomass consists of many components, which have different pyrolysis reaction behaviors, it is difficult to relate the kinetic parameters determined from different laboratories. A way to partially deal with this problem is to solve through the use of the *compensation effect* which is a correlation between activation energy and pre-exponential

factor; this is used to check whether the kinetic parameters are characteristic of a material from same family or not.

If there are n substrates in the family and i represent each substrate, the rate constant is given as,

$$k_i = A_i \exp(-E_i / RT) \tag{3.7}$$

or

$$\ln A_i = \ln k_i + E_i / RT \tag{3.8}$$

There is a compensation effect if a linear correlation is experimentally found between $\ln A_i$ and E_i for all i:

$$\ln A_i = a + bE_i \quad i = 1.....n \tag{3.9}$$

Subtract equations (3.2.2-9) with (3.2.2-8) lead to

$$a - \ln k_i + E_i\left(b - \frac{1}{RT}\right) = 0 \tag{3.10}$$

Equation (3.2.2-10) holds only when $T = T_{iso}$

$$T_{iso} = \frac{1}{Rb} \tag{3.11}$$

$$a - \ln k_i = 0 \Rightarrow k_i = e^a \qquad i = 1.....n \tag{3.12}$$

Since a is constant we have

$$k_i(T_{iso}) = k_{iso} \qquad i = 1.....n \tag{3.13}$$

In case there is a compensation effect, there is an isokinetic temperature where all components i have the same pyrolysis rate constant.

$$\ln A_i = \ln k_{iso} + {E_i}/{RT_{iso}} \qquad i = i.....n \tag{3.14}$$

Some researchers feel that the *compensation effect* isnot a valid criterion to verify kinetic parameter such as pre-exponential factor. For example Bellais[13] shows that the compensation effect is not applicable to his data.

Although the power law model is rather simple from a reaction engineering point of view, the fact is it is very popular in the community of biomass pyrolysis researchers. One reason is the complexity of components and the uncertainty in the component fractions in biomass.

(II) Competing Models

Thurner et al [14] used other models for wood pyrolysis. The wood was pyrolyzed into three different products namely gases, bio-oil, and char as shown in Figure 3.1

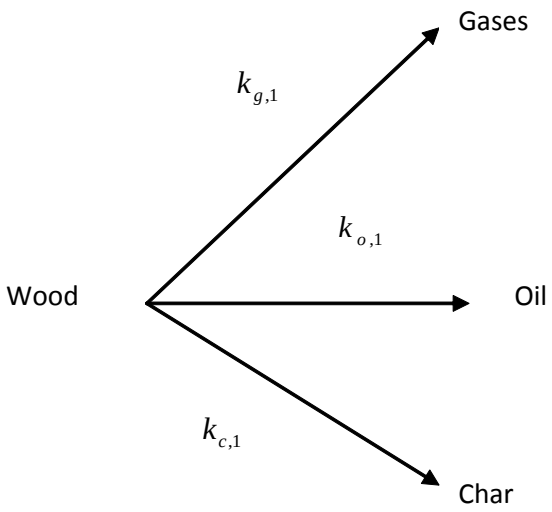

Figure 3.1 kinetic mechanism for Thurner et al[14] work

Thurner et al [14] assumed that the activation energies for char-formation reaction were the same as weight-loss reactions. As a result, the final residual weight was independent of the pyrolysis temperature.

$$\frac{dY_i}{dt} = -k_i Y_i \tag{3.15}$$

$$k_i = A_i \exp^{(-E_i/RT)} \tag{3.16}$$

While i represents three different reaction.

(III) Parallel Reaction Models

Alves et al [15] presented the model of the pyrolysis of wet particles of wood. They have presented a new reaction

mechanism. The reaction scheme assumed and the corresponding kinetics were experimentally determined for very small samples of dry pine wood sawdust. The model neglected internal temperature gradients. Six independent reactions were identified:

$$S_{v1} \xrightarrow{1} G \uparrow$$

$$S_{v2} \xrightarrow{2} G \uparrow$$

$$S_{v3} \xrightarrow{3} G \uparrow$$

$$S_{v4} \xrightarrow{4} G \uparrow$$

$$S_{v5} \xrightarrow{5} G \uparrow$$

$$S_{v6} \xrightarrow{6} G \uparrow$$

Figure 3.2 Six independent reaction from Alves et al [15]

Where S_{vi} is the volatile part of component i of wood. Components are numbered in order of increasing thermal stability. Component 1 is thought to correspond mostly to hemicelluloses, component 2 is mostly to cellulose, while components 3 to 6 correspond mainly to parts of the lignin macromolecule.

Gronli[16]developed a model for birch wood. The model assumed that birch wood was composed of four components: hemicelluloses(1), hemicelluloses(2), cellulose, and lignin.

(IV) Secondary tar cracking

In the work of Bradbury et al [17], a kinetic model for pyrolysis of cellulose was presented. The active cellulose has been presented in his work. The reaction started with transformation of cellulose to active cellulose. Then, the active cellulose decomposed through two competitive first-order-reactions, one produced volatiles and the other produced char and gases. The reaction scheme is shown in figure below:

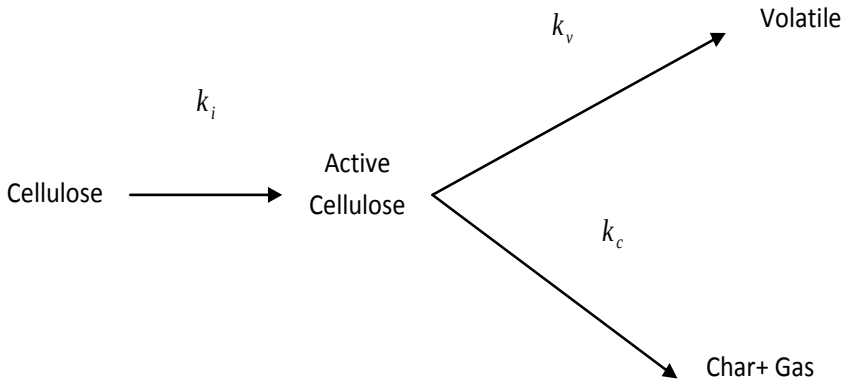

Figure 3.3 Reaction scheme from Bradbury et at [17]

Koufopanos et al[18], presented a model which correlates the pyrolysis rate of biomass with its composition. They suggested that the pyrolysis rate of biomass was a summation of the rates of the main chemical compositions in biomass: cellulose, hemicelluloses, and lignin. The Koufopanos's mechanism started with a zero-order reaction. This reaction was not related with any weight loss. The intermediate subsequently

decomposed by two competitive first-order reactions, one yielding char and the other volatile and gases. It was assumed that the reactions follow the Arrhenius law.

In his further work[19], the model included the secondary reactions which were first-order reactions between charcoal and volatile pyrolysis products. The reaction scheme is shown in the figure below.

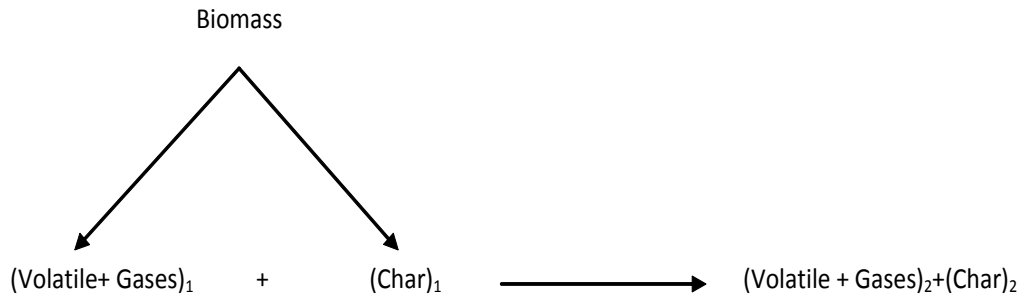

Figure 3.4 Pyrolysis reaction scheme for Koufopanos et al [19]

Varhegyi et al [20]presented the model that eliminated the simplicity of "Broido-Shafizadeh model". Varhegyi's model started with a partial reaction. In Reaction(0), the cellulose partially transformed into char, volatiles, water, and gases. This was a non-catalyzed decomposition reaction. The other part of cellulose was reacted under a hydrolysis reaction. This hydrolysis reaction transformed cellulose into intermediates. This was Reaction (1). Then, the intermediates decomposed into

char, water, and gases by hydrolysis reaction. This was Reaction (2). The reaction scheme is showed in figure below.

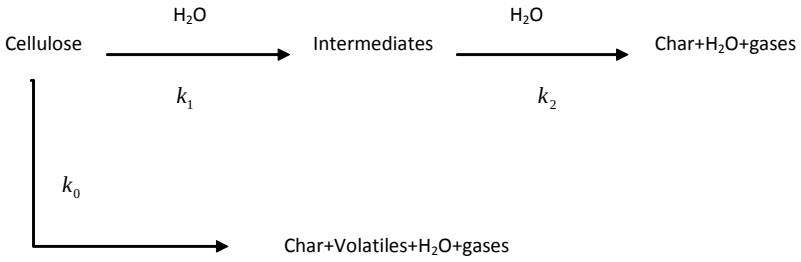

Figure 3.5 the reaction scheme by Varhegyi et al [20]

(V) Other Models

There are many other models that have been developed, such as the semi-global reaction mechanism from Branca et al [21][22]. Grioui et al [23] also developed a two stage, semi-global multi-reaction kinetic model. In this model, the wood was subdivided into three pseudo-components. Each component corresponds to a specific kinetic reaction. However, one step global models were weak when compared to models with secondary tar cracking.

(2) Literature review and theory behind ANFIS

The ANFIS system employs fuzzy modeling first introduced by LotfiZadeh[24]. Problems such as human reasoning in an imprecise environment can be handled using fuzzy logic theory. The theory is particularly applicable to uncertain problems, such as what occurs in pyrolysis. The ANFIS combines fuzzy logic concepts (Takagi-Sugeno fuzzy inference) with neural network concepts[25][26]. While Artificial Neural network (ANN) has the ability to learn from a system, the ANN knowledge is stored in an unreadable table, which is hard to interpret. On the other hand, the fuzzy inference system is able to translate the unreadable table into human language. However, the fuzzy system by itself lacks a learning ability and thus the membership function parameters have to be manually tuned. The combination of ANN and fuzzy inference system creates an approximator that has the ability to learn from samples and translate the unreadable result into human language.

(I) ANFIS Architecture

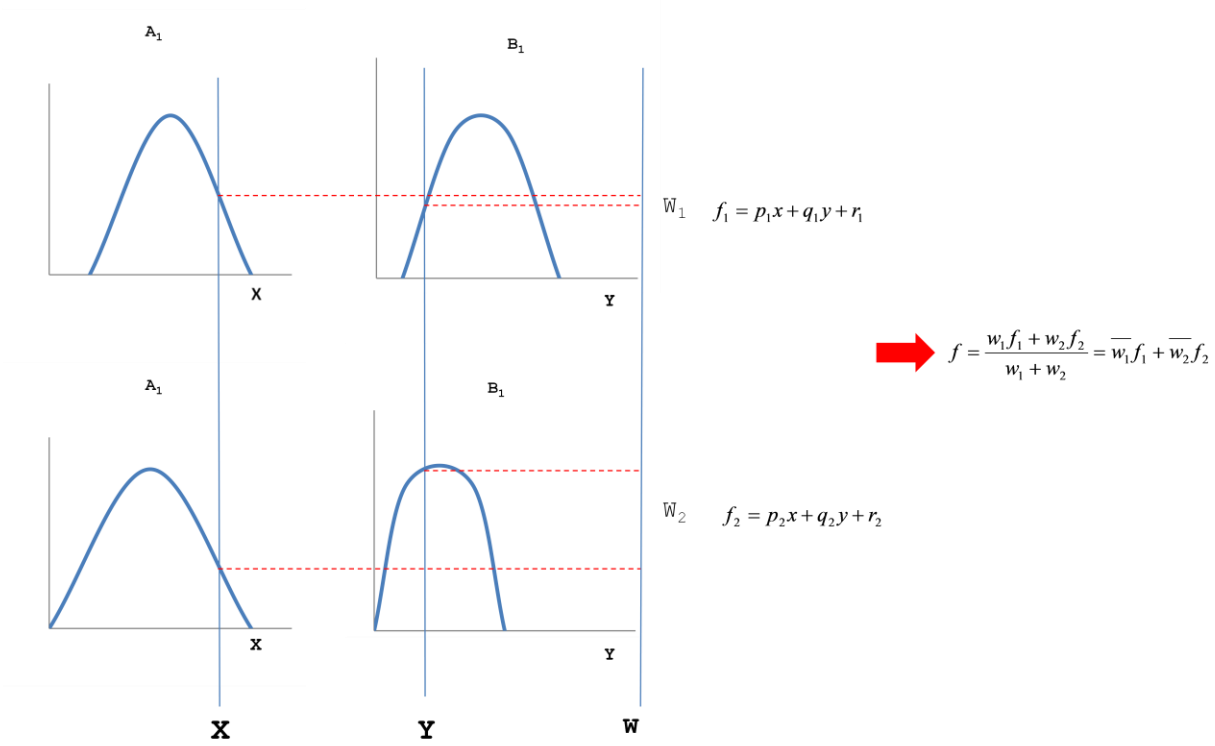

Figure 3.6 A two-input first-order Sugeno fuzzy model with two rules

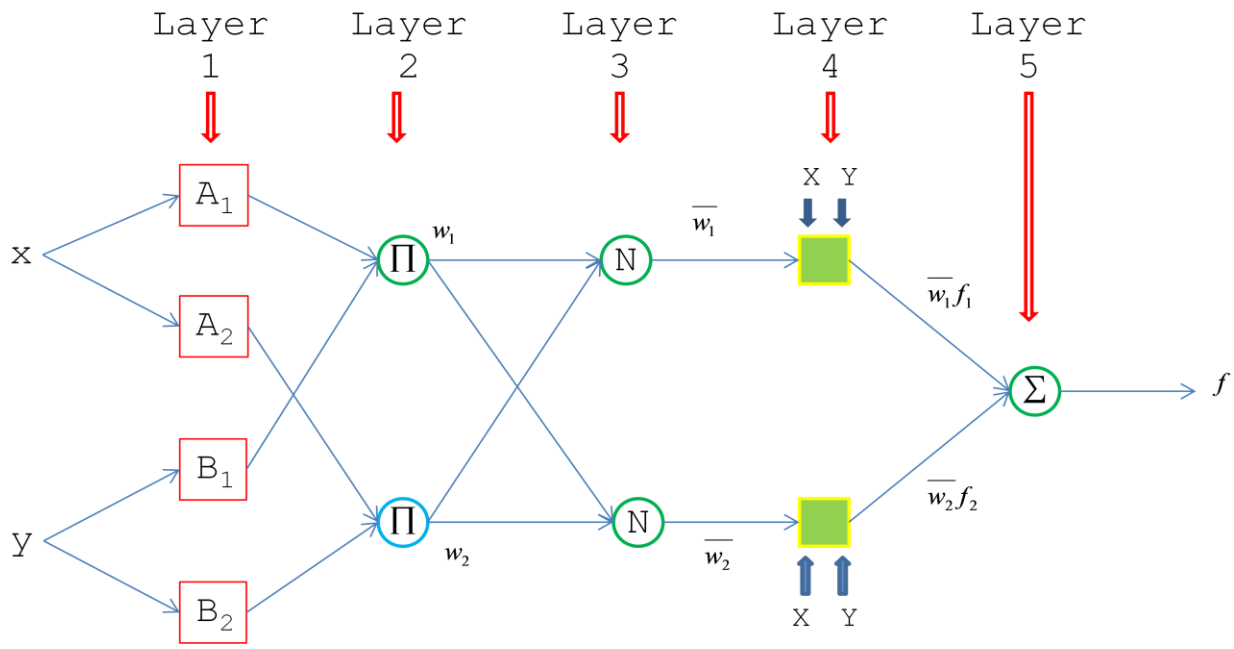

Figure 3.7 ANFIS architecture

From Figure 3.7, each node processes incoming signals; each node has a set of parameters associated with it. The square node is an adaptive node with parameters while a circle node is a fixed node with no parameters.

For simplicity, we assume that the fuzzy inference system under consideration has two inputs, x and y, and one output f. From Figure 3.7, for a first-order Sugeno fuzzy model, a common rule set with two fuzzy if-then rules is the following[25][27][26]:

Rule 1: If x is A_1 and y is B_1, then $f_1 = p_1 x + q_1 y + r_1$,

Rule 2: If x is A_2 and y is B_2, then $f_2 = p_2 x + q_2 y + r_2$.

Layer 1: Every node in this layer is a square node with node function:

$$O_{1,i} = \mu_{A_i}(x) \qquad \text{for } i = 1,2$$
$$O_{1,i} = \mu_{B_{i-2}}(y) \qquad \text{for } i = 3,4 \tag{3.17}$$

Here x is one of the input variables to node i, and A_i or B_{i-2} is the linguistic label associated with this node. $O_{1,i}$ is the membership function of A_i and it specifies the degree to which the given input x (or y) satisfies the quantifier A. The input

in this layer can be any continuous and piecewise differentiable function. For instance, the Gaussian membership function:

$$\mu_A(x) = \exp\left[-\left(\frac{x - c_i}{a_i}\right)^2\right] \qquad (3.18)$$

where $\{a, c\}$ is the parameter set. As the values of a and c change, this bell-shaped node function varies accordingly, thus exhibiting various concepts of corresponding linguistic term. Parameters in this layer are called *premise parameters*.

Layer 2: Every node in this layer is a circle node labeled Π which calculates all the incoming signals and sends the product out. Each node output corresponds to the weight of the rule.

$$O_{2,i} = w_i = \mu_{A_i}(x) \times \mu_{B_i}(y) \qquad \text{for } i = 1,2 \qquad (3.19)$$

Layer 3: Every node in this layer is a circle node labeled N. The $i-th$ node calculates the ratio of the $i-th$ rule's weight to the sum of all rules' weight.

$$O_{3,i} = \overline{w_i} = \frac{w_i}{w_1 + w_2} \qquad \text{For } i = 1,2 \qquad (3.20)$$

Layer 4: Every node in this layer is a square node with node function:

$$O_{4,i} = \overline{w_i} f_i = \overline{w_i}(p_i x + q_i y + r_i) \qquad \text{for } i = 1,2 \qquad (3.21)$$

Here $\overline{w_i}$ is an output from layer 3, and { p_i , q_i , r_i } is the parameter set. Parameters in this layer are usually called *consequence parameters*.

Layer 5: It's a circle node labeled Σ that sum all in coming signals and give the overall output

$$O_{5,i} = \sum_i \overline{w_i} f_i = \frac{\sum_i w_i f_i}{\sum_i w_i} \qquad \text{for } i = 1,2 \qquad (3.22)$$

In ANFIS, the set of parameter values is systematically modified using the training data and a learning algorithm. The basic learning method is gradient-based; this is slow and tends to be trapped in a local minimum. In contrast the ANFIS model uses a faster hybrid-learning algorithm. The hybrid-learning algorithm combines least-squares estimator and the gradient descent method; this can still be trapped in a local minimum. There are two passes in the hybrid algorithm; the forward pass calculates the vectors, which are outputs from each node in each layer. The backward pass uses a steepest descent algorithm (backpropagation) [25][26].

The parameter set S can be divided into two sets as

$$S = S_1 \oplus S_2 \tag{3.23}$$

where $\oplus$ represent direct sum.

S = set of total parameters

S_1 = set of premise parameters which is nonlinear parameters

S_2 = set of consequent parameters which is linear parameters

In the forward pass, the parameter S_2 is calculated and modified using a least squares estimator, while S_1 is unmodified.

In the backward pass, the parameter S_1 is calculated and modified using the steepest descent, while S_2 is not modified.

Through this hybrid learning method, the parameters in ANFIS are updated.

3.2. Deterministic and fuzzy model development

3.2.1. Deterministic model (power law model)

We start by modeling the pyrolysis of Canarygrass at different temperatures from 600 ˚C to 1050 ˚C. The data was obtained from Boateng[28]. The reaction time is 20seconds and the heating rate is 20 C/ms.The authors used the first order reaction kinetic model.

$$\frac{dm}{dt} = A_0 \exp\left(-E_m \big/ RT\right)\left(m_f - m\right) \tag{3.24}$$

Where m is the yield of any product of the gases quantified (i.e., CO_2, CO, CH_4, C_2H_6, C_2H_4, C_3H_8, etc); A_0 is the frequency factor corresponding to product m[1/s]; E_m is the activation energy corresponding to product m [MJ mol^{-1}]; R is the universal gas constant [8.314 kJ $mol^{-1}K^{-1}$]; m_f is the final yield of product "m" and T is the temperature in Kelvin.

3.2.2. ANFIS model

Since there are a lot of uncertainties in the pyrolysis, the deterministic model, which is designed to model a well-defined system, fails to model the pyrolysis. Here, we tackle the same problem while considering uncertainty. ANFIS is utilized to model the pyrolysis reaction. There are two input variables namely the reaction temperature (°C) and the reaction time (s). The output of this model is the production rate of the gases quantified from pyrolysis of Reed Canarygrass.

(1) ANFIS rules and membership functions

The model consists of nine rules since there are two inputs. There are three membership functions for each input. The linguistic terms for temperature are high temperature, medium temperature and low temperature. With three linguistic terms from temperature, we can generate three membership functions to match the fuzzy membership function. The linguistic rules for time of reaction are long period of time, mid-range period of time, and short period of time. Therefore the set of linguistic rules for fuzzy model can be stated as rule (I) to (IX) below:

(I) If (Time is short (in1mf1)) and (Temperature is low (in2mf1)) then (the production is (out1mf1))

(II) If (Time is short (in1mf1)) and (Temperature is medium (in2mf2)) then (the production is (out1mf2))

(III) If (Time is short (in1mf1)) and (Temperature is high (in2mf3)) then (the production rate is (out1mf3))

(IV) If (Time is mid-range (in1mf2)) and (Temperature is low (in2mf1)) then (the production rate is (out1mf4))

(V) If (Time is mid-range (in1mf2)) and (Temperature is medium (in2mf2)) then (the production rate is (out1mf5))

(VI) If (Time is mid-range (in1mf2)) and (Temperature is high (in2mf3)) then (the production rate is (out1mf6))

(VII) If (Time is long (in1mf3)) and (Temperature is low (in2mf1)) then (the production rate is (out1mf7))

(VIII) If (Time is long (in1mf3)) and (Temperature is medium (in2mf2)) then (the production rate is (out1mf8))

(IX) If (Time is long (in1mf3)) and (Temperature is high (in2mf3)) then (the production rate is (out1mf9))

(2) ANFIS calculation procedure

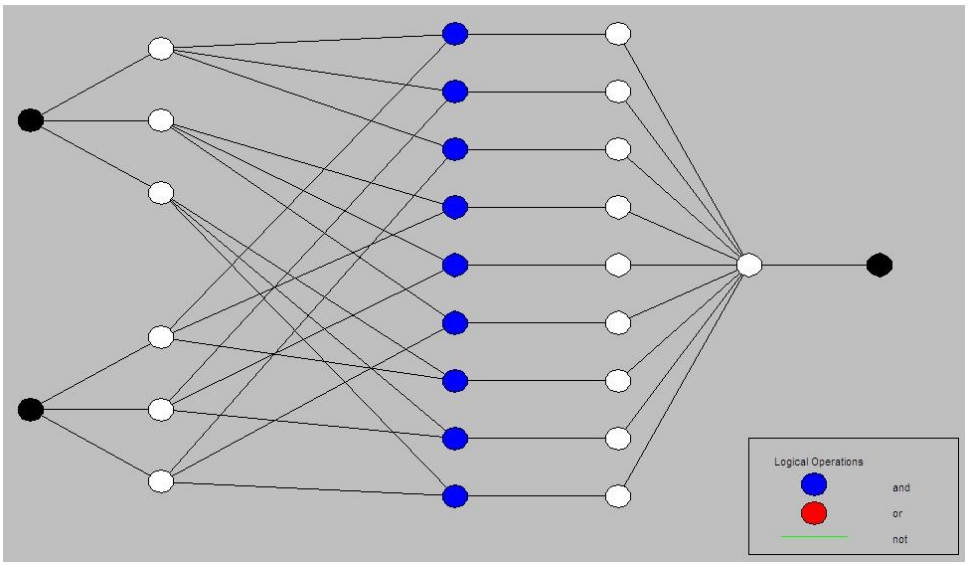

Figure 3.8 FIS mapping

Figure 3.8 displays the calculation procedure for the ANFIS model by layer. The first two nodes display two inputs, which are time of reaction and temperature of reaction. The second layer with six nodes displays membership functions. There are three membership functions for each input. A fuzzification process with the Gaussian membership function is executed over this layer. The inputs are determined by the degree to which they belong to each of the appropriate fuzzy sets via membership functions. The third layer displays rules. There are nine rules in this calculation. The fourth layer displays output membership functions for each rule. The fifth layer output is an aggregation of the fourth layer output. The defuzzified output is displayed in the last layer.

3.3. Result, discussion and conclusion

3.3.1. Deterministic model (power law model)

The results from the model are shown below:

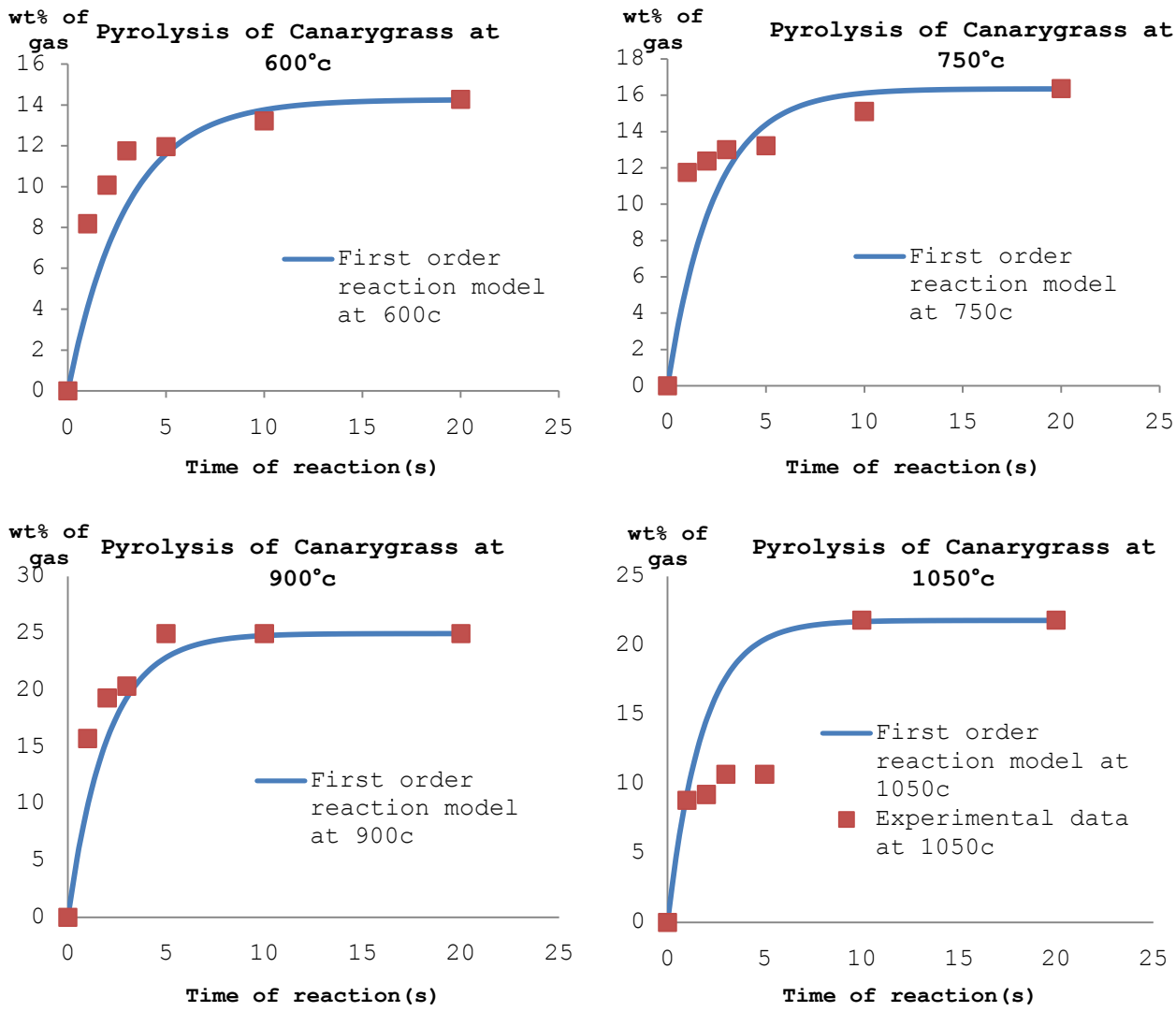

Figure 3.9 Pyrolysis of Canarygrass at different temperature using first order kinetic reproduced from Boateng et al [73]

From the graph, the first kinetic reaction cannot successfully predict the pyrolysis of Canarygrass at

temperatures of 750°C and 1050°C. At the temperature of 750°C, we can see from the graph that the model fails to predict the pyrolysis reaction during the first 5 seconds. In addition, at the temperature of 1050°C, the model fails to predict the reaction at 2-5 seconds. The graph's prediction completely fails to predict the reaction at the stated time. However, the model performs well at temperatures of 600°C and 900°C. From the graphs, we can say that the first kinetic model does not consistently perform well in a specific region. It performs well at 600°C; however, it fails at 750°C. Later on, it performs well again at 900°C. Finally, it fails at 1050°C. This means the model is not a consistent model at low or high temperatures. We will compare their results with our results later.

3.3.2. ANFIS model

There are two inputs, which are temperature and time of reaction. Each of input consists of three different membership functions. All the membership functions, which already trained, are shown in figures below:

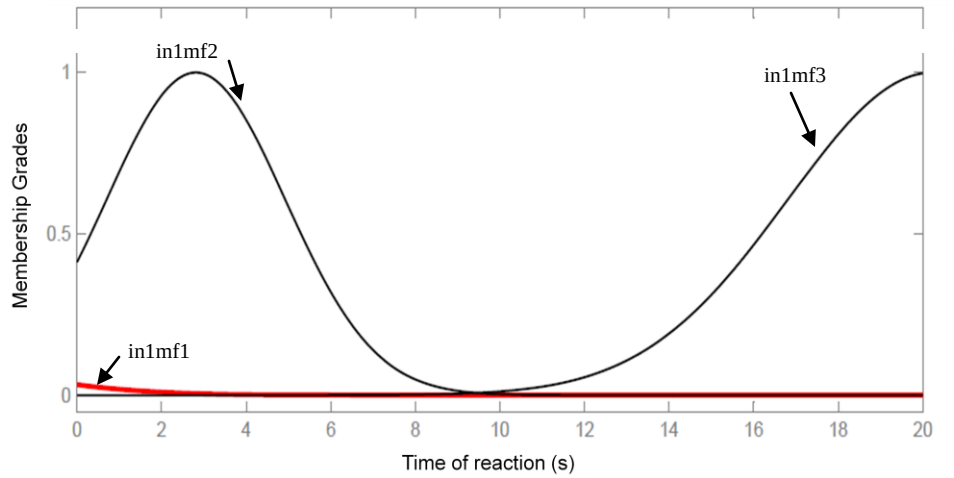

Figure 3.10 FIS represent membership function for time of the reaction

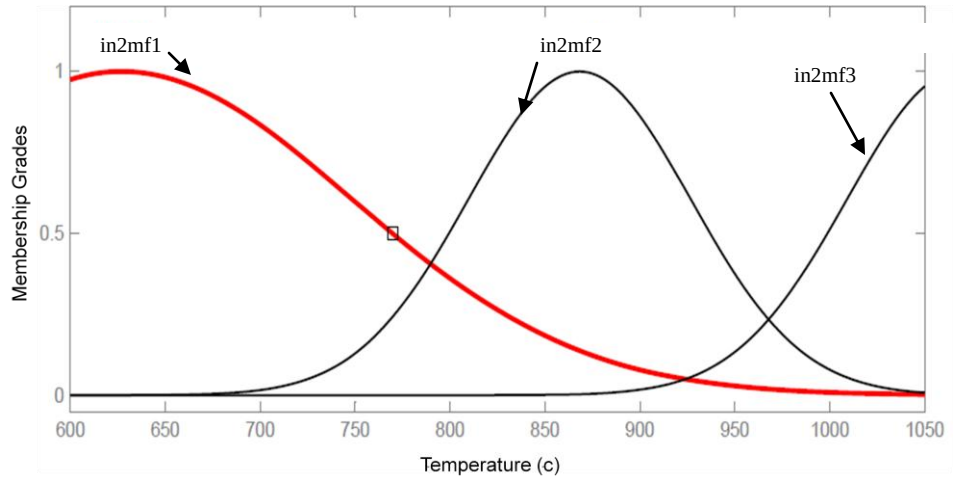

Figure 3.11 FIS represent membership function for temperature

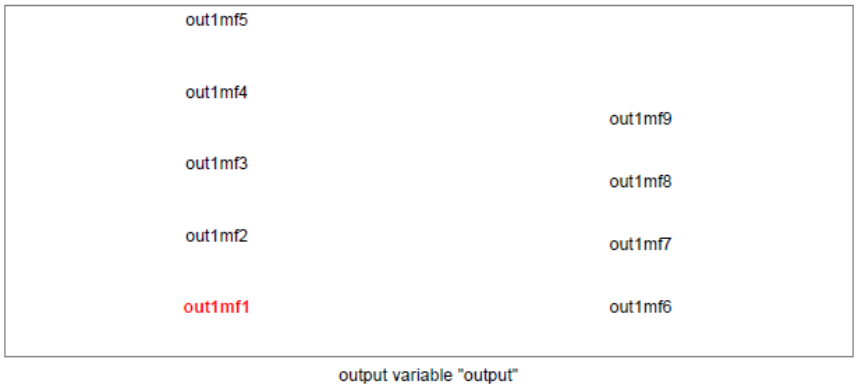

Figure 3.12 FIS represent membership function for output, which is production from pyrolysis reaction

Figure 3.10 represents the membership function of the reaction time. There are three different membership functions, namely short reaction time, mid-range reaction time, long reaction time. The membership function is calculated from the hybrid learning method. From0 to 8 seconds, the reaction is mostly represented by the mid-range time membership function. From 0 to 2 seconds, there is still some influence from the short reaction time membership function. However, from Figure 3.10, the effect of the short reaction time is very little. The effect of long reaction time begins after 8 seconds. From the experimental result, the reaction takes place mostly in the time of 0-8 seconds and reaches equilibrium after 10 seconds for all temperatures. This means the mid-range reaction time membership function is highly affected by the reaction in the transient range. On the other hand, the long time of reaction membership

function has an effect when the reaction reaches the equilibrium.

Figure 3.11, the temperature is also separated into three different membership functions which is low temperature of reaction, medium temperature of reaction, and high temperature of reaction. The temperature of 600°C is influenced by only low temperature membership function. The 750°C is influenced by low and medium temperature membership function, with the low temperature having the most influences. The 900°C is influenced by all three membership functions. The medium temperature is the most influenced. The 1050°C is influenced mostly by high temperature membership function. However, there is very little effect from medium temperature.

From Figure 3.12, there are nine outputs in layer 5 from the calculation, which are affected by two inputs.

(1) ANFIS model result with training data result

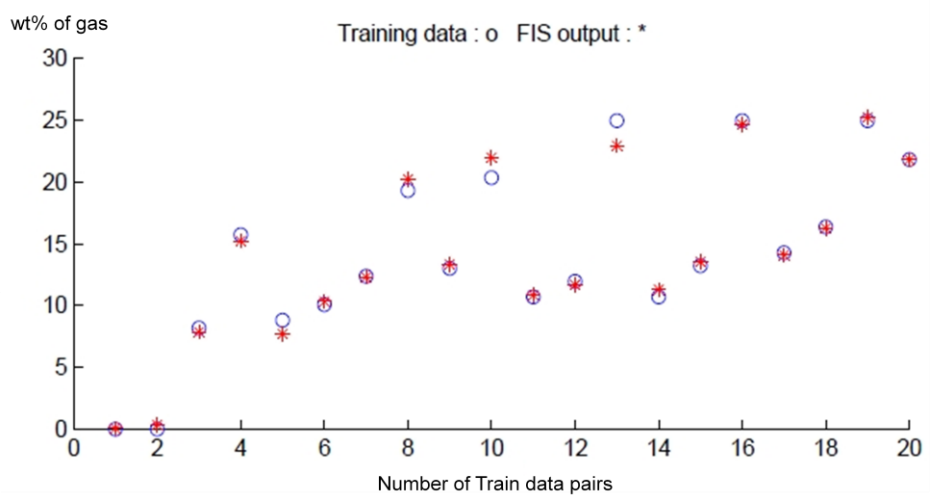

Figure 3.13 wt% of gas vs number of train data pairs

Figure 3.13 represents training data set. The output is the weight of pyrolysis production while the inputs are a set of temperatures and a set of times. From Figure 3.13, we can see that with this method the output in a training section is closed to the experimental data.

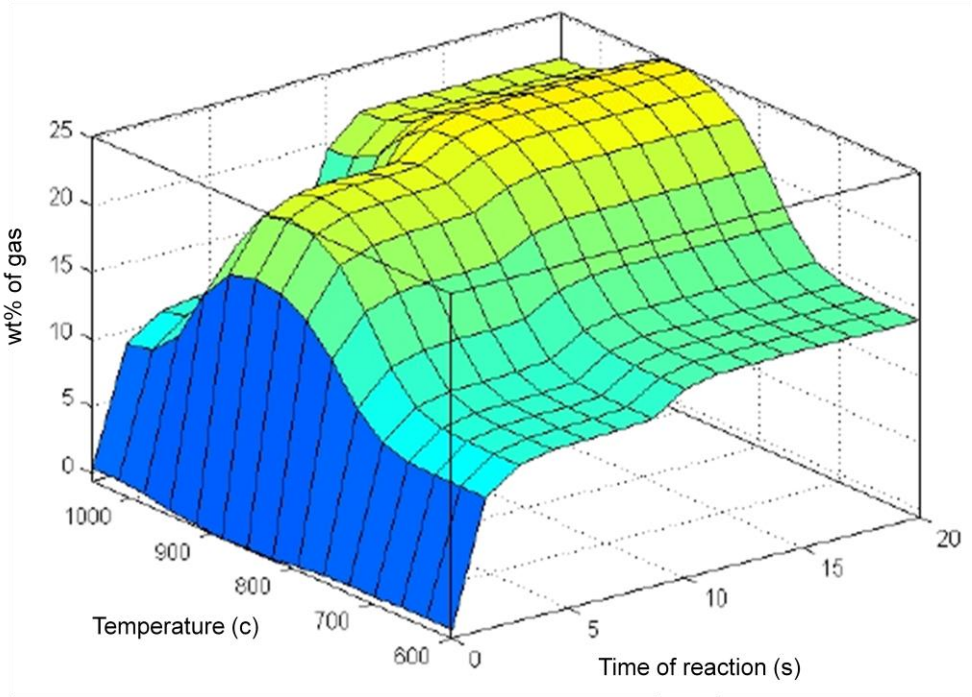

Figure 3.14 %wt of gas depend on temperature (C) and time of reaction (s)

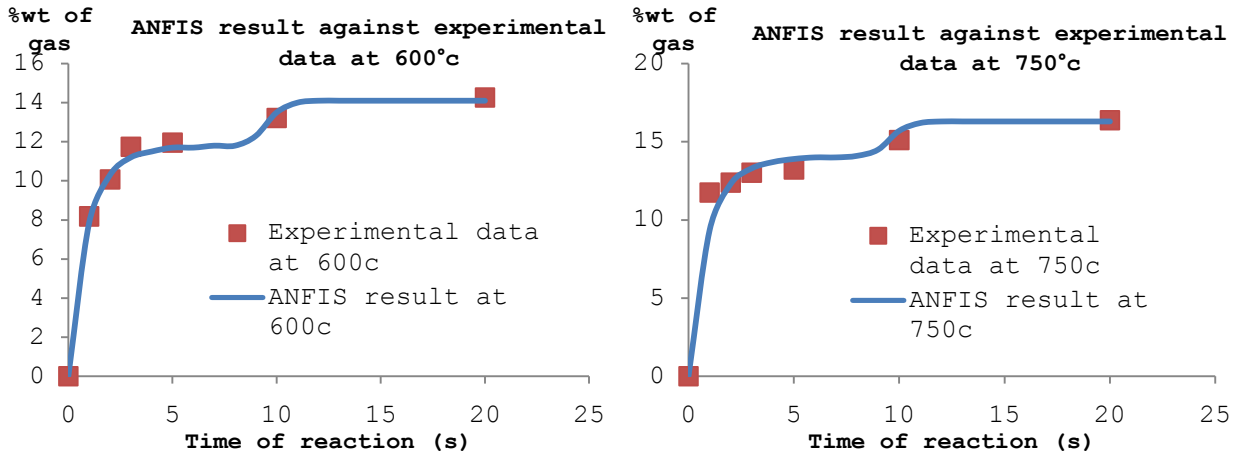

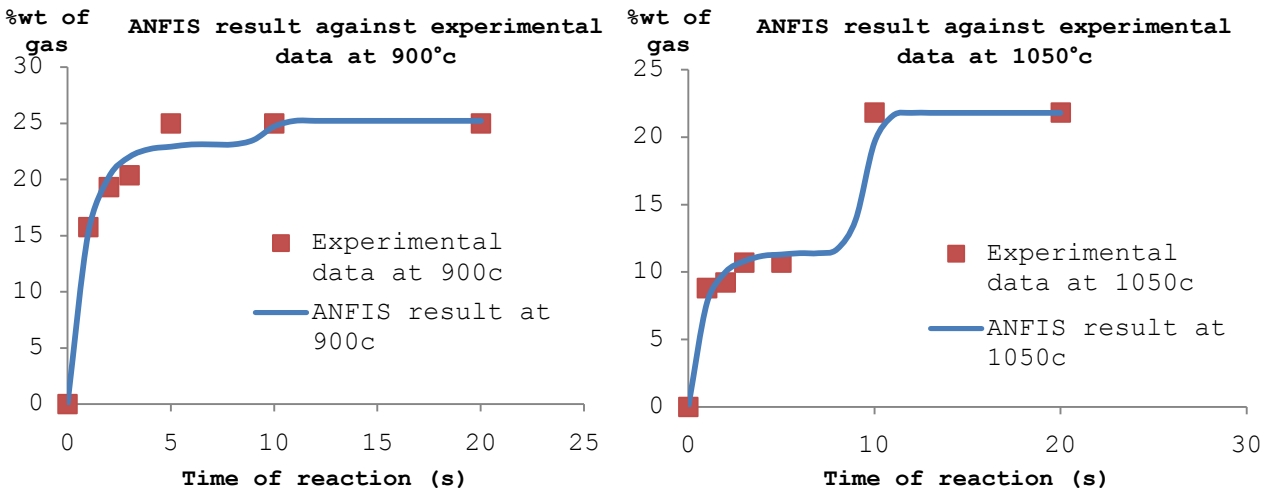

Figure 3.15 ANFIS result against experimental data at 600°c to 1050°c

Figure 3.14 shows 3D results from Matlab calculation for the reaction by using the ANFIS method. Figure 3.15 displays the ANFIS calculation result against the experimental data at different temperatures. The result from the ANFIS model is close to the experimental data from the pyrolysis reaction of Reed Canarygrass.

(2) ANFIS model result with testing data result

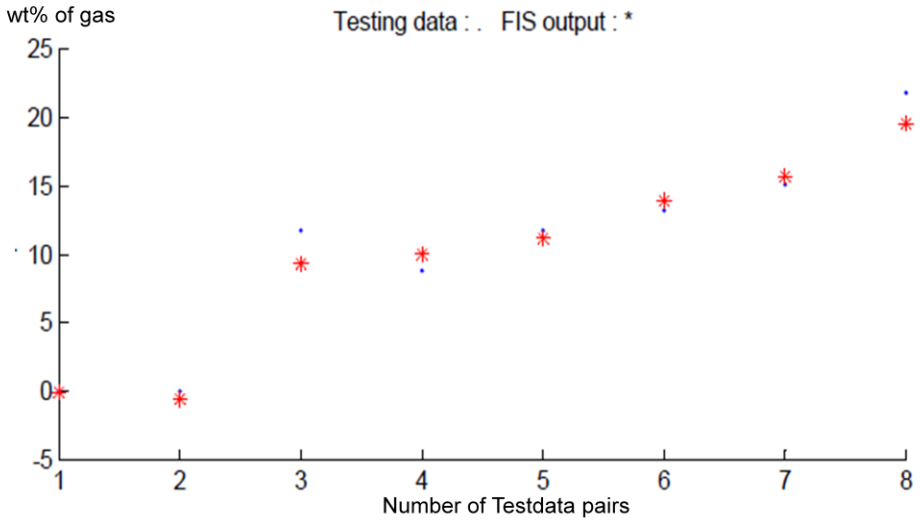

Figure 3.16 wt% of gas vs number of test data pairs

Figure 3.16 represents testing data set. The output is the weight of pyrolysis production, while the inputs are sets of temperatures and times. The ANFIS model successfully predicts the output. The result means that the model is robust and can be use to predict the weight of pyrolysis production.

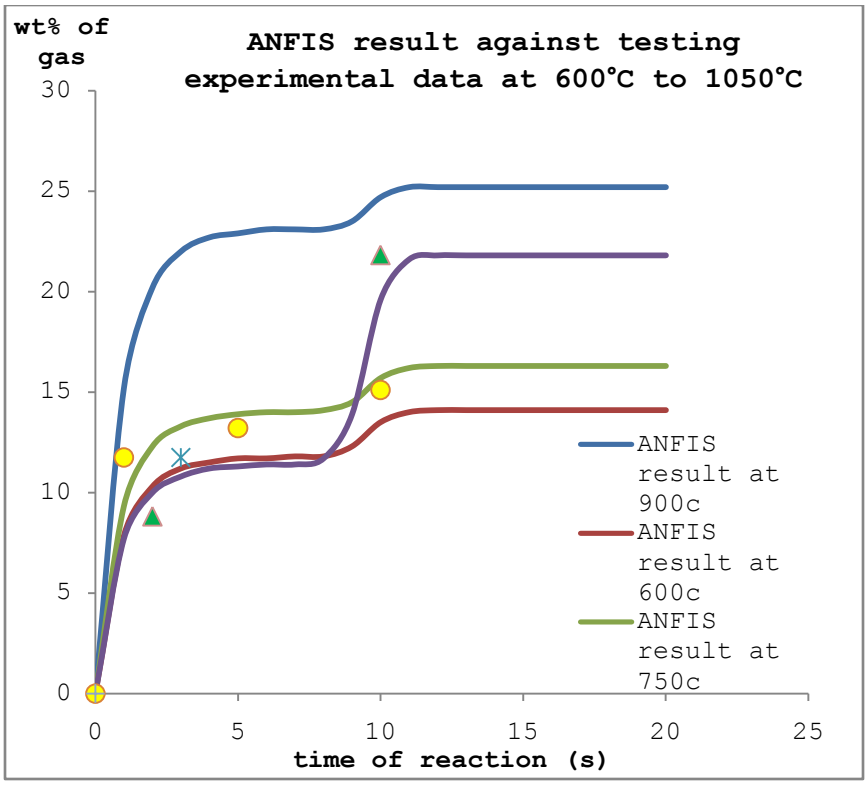

Figure 3.17 testing ANFIS model with the testing data

Figure 3.17 displays the result from ANFIS with the testing data set. The results from the ANFIS model are similar to the testing data, demonstrating the model can predict the pyrolysis production weight at temperatures from 600°C to 1050°C and reaction times from 0s to 20s.

(3) Comparison of Deterministic model and ANFIS model result

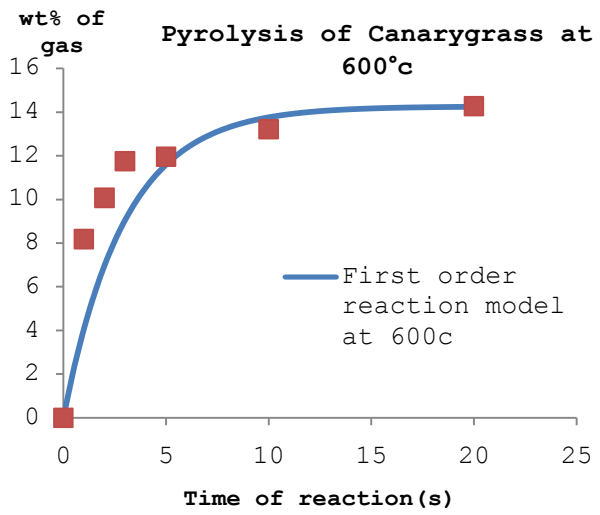

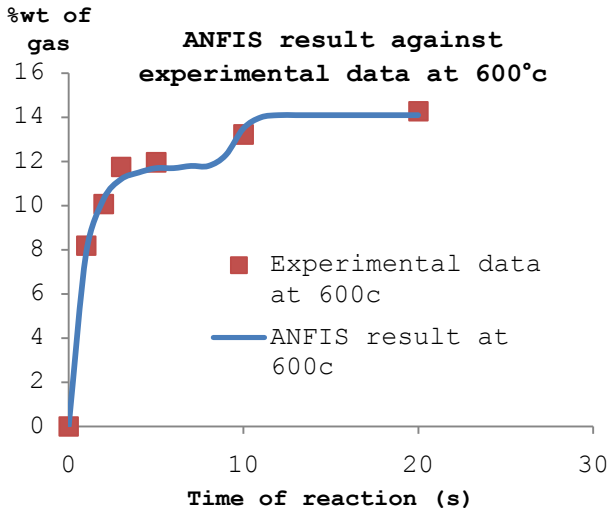

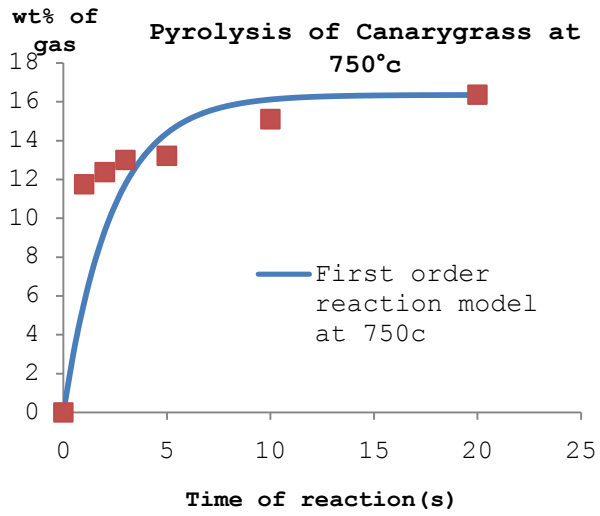

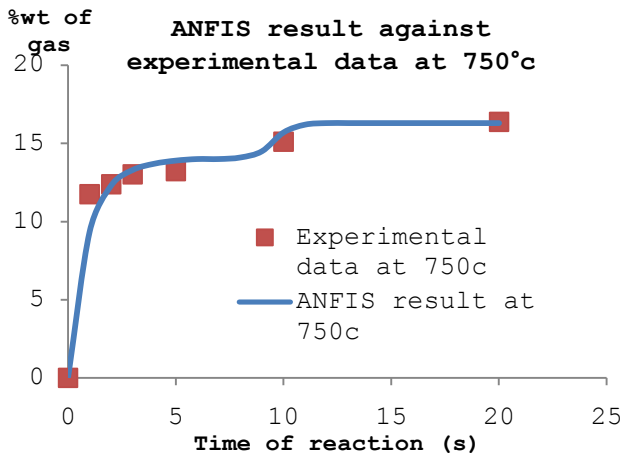

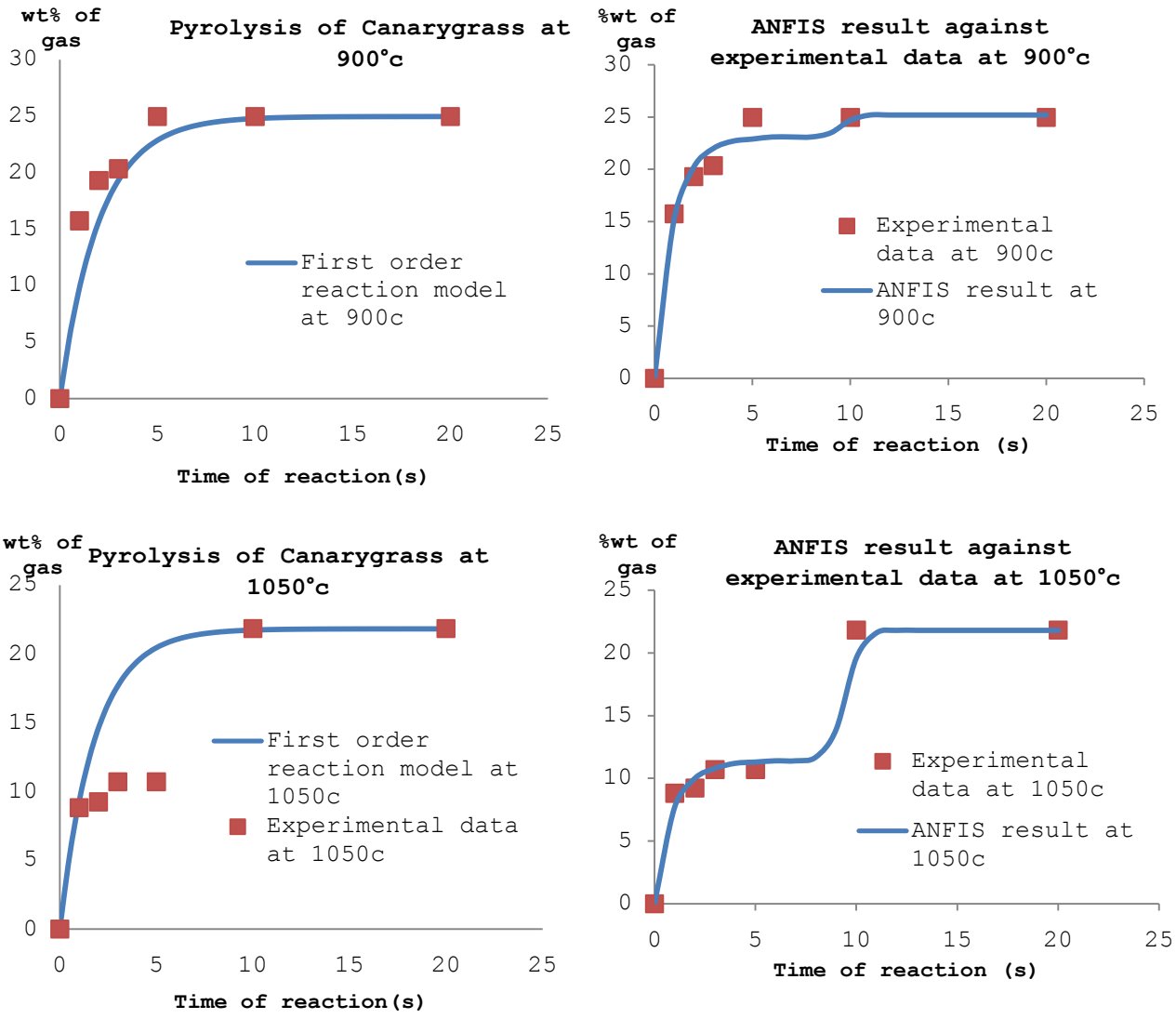

Figure 3.18 Comparison result from two different models left side is first order kinetic reaction and right side is ANFIS model

Figure 3.18 displays the results from two different models. The left side shows the results from the first order kinetic reaction model, while the right side shows the results from the ANFIS model we developed. From the results, the ANFIS model better predicts pyrolysis reaction than the first order kinetic reaction model.

3.3.3. Verification of ANFIS model with Pyrolysis of wood and model discussion

We model the pyrolysis of wood with the ANFIS system and compare it with the power law model, which is conventionally used. We obtained the pyrolysis data from Adrian[29]. The wood particle is pyrolyzed at three different temperatures, namely 600, 800 and 1000°C.

Firstly, we consider the first order power law model. The model results are shown below.

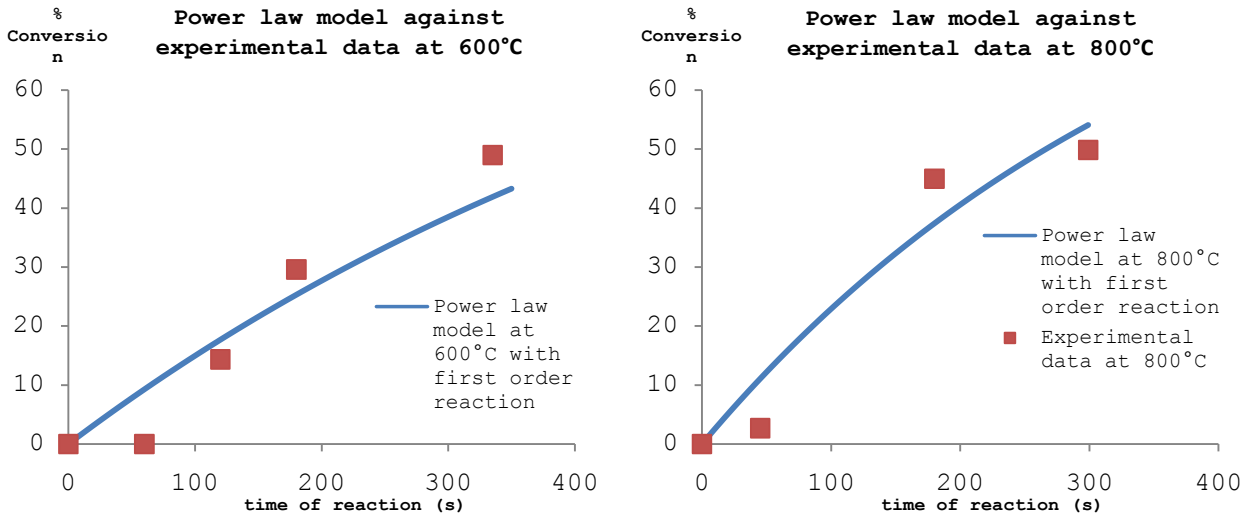

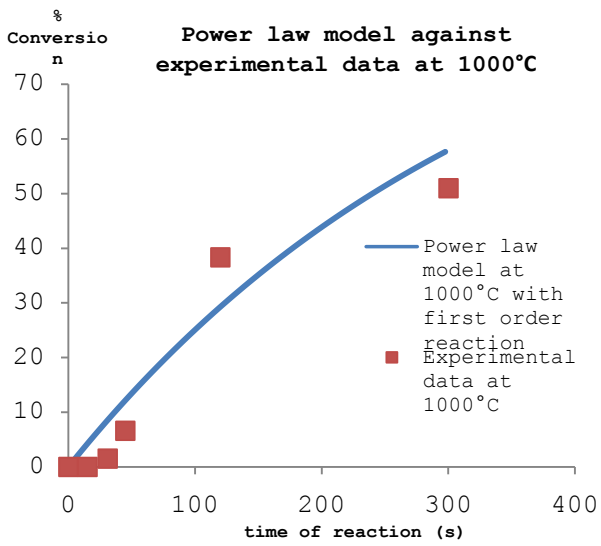

Figure 3.19 Power law model against experimental data at different temperature

From Figure 3.19, the power law with the first order reaction model is not adequate to model the pyrolysis of wood. There are too many discrepancies between the model and experimental data. Therefore, we determined an optimum order of reaction at different temperatures to fit the experimental data.

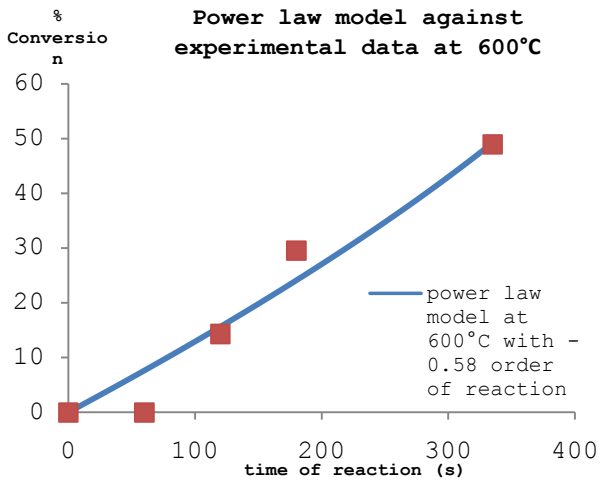

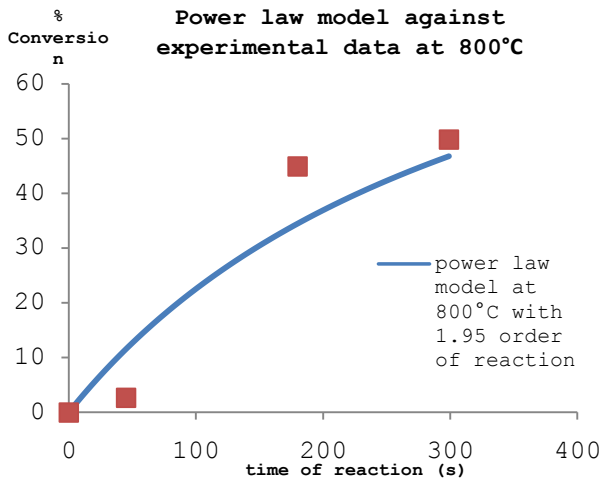

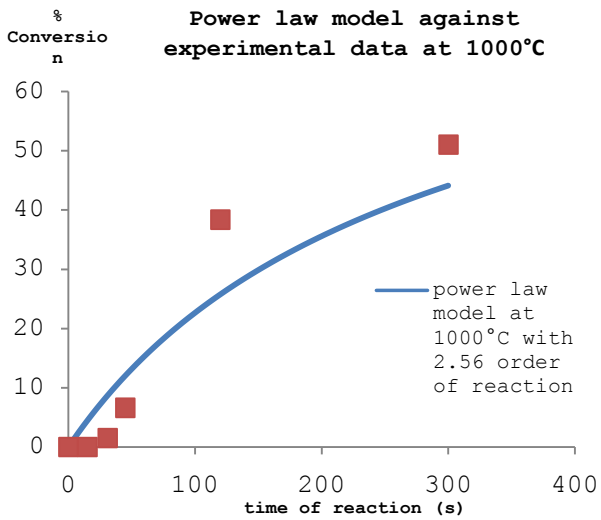

Figure 3.20 Power law model against experimental data at different temperature with optimum order of reaction

From Figure 3.20, we model the reaction by using the power law model with the optimum order of reaction for each temperature. The order of reactions is 0.58, 1.95 and 2.56 at the temperature of 600, 800 and 1000˚C respectively. We can see that the order of the reaction is increasing as the temperature is rising. This means that the reaction is faster at higher temperatures. However, the model results are not suitable for describing the pyrolysis of wood. We conclude that the power law does not adequately model the experimental data. Next we consider the ANFIS model of the same system.

In the ANFIS model, we first create membership functions. There are two different inputs, which are reaction time and temperature. There are three membership functions for each

input. The linguistic terms for temperature are high temperature, medium temperature and low temperature. With three linguistic terms for temperature, we can generate three membership functions to match the fuzzy membership function. The linguistic membership function for time of reaction are long period of time, mid-range period of time, and short period of time. Therefore the set of linguistic rules for fuzzy model can be stated as rule (I) to (IX).

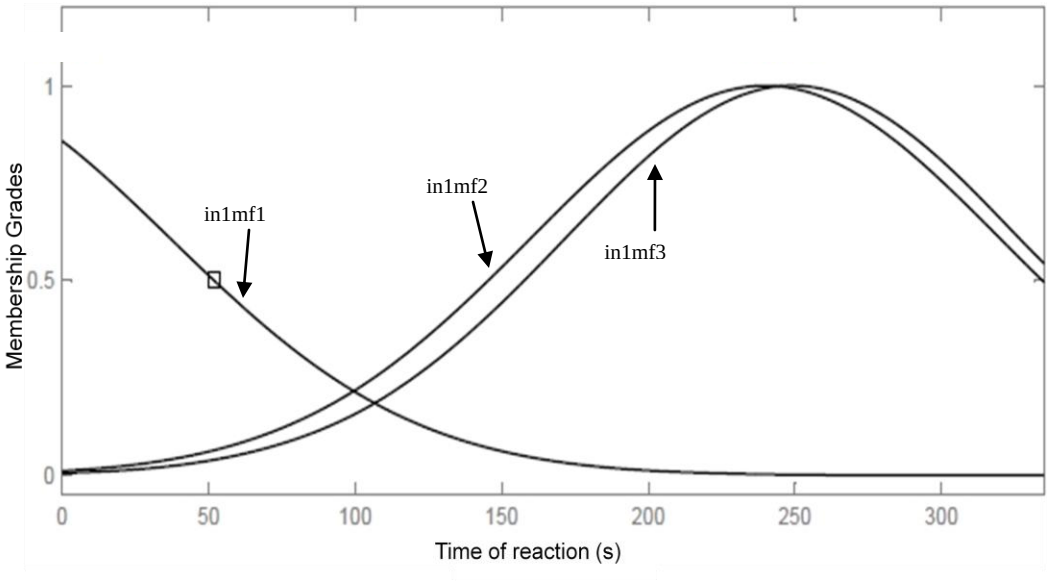

Figure 3.21represent membership function for time of the reaction

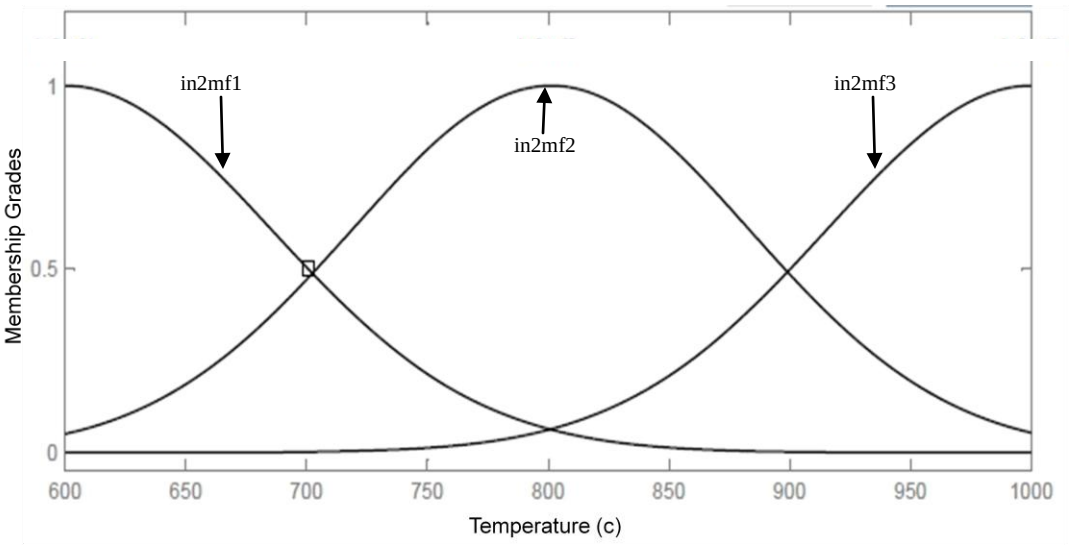

Figure 3.22 FIS represent membership function for temperature

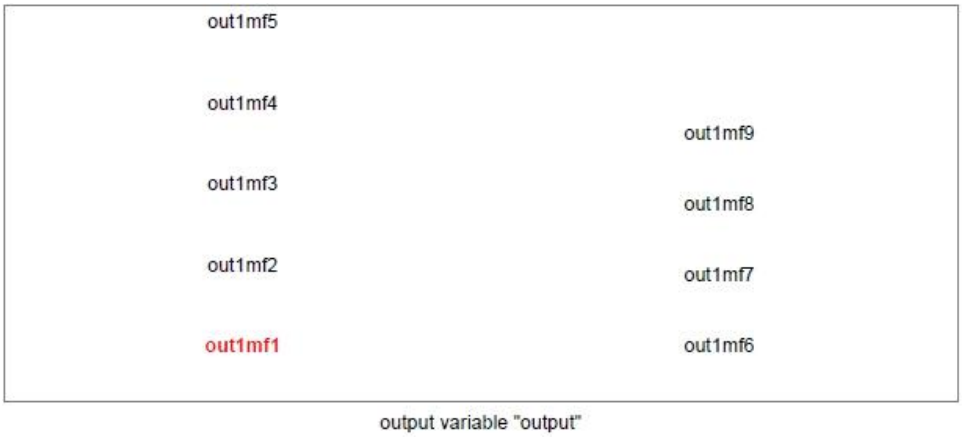

Figure 3.23 FIS represent membership function for output which is production from pyrolysis reaction

From Figure 3.21, for the first 100 seconds of the reaction, the membership function is controlled mostly by the *short time* membership function. The reaction after 100 seconds is controlled by two membership functions which are *mid-range and long time* membership functions. Both *mid-range and long time*

membership functions take effect on the transient of reaction until the reaction reaches equilibrium stage.

From Figure 3.22, there are three membership functions, which are *low, medium, and high temperature* membership functions. At 600°C, there are two membership functions that affect the reaction; these are *low and medium temperature* membership functions. The *low temperature* membership function takes most action on the reaction at 600°C while the *medium temperature* takes little effect. The *low, medium, and high temperature* membership functions take effect on the reaction at 800°C. The *medium temperature* has the most effect on the reaction at 800°C while the *low and medium temperature* membership functions have minimal effect. At temperature 1000°C, the *medium and high temperature* membership functions take effect. The *high temperature* membership function has the most of effect on the reaction at 1000°C while the *medium temperature* membership function has little effect.

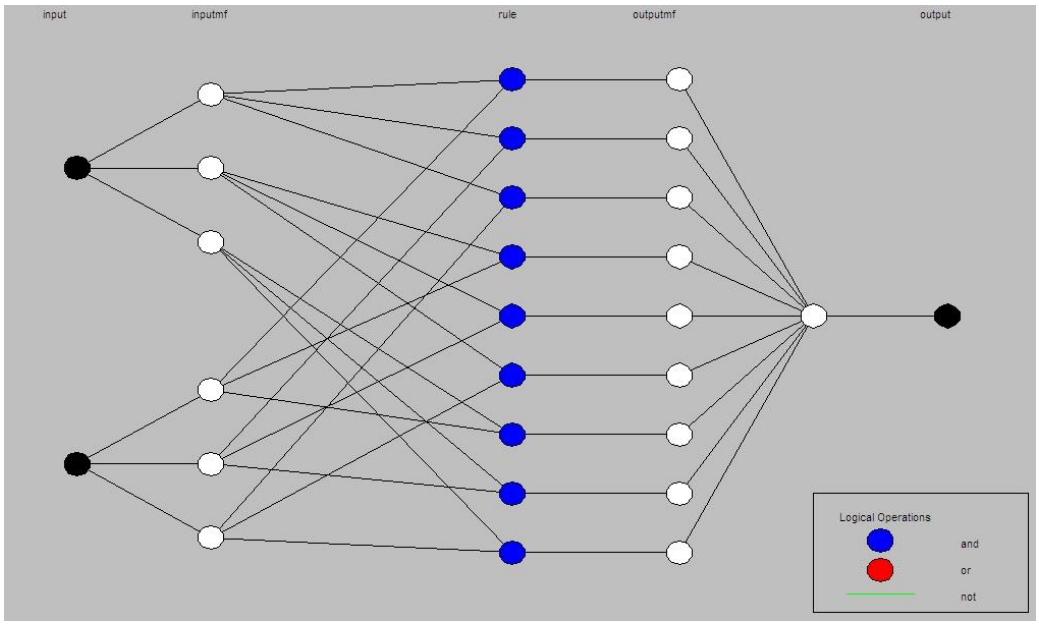

Figure 3.24 FIS mapping

Figure 3.24, the same as Figure 3.8, displays the calculation procedure by layer for the ANFIS model. The calculation consists of six layers.

Figure 3.25 % conversion vs number of train data pairs

Figure 3.25 represents the training data set. The output is the % conversion while the inputs are a set of temperatures and a set of times. In the figure, the % conversion calculated from our model matches the experimental data.

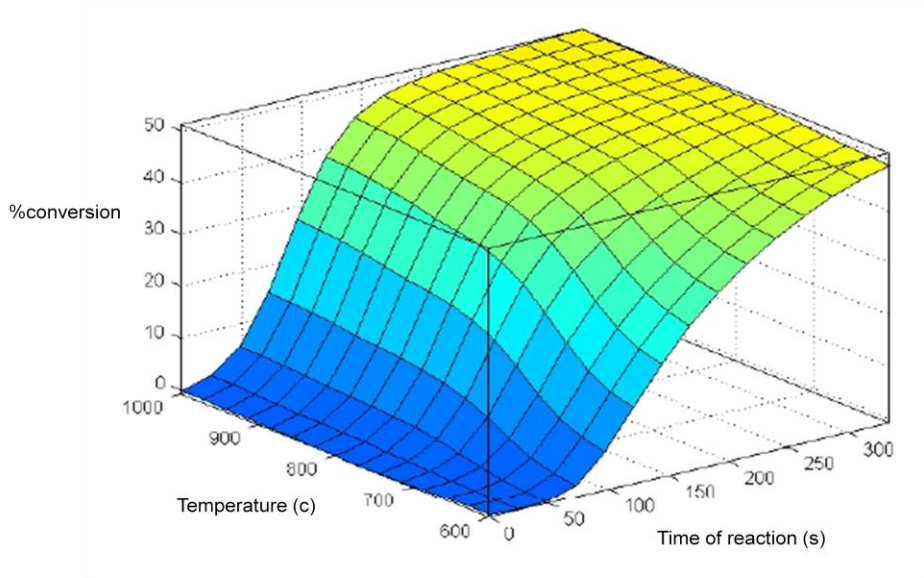

Figure 3.26 %conversion depend on temperature (C) and time of reaction (s)

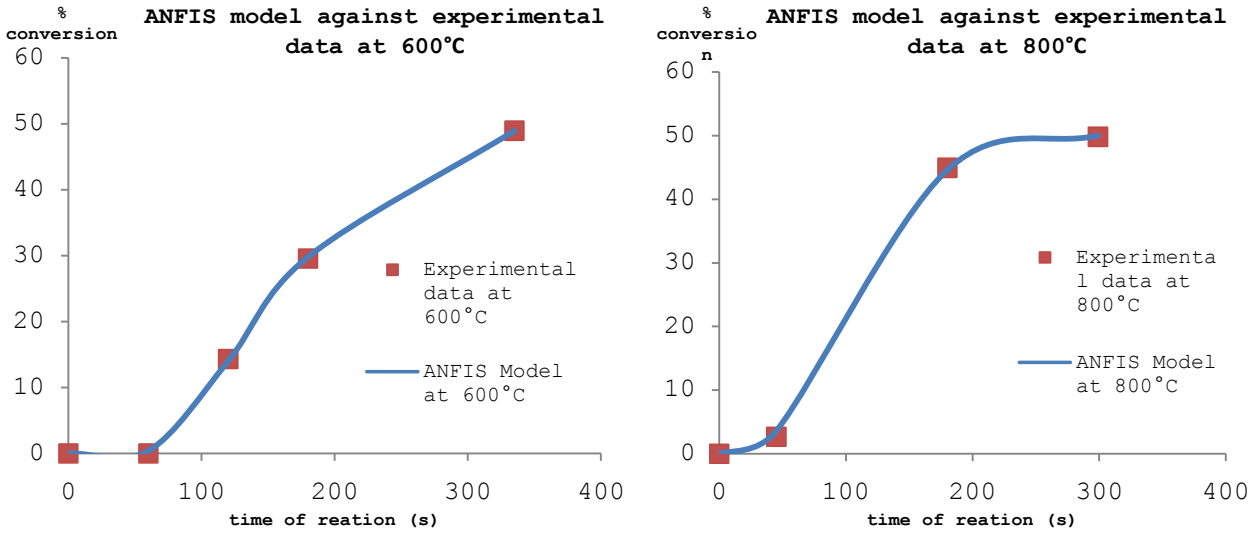

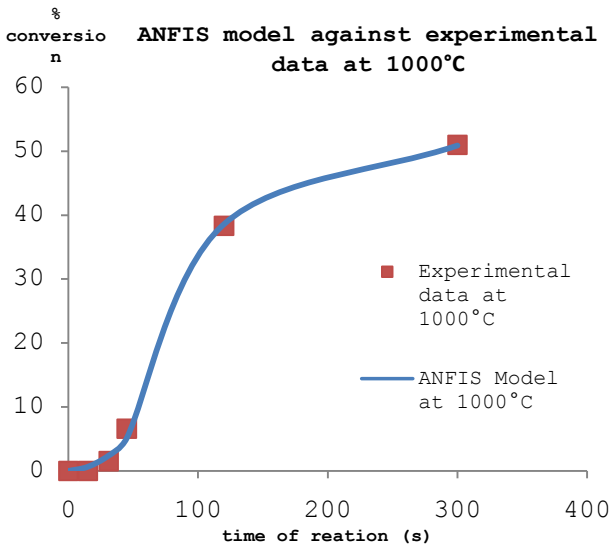

Figure 3.27 ANFIS model against experimental data at 600 to 1000°C

Figure 3.26 shows 3D results from Matlab calculations for the reaction by using the ANFIS method. Figure 3.27 displays the ANFIS calculation result against the experimental data at different temperatures. The result from the ANFIS model is close to the experimental data from the pyrolysis reaction of wood.

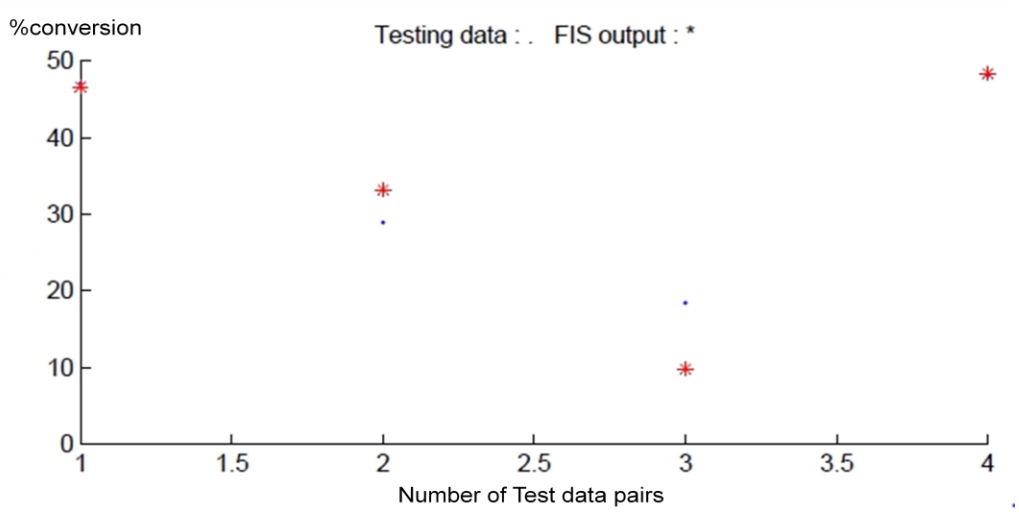

Figure 3.28 %conversion vs number of test data pairs

Figure 3.28 represents the testing data set. The output is the %conversion for the pyrolysis of wood, while the inputs are sets of temperatures and times. The ANFIS model is adequate to predict the output. The result means that the model is robust and can be used to predict %conversion of the pyrolysis of wood.

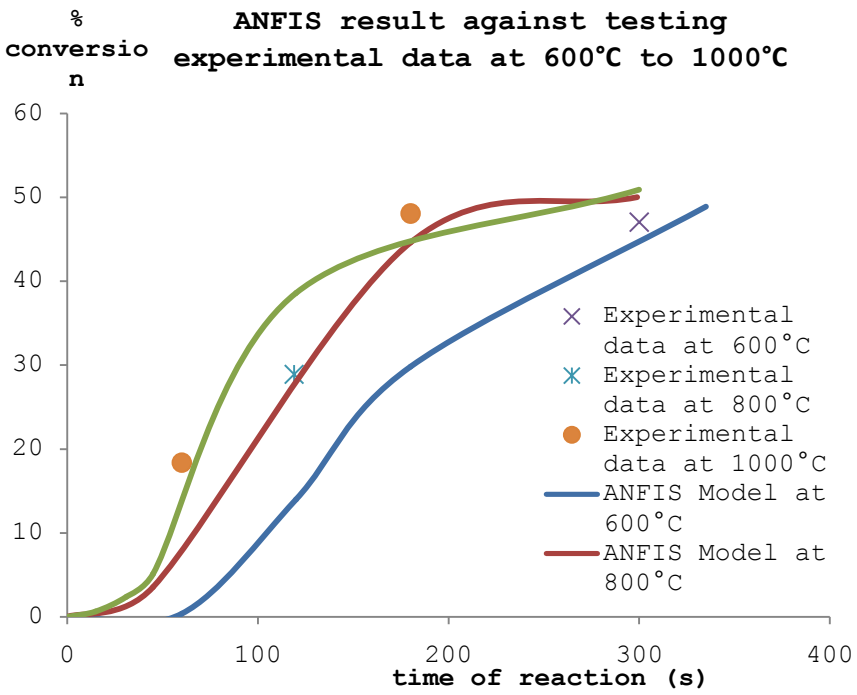

Figure 3.29 testing ANFIS model with the testing data

Figure 3.29 displays the result from the ANFIS model with the testing data set. The results from the ANFIS model are close to the testing data, and illustrate that the model can predict the pyrolysis production of wood from 600°C to 1000°C and reaction times from 0s to 330s.

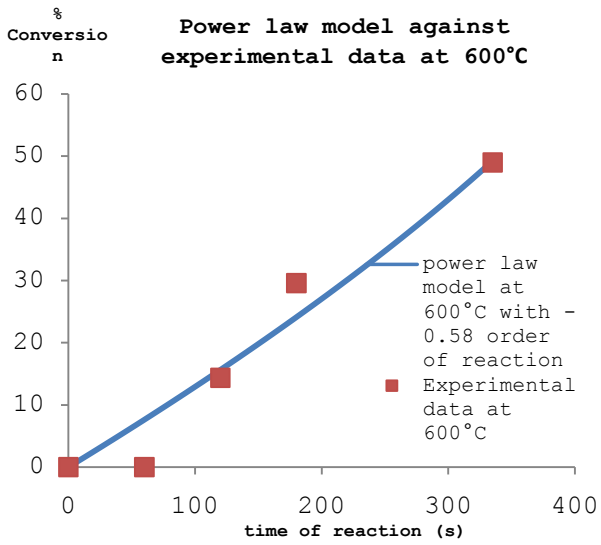
% Conversion
Power law model against experimental data at 600°C
60
50
40
30
20
10
0
0
100
200
300
400
time of reaction (s)
power law model at 600°C with -0.58 order of reaction
Experimental data at 600°C

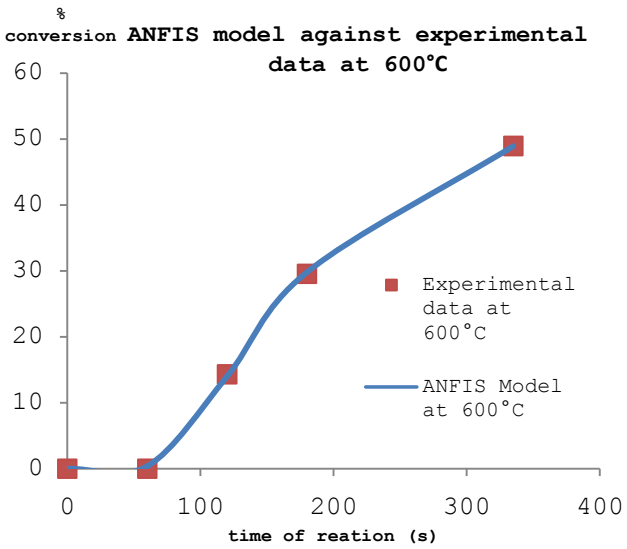
% conversion
ANFIS model against experimental data at 600°C
60
50
40
30
20
10
0
0
100
200
300
400
time of reation (s)
Experimental data at 600°C
ANFIS Model at 600°C

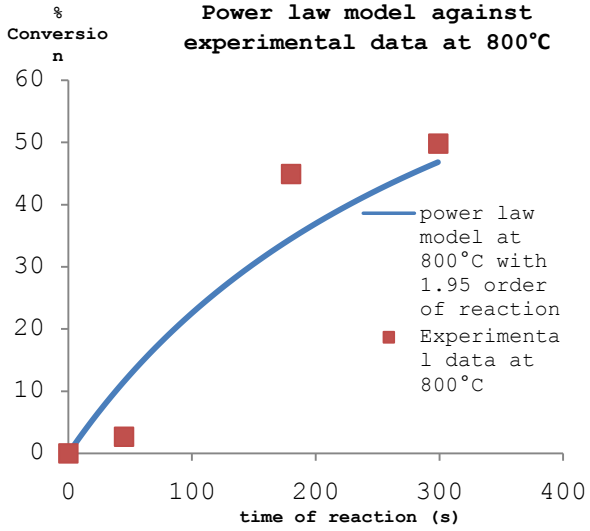
% Conversion
Power law model against experimental data at 800°C
60
50
40
30
20
10
0
0
100
200
300
400
time of reaction (s)
power law model at 800°C with 1.95 order of reaction
Experimental data at 800°C

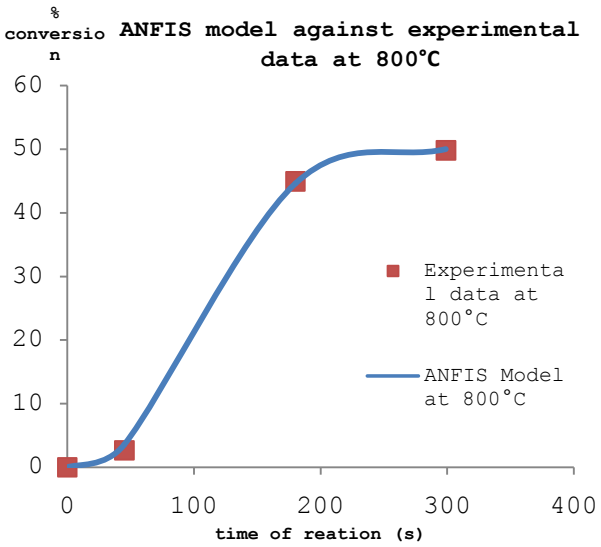
% conversion
ANFIS model against experimental data at 800°C
60
50
40
30
20
10
0
0
100
200
300
400
time of reation (s)
Experimental data at 800°C
ANFIS Model at 800°C

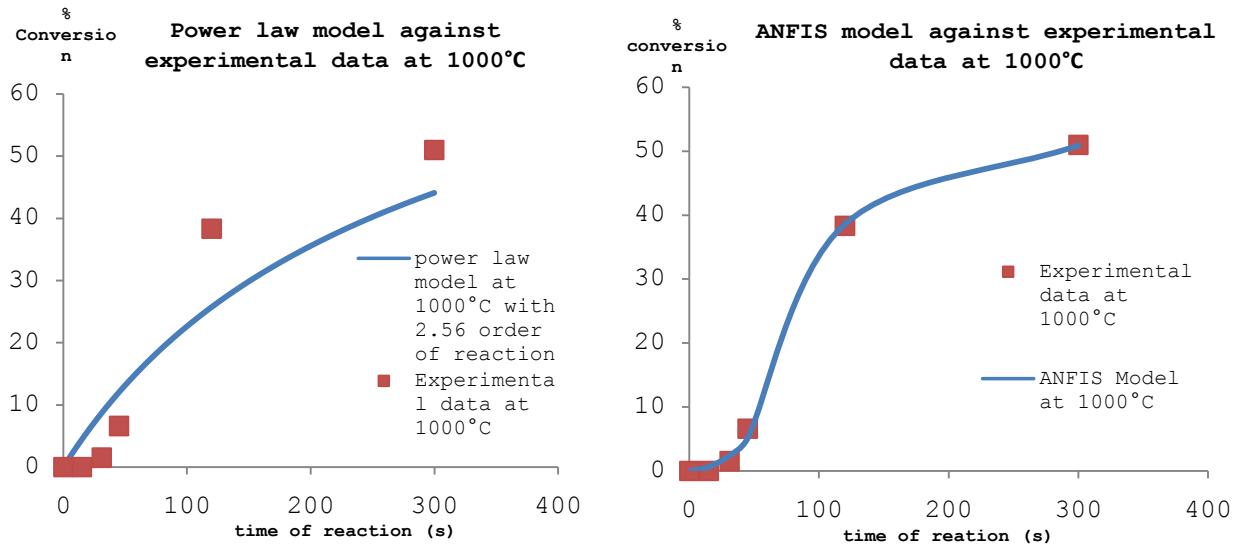

Figure 3.30 Power law model vs ANFIS model for pyrolysis of wood

Figure 3.30 displays the results from two different models. The left side shows the results from the power law model, while the right side shows the results from the ANFIS model we developed. From the results, the ANFIS model better predicts pyrolysis reaction than the power law model.

From both experimental data sets, the pyrolysis of Reed Canary grass is faster than the wood particles. For pyrolysis of Reed Canary grass, the reactions mostly take place in the first 8 seconds. The *short time of the reaction* membership function has maximum effect in the first 8 seconds. After that, the reaction almost reaches the equilibrium state. The transients in the reaction are controlled by the *mid-range time of the reaction* membership function, while the equilibrium stage is influenced mostly by the *long time of reaction* membership

function. On the other hand, for the pyrolysis of the wood particle, the reaction is slower. At 600°C and 800°C, there is not much conversion that appears on the first 50 seconds. There is a little higher conversion at first 50 seconds at 1000°C. At 100s, the reactions at 600°C to 1000°C are influenced by short time of the reaction membership function. The transient and equilibrium stage for pyrolysis of wood are influenced by mid-range and the long time of the reaction membership function.

3.3.4. Conclusion and future work

We have shown another way to model the pyrolysis reaction of biomass such as Reed Canary grass and wood. Instead of using a standard power law model, we propose the use of the ANFIS model, which combines the fuzzy inference system and neural network. We were inspired to use this model due to the uncertainty in the pyrolysis of biomass. Modeling is complex because of short reaction times, temperatures as high as a thousand degree Celsius, and biomass of unknown chemical compositions. Deterministic models, such as the first order reaction model, may not be able to give a good prediction of the reaction. The results from the ANFIS model give both a good fit to the experimental results and a good prediction when testing the model with the testing data set. Also, with the advantage from a fuzzy inference system, we can give a linguistic

interpretation in the form of rules. After validating the ANFIS model with another source of biomass, namely, wood, the ANFIS model is working well and better than the traditional power law model.

For future work, we can extent the work to different sources of biomass including rice hulk and chicken litter (with diverse and unknown components).

Reference

[1] International Energy Agency. Climate and Electricity Annual 2011. OECD Publishing; 2011.

[2] Goswami DY. A Review and Future Prospects of Renewable Energy in the Global Energy System. In: Goswami DY, Zhao Y, editors. Proc. ISES World Congr. 2007, Springer Berlin Heidelberg; 2008, p. 3–10.

[3] Faaij A. Modern Biomass Conversion Technologies. Mitig Adapt Strateg Glob Chang 2006;11:335 – 367.

[4] Li Z, Zhao W, Meng B, Liu C, Zhu Q, Zhao G. Kinetic Study of Corn Straw Pyrolysis: Comparison of Two Different Three-Pseudocomponent Models. Bioresour Technol 2008;99:7616 – 7622.

[5] Chiang W, Fang H, Wu C, Chang C, Chang Y-M, Shie J-L. Pyrolysis Kinetics of Rice Husk in Different Oxygen Concentrations. J Environ Eng 2008;134:316 – 326.

[6] Gašparoviè L, Labovský J, Markoš J. Calculation of Kinetic Parameters of the Thermal Decomposition of Wood by Distributed Activation Energy Model (DAEM) 2012;26:45–53.

[7] Sohpal VK, Singh A, Dey A. Fuzzy Modeling to Evaluate the Effect of Temperature on Batch Transesterification of Jatropha Curcas for Biodiesel Production. Bull Chem React Eng Catal 2011;6:31 – 38.

[8] Fazilat H, Akhlaghi S, Shiri ME, Sharif A. Predicting Thermal Degradation Kinetics of Nylon6/Feather Keratin Blends Using Artificial Intelligence Techniques. Polymer (Guildf) 2012;53:2255 – 2264.

[9] Lertworasirikul S. Drying Kinetics of Semi-Finished Cassava Crackers: A Comparative Study. LWT-Food Sci Technol 2008;41:1360 – 1371.

[10] Lerkkasemsan N, Achenie LEK. Life Cycle Costs and Life Cycle Assessment for the Harvesting, Conversion, and the Use of Switchgrass to Produce Electricity. Int J Chem Eng 2013;2013:1 – 16.

[11] Keattch CJ, Dollimore D. An Introduction to Thermogravimetry. 2nd ed. London: Heyden; 1975.

[12] Coats A, Redfern J. Kinetic Parameters from Thermogravimetric Data. Nature 1964;201:68 – 69.

[13] Bellais M. Modelling of the Pyrolysis of Large Wood Particles. KTH, 2007.

[14] Thurner F, Mann U. Kinetic Investigation of Wood Pyrolysis. Ind Eng Chem Process Des Dev 1981;20:482 – 488.

[15] Alves SS, Figueiredo JL. A Model for Pyrolysis of Wet Wood. Chem Eng Sci 1989;44:2861 – 2869.

[16] Grønli MG. A Theoretical and Experimental Study of the Thermal Degradation of Biomass. Norwegian University of Science and Technology, 1996.

[17] Bradbury AGW, Sakai Y, Shafizadeh F. A Kinetic Model for Pyrolysis of Cellulose. J Appl Polym Sci 1979;23:3271 – 3280.

[18] Koufopanos CA, Lucchesi A, Maschio G, Koufopanosi CA. Kinetic Modelling of the Pyrolysis of Biomass and Biomass Components. Can J Chem Eng 1989;67:75 – 84.

[19] Koufopanos CA, Papayannakos N, Maschio G, Lucchesi A. Modelling of the Pyrolysis of Biomass Particles. Studies on Kinetics, Thermal and Heat Transfer Effects. Can J Chem Eng 1991;69:907 – 915.

[20] Varhegyi G, Jakab E, Antal MJ. Is the Broido-Shafizadeh Model for Cellulose Pyrolysis True? Energy & Fuels 1994;8:1345 – 1352.

[21] Branca C, Di Blasi C. Kinetics of the Isothermal Degradation of Wood in the Temperature Range 528–708 K. J Anal Appl Pyrolysis 2003;67:207 – 219.

[22] Branca C, Albano A, Di Blasi C. Critical Evaluation of Global Mechanisms of Wood Devolatilization. Thermochim Acta 2005;429:133 – 141.

[23] Grioui N, Halouani K, Zoulalian A, Halouani F. Thermogravimetric Analysis and Kinetics Modeling of Isothermal Carbonization of Olive Wood in Inert Atmosphere. Thermochim Acta 2006;440:23 – 30.

[24] Zadeh LA. Fuzzy sets. Inf Control 1965;8:338 – 353.

[25] Jang J-SR. ANFIS: Adaptive-Network-Based Fuzzy Inference System. IEEE Trans Syst Man Cybern 1993;23:665 – 685.

[26] Jang J-SR, Sun C-T, Mizutani E. Neuro-Fuzzy and Soft Computing: A Computational Approach to Learning and Machine Intelligence. Upper Saddle River, NJ: Prentice Hall; 1997.

[27] Jang J. Fuzzy Modeling Using Generalized Neural Networks and Kalman Filter Algorithm. Proc. 9th Natl. Conf. Artif. Intell., vol. 91, 1991, p. 762 – 767.

[28] Boateng A, Jung H, Adler P. Pyrolysis of Energy Crops Including Alfalfa Stems, Reed Canarygrass, and Eastern Gamagrass. Fuel 2006;85:2450 – 2457.

[29] Badea A, Gheorghe C, Marculescu C, Minciuc E. Biomass Pyrolysis Experimental Investigations. Sci Bull Ser C 2008;70:129 – 138.

Chapter 4 Summary and Conclusions

4. Summary and Conclusions

4.1. Overall Summary

In this dissertation, we considered different aspects of bioenergy from the molecular level to the macro-scale level (unit operations), namely using bioenergy to produce electricity. This work has been separated into three specific aims. The first aim mainly focuses on biodiesel production via heterogeneous catalyst. Two catalysts have been studied. Proper deterministic models and stochastic models have been successfully developed. The results from both models agree with each other. The second aim focuses on the production of energy from biomass. Our work considers both life-cycle analysis and life-cycle cost for electricity production using pyrolysis oil from switchgrass conversion. The results show that the electricity produced by biomass is environmentally friendly since it reduces GHG emissions. The results also show that electricity produced by biomass can be competitive with fossil fuel energy sources if there is government subsidy. However, with good farming and transportation management, the process might be able to compete with fossil fuels without government subsidy. The final aim focuses on modeling of pyrolysis of biomass. Modeling of biomass is extremely difficult, mostly due to the presence of many sources of uncertainty. Therefore, we

have proposed fuzzy modeling as a way to address some of the uncertainty.

These three aims are connected by addressing and solving bio energy topic of one popular bio energy type that is bio-oil. However, the bio-oil in these aims comes from two popular implements that are esterification and pyrolysis. These two aims focus on the study of reaction mechanism and the prediction of the reactions yield. One of the aims focused mainly on life-cycle analysis and life cycle cost. They can be put together to address many important decisions. For example, which transform process is suitable for a different location? Or, which process is more environmentally friendly in a certain circumstance? Since we can predict the yield of bio oil from two different reactions by kinetic models that we developed, we can help address this issue by combining the models with life cycle analysis and life cycle cost models that we developed.

However, our models also have limitations mostly on data acquisition. The biodiesel models are only focus on some of solid acid catalysis. The model can be more broadly studied in the future with good supplied data. Likewise, life cycle analysis and life cycle cost are also limited by data. Most of the time, we cannot get exact data on some processes. This

problem can be addressed by cooperating with other researchers, government agencies, or people who work on that particular process for more accurate data. The fuzzy modeling also has limitations on data. The models can perform with more biomass source and that proves its strong point.

With the success of shale oil production in the United State, there is a huge effect on bio energy. The shale oil can produce with cheaper price than bio energy. This gives negative impacts to bio energy development in the United State. However, bio energy still holds its strong point as a renewable source over the shale oil in many countries that do not own a shale oil reservoir and have agriculture as their economic backbone. The most important strong point of bio energy in the future from author point of view is a clean energy that can reduce GHG emission. In the future, when the carbon credit play important role, the bio energy can compete with shale oil or other fossil fuels.

4.2. Research contribution

(1) We have proposed a good model for biodiesel reaction via heterogeneous catalysts. We have studied the reactions over a small number of molecules using the stochastic model. With the model, we can deliver proper mechanism of the reaction over the heterogeneous catalysts.

(2) We have developed the life-cycle analysis and life-cycle cost model switchgrass pyrolysis for use in power plants. We have proved that the energy from switchgrass is clean energy and can be competitive with fossil fuels. Since meso level in LCA needs more research to address the scope and methodology, our contribution is not only to determine the GHG emission we also address the scope and methodology for life-cycle analysis of the miso level. We hope that with the success of our model, the scope and methodology will be recognized for further research.

(3) We have tried to address the uncertainty associated with biomass conversion by using fuzzy logic and inference tools. The models work well and surpass popular power law models. With the results, we proved that this new aspect of modeling the pyrolysis of biomass is suitable for the system.

4.3. Research papers and presentations

4.3.1. Research papers

(1) Lerkkasemsan, N.; Achenie, L.E.K. Pyrolysis of Biomass - Fuzzy Modeling. Renewable Energy, Volume 66, pp.747–758, 2014

(2) Lerkkasemsan, N.; Achenie, L.E.K. Life cycle costs and life cycle assessment for the harvesting, conversion and the use of switchgrass to produce electricity. International Journal of Chemical Engineering ,Vol. 2013

(3) Lerkkasemsan, N.; Abdoulmoumine, N.; Achenie, L.; Agblevor, F. Mechanistic modeling of palmitic acid esterification via heterogeneous catalysis, Industrial and Engineering Chemistry Research volume 50, issue 3, pp. 1177 – 1186, 2011

4.3.2. Presentations

(1) Lerkkasemsan ,N.; Pyrolysis of Reed Canary Grass. AICHE meeting, 2014

(2) Lerkkasemsan,N.; Pyrolysis of Reed Canary grass. 5th Annual Chemical Engineering Research Symposium, 2013

4.4. Recommendation and continued research

4.4.1. Specific Aim 1

A more-detailed model can be delivered. For example, in our research, we assumed that the reaction mechanism was not affected by the transport of fluid. If we do not use this assumption, we can deliver the more-detailed model.

4.4.2. Specific Aim 2

In the future, when more data are available, a more-comprehensive model can be delivered. The models in this dissertation have not concluded environmental impacts from other chemicals.

In cases where there are available data, the life cycle cost model can be extended. We can also integrate optimization calculation into the life cycle cost model. The optimized life cycle cost model can help researchers determine the best scenario for different plants.

4.4.3. Specific Aim 3

The pyrolysis of each biomass compound such as cellulose, hemicelluloses and lignin can be used to train membership functions. We can use these trained membership functions to help predict the pyrolysis of actual biomass.

In cases where data are available, our model can be extended to consider the effects of other factors such as shape of biomass, moisture, other chemicals, etc. With the extensive model, it may give a better prediction on the biomass pyrolysis.

Appendices

Appendix A: Nomenclature

A	Palmitic acid
E	Palmitic acid methyl ester
M	Methanol
S	Catalyst active site
W	Water
C_T	Total catalyst active sites
AS	Palmitic acid adsorbed on an active site
ES	Intermediate palmitic acid methyl ester on the catalyst surface
C_A	Concentration of palmitic acid, M
C_B	Concentration of methanol, M
C_E	Concentration of palmitic acid methyl ester, M
C_W	Concentration of water, M

C_{A0}	Initial concentration of palmiticacid, M
K_{AB}	Adsorption parameter of palmitic acid, $\frac{dm^3}{mol}$
K_{DB}	Desorption parameter of palmitic acid, $\frac{mol}{dm^3}$
K_{AM}	Adsorption parameter of methanol, $\frac{dm^3}{mol}$
K_S	Reaction rate constant, $K_s = \frac{k_{-s}}{k_s}$
k_{-S}	Kinetic constants of the forward reaction, $\frac{dm^3}{g_{cat}\, min}$
k_S	Kinetic constants of the reverse reaction, $\frac{dm^3}{g_{cat}\, min}$
X	Conversion of palmitic acid

Appendix B: Esterification of palmitic acid on SO_4/ZrO_2-550°C

Time (min)	Temperature (°C)	% catalyst loading (w/w)	Xa	StdDev	[Ca], mol/l	[Cb], mol/l	[Cc], mol/l	[Cd], mol/l
0	40°C	10	0.0000	0.0185	0.2465	24.7129	0.0000	0.0000
30			0.1370	0.0422	0.2250	24.6914	0.0215	0.0215
40			0.1619	0.0705	0.2085	24.6749	0.0379	0.0379
50			0.2041	0.0663	0.1961	24.6625	0.0504	0.0504
60			0.2044	0.0783	0.1623	24.6287	0.0842	0.0842
80			0.3414	0.0783	0.1608	24.6272	0.0857	0.0857
100			0.3360	0.0231	0.1608	24.6272	0.0857	0.0857
140			0.4020	0.0478	0.1474	24.6138	0.0991	0.0991
180			0.4335	0.0361	0.1396	24.6060	0.1069	0.1069
0	60°C	10	0.0000	0.0000	0.2465	24.7129	0.0000	0.0000
20			0.1680	0.0748	0.2051	24.6714	0.0414	0.0414
40			0.2910	0.0396	0.1747	24.6411	0.0717	0.0717
60			0.4309	0.0478	0.1403	24.6066	0.1062	0.1062
80			0.4875	0.0281	0.1263	24.5927	0.1202	0.1202
110			0.5551	0.0190	0.1097	24.5760	0.1368	0.1368
140			0.5767	0.0483	0.1043	24.5707	0.1421	0.1421
180			0.6014	0.0318	0.0982	24.5646	0.1482	0.1482

Time (min)	Temperature (°C)	% catalyst loading (w/w)	Xa	StdDev	[Ca], mol/l	[Cb], mol/l	[Cc], mol/l	[Cd], mol/l
0	80°C	10	0.0000	0.0000	0.2465	24.7129	0.0000	0.0000
20			0.2597	0.0367	0.1825	24.6489	0.0640	0.0640
30			0.3338	0.0870	0.1642	24.6306	0.0823	0.0823
40			0.5083	0.0371	0.1212	24.5876	0.1253	0.1253
60			0.6540	0.0656	0.0853	24.5517	0.1612	0.1612
80			0.7083	0.0100	0.0719	24.5383	0.1746	0.1746
120			0.8426	0.0085	0.0388	24.5052	0.2077	0.2077
180			0.8729	0.0159	0.0313	24.4977	0.2151	0.2151

Appendix C: Esterification of palmitic acid on $AcAl_2O_3$

Time (min)	Temperature, K	Temperature (°C)	% catalyst loading (w/w)	Xa	StdDev	[Ca], mol/l	[Cb], mol/l	[Cc], mol/l	[Cd], mol/l
0	313K	40°C	100	0.00	0.0000	0.2465	24.7129	0.0000	0.0000
20				0.17	0.0093	0.2042	24.6706	0.0423	0.0423
40				0.24	0.0187	0.1877	24.6541	0.0587	0.0587
60				0.25	0.0080	0.1844	24.6507	0.0621	0.0621
90				0.29	0.0174	0.1743	24.6406	0.0722	0.0722
120				0.35	0.0108	0.1604	24.6268	0.0861	0.0861
130				0.36	0.0514	0.1575	24.6239	0.0889	0.0889
180				0.39	0.0041	0.1514	24.6178	0.0950	0.0950
0	333K	60°C	100	0.00	0.0000	0.2465	24.7129	0.0000	0.0000
10				0.17	0.0995	0.2055	24.6719	0.0410	0.0410
20				0.20	0.0553	0.1962	24.6626	0.0502	0.0502
50				0.31	0.0708	0.1706	24.6370	0.0758	0.0758
70				0.39	0.0757	0.1509	24.6172	0.0956	0.0956
120				0.45	0.0605	0.1365	24.6029	0.1099	0.1099
180				0.47	0.0175	0.1301	24.5965	0.1163	0.1163

Time (min)	Temperature, K	Temperature (°C)	% catalyst loading (w/w)	Xa	StdDev	[Ca], mol/l	[Cb], mol/l	[Cc], mol/l	[Cd], mol/l
0	353K	80°C	100	0.00	0.0000	0.2465	24.7129	0.0000	0.0000
20				0.29	0.0762	0.1740	24.6404	0.0725	0.0725
30				0.43	0.0592	0.1393	24.6057	0.1072	0.1072
40				0.48	0.0360	0.1281	24.5945	0.1184	0.1184
60				0.55	0.0166	0.1098	24.5762	0.1367	0.1367
80				0.59	0.0250	0.1007	24.5671	0.1458	0.1458
120				0.66	0.0313	0.0842	24.5505	0.1623	0.1623
180				0.71	0.0256	0.0716	24.5380	0.1748	0.1748

Appendix D: Experimental data for esterification of FFA on SO_4/ZrO_2-550°C for verifying model

Temperature	**Time**	X_A	**Deviation**
40°C	210min	0.4649	0.0455
	240min	0.4926	0.0469
60°C	210min	0.6175	0.0146
	240min	0.6330	0.0144
80°C	210min	0.9160	0.0094
	240min	0.9230	0.0048

Appendix E: Result of esterification from experiment for $AcAl_2O_3$ for verifying model

Temp, °C	**time,min**	***X***	**Deviation**
40	210	0.4387	0.0245
	240	0.4358	0.04
60	210	0.5211	0.0253
	240	0.5739	0.0251
80	210	0.7281	0.0446
	240	0.7572	0.0061

Appendix F: Notation for ANFIS membership function

Notation	Meaning
in1mf1	Membership function for short time of reaction
in1mf2	Membership function for mid-range time of reaction
in1mf3	Membership function for long time of reaction
in2mf1	Membership function for low temperature
in2mf2	Membership function for medium temperature
in2mf3	Membership function for high temperature
out1mf1 to out1mf9	Membership function for product from the reaction at different condition of reaction